7907-00

FINAL REPORT ON THE DEVELOPMENT OF A RAYLEIGH SCATTERING DIAGNOSTIC FOR DENSITY AND TEMPERATURE MEASUREMENTS

Prepared by:

K. Annen and R. Joklik
Aerodyne Products Corporation
76 Treble Cove Road
North Billerica, MA 01862

Prepared for:

NASA Lewis Research Center

Under Contract No. NAS3-24613
Period Covered: 4 April, 1985 through 4 April, 1987

October, 1987

ABSTRACT

This report covers the design, development, and initial testing of the Rayleigh scattering diagnostic system. The system performs measurements of gas density and temperature at rates up to 10 kHz. The system utilizes both the 510 nm and 578 nm lines of a copper vapor laser in measuring the Rayleigh scattering signal and in subtracting out interference due to surface-scattered laser light. The system features a 1 inch diameter Rayleigh scattering probe which contains the laser focusing optics, the collection optics, and a pressure transducer. The probe is water-cooled and the optics and pressure transducer are protected with a purge gas flow for use in combustion environments. The system includes PC-based data acquisition and reduction. The small measurement volume created by the probe optics, together with a particle identification and rejection routine in the data reduction software, allow the system to perform measurements in environments having a particle density of $10^4/cm^3$ with little or no reduction in precision or accuracy. The precision of single pulse measurements of density in a 1200 K, 20 atm environment is projected to be 1.7% based on tests of the system performance at ambient density. Recommendations for improvements in the system are presented.

TABLE OF CONTENTS

TABLE OF CONTENTS, Cont'd

LIST OF FIGURES

LIST OF TABLES

I. RAYLEIGH SCATTERING DIAGNOSTIC SYSTEM AND COMPONENT DESCRIPTION

1.1 System Overview

The Rayleigh Scattering Diagnostic (RSD) system uses the principle of Rayleigh Scattering to measure gas density and temperature. Rayleigh scattering is the elastic scattering of light by molecules and small particles (particles whose size is small compared with the wavelength of light). Since the scattering is elastic, the scattered light has the same wavelength as the incident light. In the RSD system, the Rayleigh scattering signal is directly proportional to the density of the gas in the measurement volume. The most appropriate applications for the RSD system are in measurement environments having elevated pressures and low levels of particulates.

The RSD system developed under this contract was designed to perform measurements of gas density and temperature at rates up to 10 kHz in enclosed environments having limited optical axis and low particulate loadings. The optical components for generating and measuring the Rayleigh scattering signal are housed in a water cooled probe having a main body diameter of 2.54 cm (1"). The measurement volume is located 3 cm from the front face of the probe and has nominal spatial dimensions of 200 μm x 400 μm x 600 μm.

A general schematic of the RSD system is given in Figure 1.1. The main components are: the copper vapor laser, the Rayleigh scattering probe, the optical fibers coupling the laser and detectors to the probe, photomultiplier tube (PMT) detectors for the Rayleigh scattering signal, photodiode detectors for the power monitor signals, gated integrators for the Rayleigh scattering signals and gated integrators/long term averagers for the power monitor signals, an analog-to-digital (A/D) conversion board, a microcomputer, a clock, and a timing module which controls the triggering of the laser and electronics. Not shown in Figure 1.1 is the calibration cell which is used to obtain an absolute calibration of the RSD system.

The sequence of steps which is performed and repeated by the RSD system in the measurement process is shown in Figure 1.2. The sequence is initiated

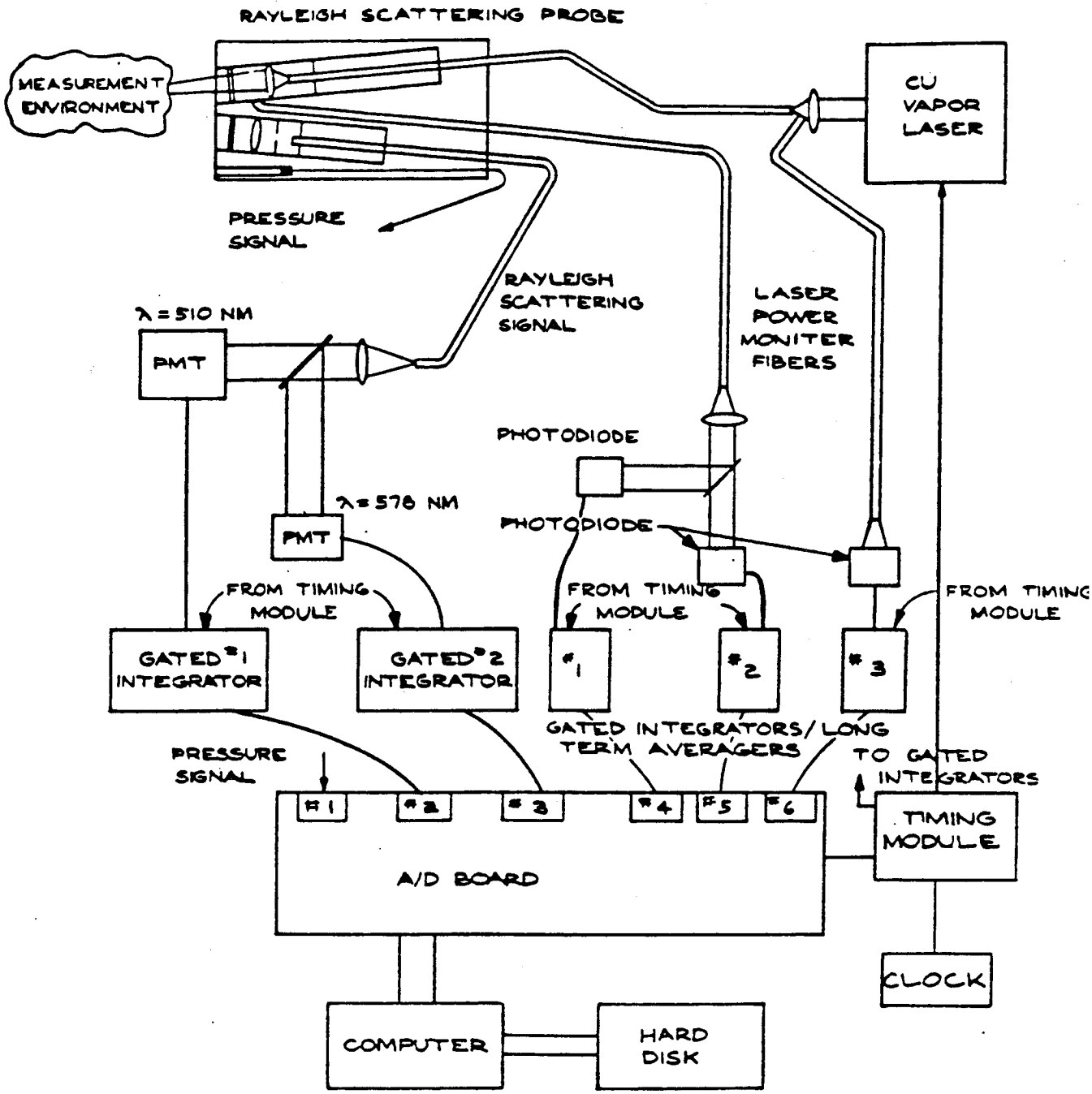

Figure 1.1 Schematic of Rayleigh Scattering Diagnostic System

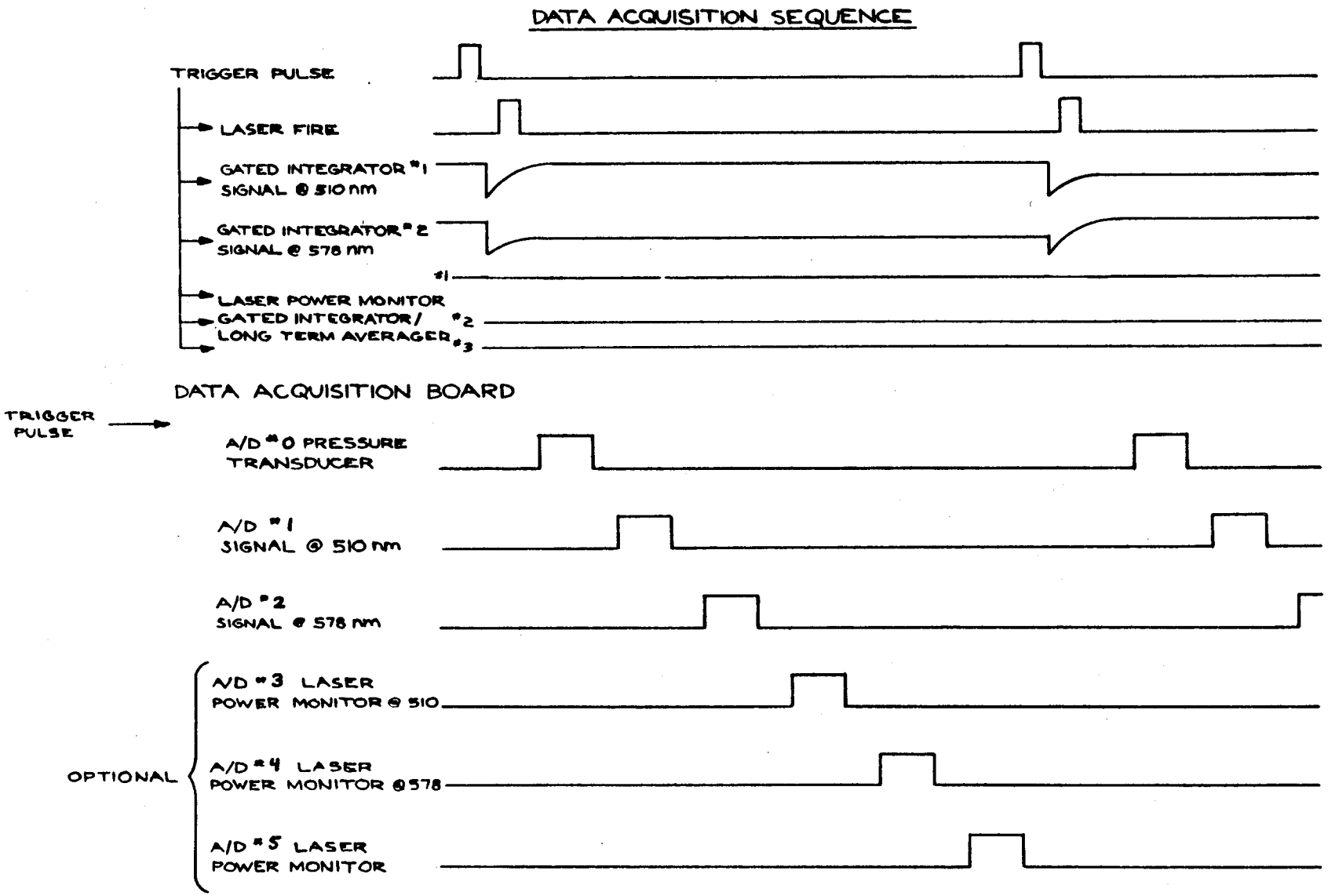

Figure 1.2 Data Acquisition Sequence for Rayleigh Scattering Measurements

by a TTL pulse from the clock to the timing module which then sends out trigger pulses to the laser, the gated integrators, and the A/D board. The adjustable delay on the gated integrators is set so that the gate opens shortly before the laser fires and closes shortly after the ~25 ns laser pulse has ended. The gated integrators then produce output voltages which are proportional to the average signal acquired during the period in which the gate was open. The modes in which the gated integrators are used differ, however, between the Rayleigh scattering signals and power monitor signals. For the Rayleigh scattering signals, the output voltages of the gated integrators remain constant until the next trigger pulse is received, at which time the voltage falls to zero and then rises to reflect the average signal acquired during the new gate period. The voltage can be read on the A/D board any time before the next trigger pulse, and reflects the signal acquired during one gate period. This is contrasted with the gated integrators for the laser power monitor signals which are used in a long term averaging mode (having a time constant of ~0.1 s). The output voltages of the power monitor gated integrator/long term averagers reflect an average of the signals acquired in the gate periods during the previous time constant. Since the pulse-to-pulse power variation of the laser is small, the long term averaging mode of the power monitor gated integrators is acceptable.

The first signal acquired by the A/D board is the output from the pressure transducer. This signal is read first to allow the pressure signal to be acquired as close in time as possible to the Rayleigh scattering signals. Acquisition of this signal first also allows additional time for the gated integrators to produce the proper output voltage. The next two signals acquired by the A/D converter are the Rayleigh scattering signals at 510 nm and 578 nm from the gated integrators. Acquisition of the power monitor signals for each measurement is optional since they reflect an average of the laser power over many pulses. (In particular, the last power monitor signal on A/D channel #5 is intended only as a diagnostic and is not used in the computation of density or temperature. This signal is not normally read for each laser pulse). If the power monitor signals are not read for each measurement, they are read at the start and end of each measurement series. An advantage of reading the power monitor signals only at the start and end of

a measurement series is that the amount of data per measurement is reduced by 40%.

The sequence of steps shown in Figure 1.2 and discussed above, is repeated continuously until one DMA segment in the computer memory is filled. In subsequent sections of this report, this will be referred to as the acquisition of a "frame" of data. After the DMA segment is filled, the data are transferred to the hard disk, and "on-line" data can be computed and displayed, and the power monitor signals can be read. Then the acquisition of frames of data can be repeated until either the desired number of measurements have been taken or until the 20 Mbyte hard disk is full.

An important step in the Rayleigh scattering measurement procedure is the calibration system. The calibration provides the reference from which the absolute values of measured densities and temperatures are determined. The calibration procedure can be simply performed with the calibration cell which is part of the RSD system, or it can possibly be performed in the actual measurement environment. The main requirements for the calibration procedure are that the temperature and pressure of the measurement volume be stable and accurately known. Since the Rayleigh scattering signal is directly proportional to density, the density of the gas in the measurement volume during a measurement is related to the density during the calibration by the ratio of signal intensities.

The initial objectives of the Rayleigh Scattering program were: 1) the measurement of density with a precision error of 1% at elevated pressures (20 atm, or greater) and a measurement rate of 5 kHz; 2) the measurement of average temperature or density with an accuracy error of 2%; 3) no substantial degradation of precision or accuracy with particle concentrations up to 2×10^4 cm^{-3}; and 4) a probe design which is compatible with applications such as gas turbine engines and the SSME. Based on measurements obtained in the calibration cell at 300 K and 1 atm, the precision error which would be obtained at 1200 K, 20 atm and 5 kHz for similar background noise levels is 1.7%. This is lower than the design value for four primary reasons: laser power lower than specifications, poorer than anticipated coupling of the laser power into a fiber, greater than designed reflection from laser focusing

lenses, and a lower collection solid angle than designed. Also based on calibration cell measurements at 300 K and 1 atm, the accuracy error due to surface scattering in average density and temperature measurements at 1200 K and 20 atm is estimated to be 0.5%. This value assumes that the precision with which the surface scattering interference can be subtracted out is limited only by Poisson statistics. For this elevated pressure case, the measurement accuracy will most likely be limited by the accuracy of the electronics. No direct determination of the sensitivity of the Rayleigh scattering measurements to the level of particulate loading was made in the testing of the RSD system. However, based on our best estimates of the measurement volume dimensions and the observed ability of the RSD system to reject signals affected by particulate scattering, it is judged that particulate concentrations up to ~10^4 cm^{-3} will not have a significant effect on the measurement accuracy or precision. The probe developed in this program has not been tested in a gas turbine combustor or similar environment. The probe has, however, been designed to operate in a hot, pressurized, vibrating environment. The probe purge gas system has been designed to keep the optical components clean over a wide range of measurement environment pressures. The water cooling system of the probe has been designed to receive a heat flux as high as 500 W/cm^2 on the first surface. Optical fibers allow the laser, detectors, and electronic components to be located away from the measurement environment, while the optical components in the probe are firmly secured to ensure their proper operation under vibration.

The performance of the RSD system relative to the initial program objectives will be discussed further in this chapter in the component descriptions, and in the discussion of the RSD system tests in Chapter 3.

1.2 Copper Vapor Laser

The RSD system uses a Cooper Lasersonics (Plasma Kinetics Div.) Model 251 copper vapor laser. The nominal power rating of the laser is 20 W. This power rating is for the sum of the power on the 510.6 nm and 578.2 nm lines. The stated pulse rate range of the laser is 4 - 10 kHz, although it is capable of operating as low as 2 kHz and as high as 12 kHz for brief periods. The nominal pulse width of the laser is 25 ns, however this width can be decreased

or increased by changing the operating parameters of the laser. (The pulse width was not deliberately varied in the program). The laser beam diameter is 32 mm.

A feature of the copper vapor laser which is used to great advantage in the RSD system is the two wavelength emission of the laser. The laser emits roughly two thirds of its power at 510 nm and one third of its power at 578 nm. Due to the inverse power dependence on wavelength, the Rayleigh scattering cross section is 65% greater at 510 nm than at 578 nm. By monitoring scattered light intensities of both lines, this wavelength dependence is used to subtract out the interference caused by wall scattered laser light. (This is discussed further in Section 2.6).

The distribution of power between the 510 nm and 578 nm lines of the copper vapor laser is a function of the operating conditions of the laser - primarily the gas temperature in the plasma discharge tube. Therefore, the use of the two wavelength emission of the laser requires a measurement of the power at each wavelength.

The divergence of the beam is not characterized by a single value of the divergence, but by a distribution of divergences. With stable resonator optics, roughly 35% of the laser power is emitted with a divergence less than or equal to 3 mrad, and 70% is emitted with a divergence less than or equal to 6 mrad. These characteristics were determined by measuring the power transmitted through a known size pinhole using a known focal length lens (see section 3.3). The relationship between the divergence of the light transmitted through a pinhole, the lens focal length, and the pinhole diameter is approximately given by,

$$d_{pinhole} = (\text{lens focal length})(\text{transmitted beam divergence}).$$

Since the divergence characteristics of the laser with the stable resonator optics were judged to be unsatisfactory for the RSD system, unstable resonator optics were obtained for the laser. The divergence characteristics of the laser with unstable resonator optics are shown in Figure 1.3. As can be seen

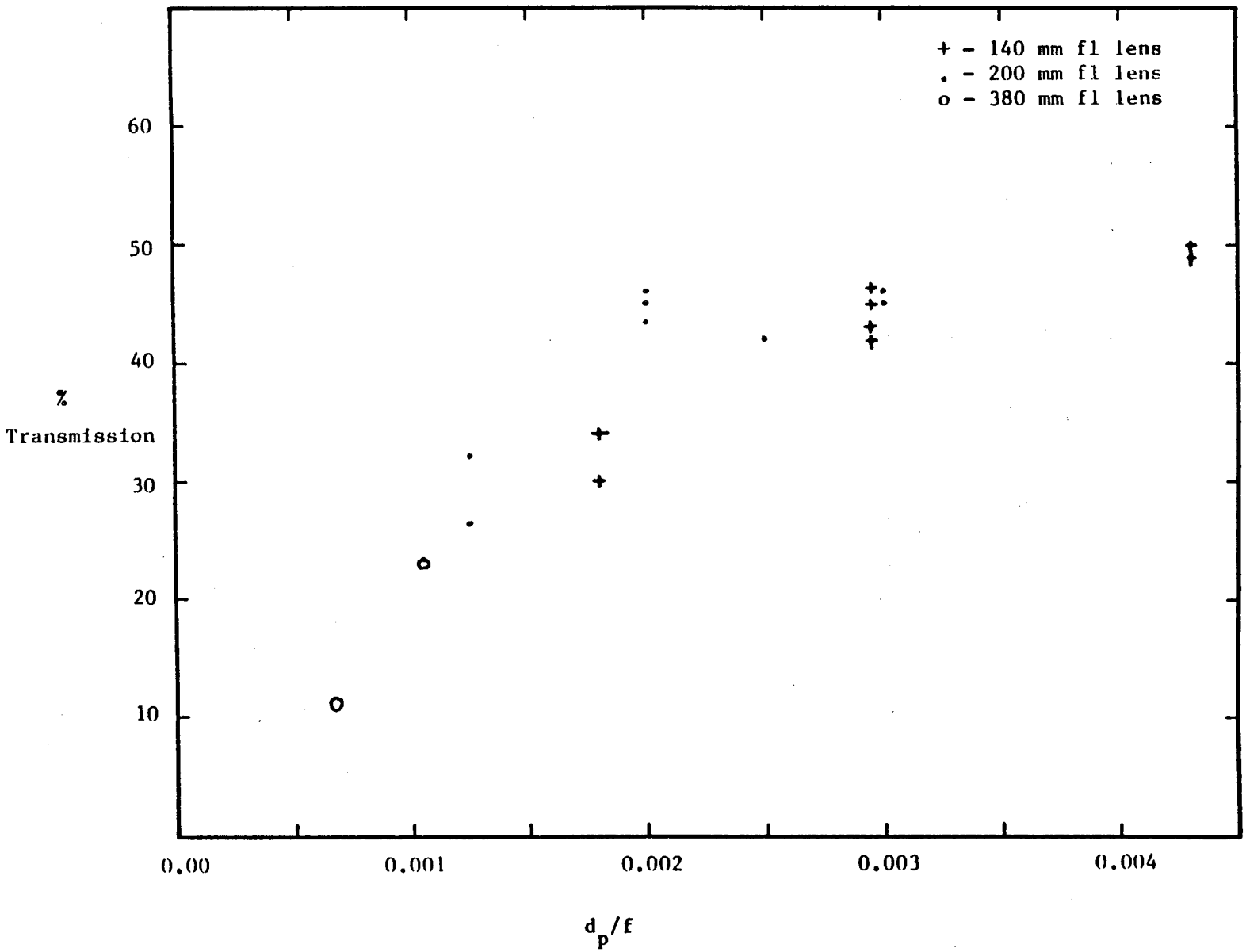

Figure 1.3 Copper Vapor Laser Divergence Measurements

from the above equation, the quantity plotted along the abscissa, d_p/f, is equal to the divergence of the transmitted laser beam. Figure 1.3 shows that the unstable resonator optics increase the fraction of power emitted at low divergences, although still less than 50% of the total laser power is emitted at a divergence less than 3 mrad.

Both the power and pulse rate of the copper vapor laser are variable, although the laser was primarily designed to operate at fixed pulse rate and power settings. The power can be varied to a limited extent by the variac setting on the front panel of the power supply. The power, however, is neither a linear nor monotonic function of this setting. (At the high end, an increase in voltage can result in a decrease in power). The pulse rate of the laser can be varied by varying the frequency of the external trigger source. The capacitor configuration inside the laser head must also be changed, however, to accommodate the change in frequency. Plasma Kinetics specifies a capacitance of 6 nF for pulse rates between 4 - 7 kHz, and 4 nF for 7 - 10 kHz. Plasma Kinetics specifies the shape of the external trigger pulse to be 10 V in amplitude with a rise time of 50 ns and a width of 300 ns (see Section 2.3.2.2 of the laser manual). Our experience indicates that the rise time and pulse width specifications for the external trigger pulse are not critical, and that a square wave input is adequate. In the RSD system, the laser is triggered by a pulse from an optoisolator circuit in the timing module. (The optoisolator electrically separates the laser firing circuit from the timing electronics).

The copper vapor laser can also be run independently from the RSD system by using the internal trigger source in the thyratron driver. This trigger source produces a fixed pulse rate of 6 kHz. The internal trigger source is used by connecting a short BNC cable as a jumper between the "Internal Source" and "External Source" plugs at the back of the laser power supply.

1.3 Optical Fibers

Optical fibers are used in the RSD system to transmit light from the laser to the probe input optics, to transmit light collected by the probe collection optics to the photomultiplier tube detectors, and to collect a

fraction of the laser input light both in the probe and in the laser hood and transmit the light to the photodiode power monitor detectors. With the exception of the power monitor which collects light in the laser hood, all of the fibers are silica core/silica clad with a core diameter of 200 μm and a cladding diameter of 250 μm. These fibers are specified to have an approximate attenuation of 17.5 db/km at 510 nm and 13 db/km at 578 nm. The fibers have cleaved ends, which is the preferred termination method for high power laser applications. Each of the fibers will now be discussed in further detail.

The most critical fiber in the RSD system is the laser input fiber. This is the only fiber in the system which is subject to laser damage, and the only fiber for which the numerical aperture (NA) and core diameter have a significant influence on the RSD system performance. (This latter point is discussed in section 1.7.2 and Appendix A). A special, low NA fiber produced by General Fiber Optics is used for the laser input fiber. This fiber has an NA of 0.13 and is produced specifically for use with high power pulsed lasers. The low NA minimizes the occurrence of self-focusing which can cause laser damage in fibers, but it also results in a "lossy" fiber in which significant transmission losses can occur due to low radius bends in the fiber. Thus, bends in the laser input fiber should be minimized to the greatest extent feasible. The fiber is made with a sheath of thin plastic and is relatively fragile. For this reason, the fiber was inserted into a 3/16" Tygon tube for additional protection. The length of the laser input fiber is nominally 10 m. A second 10 m length of this fiber is delivered with the RSD system as a spare.

A 10 m length of Diaguide ST200D-FV is used as the collection fiber. This fiber has an NA of 0.2. The Diaguide fiber is made with a thick secondary coating of nylon enclosed in a Kevlar reinforced vinyl sheath and is relatively rugged. A Diaguide D95P/250 plug is installed on the detector end of the fiber.

A 13 m length of Diaguide ST200D-FB is used as the probe power monitor fiber. This fiber is located adjacent to the laser input fiber in the probe, collecting light which is scattered off the surfaces of the laser input

optics. The detector end of the fiber is terminated with a Diaguide D95P/250 plug. Both the collection and power monitor fibers from the probe have been inserted in 1/2" Tygon tubing for convenient handling.

A 10 m length of General Fiber Optics #10-500-A plastic fiber is used to monitor the laser power in the laser hood. The fiber has a core diameter of 465 μm, a cladding diameter of 500 μm, and an NA of 0.50. This fiber was selected for the less important hood power monitor application because it is both rugged and inexpensive. The transmission of this fiber over a 10 m length is 53%, which is significantly lower than the other fibers. But due to the high strength of the hood power monitor signal, the increased attenuation is acceptable. The detector end of the fiber is terminated with a Diaguide D95P/500 plug. Due to the plastic cladding, this fiber cannot be cleaved. The best method of terminating the fiber is to cut the fiber with a sharp blade and then grind and polish the face. Acceptable performance can be obtained, however, without grinding and polishing if the cut face is reasonably free of defects.

1.4 Laser/Fiber Coupling System

The laser/fiber coupling system is a critical component of the RSD system, since it strongly influences the amount of laser power available for the Rayleigh scattering measurement and the stability and reliability of this power. A schematic of the laser/fiber coupling system is shown in Figure 1.4. The laser and the coupling system are mounted on a single 9 ft. piece of 10" aluminum channel. This allows the coupling system to be stably mounted and positioned relative to the laser. (It also allows the laser to be moved much more easily). A hood constructed of a PVC plastic frame and 3 mm thick Acrylite FF sheet walls encloses the laser/fiber coupling area. The hood serves two important functions - it protects personnel from direct or scattered laser light, and it allows the coupling area to be kept free from particles by means of a filtered air purge system. The presence of particles increases the probability of the input fiber being damaged by the laser. A 200 mm focal length, 40 mm diameter achromat lens (Melles Griot #01-LA0225) is used to focus the laser beam into the 200 μm core fiber. Before entering the fiber, the light passes through a 600 μm brass pinhole having X-Y-Z

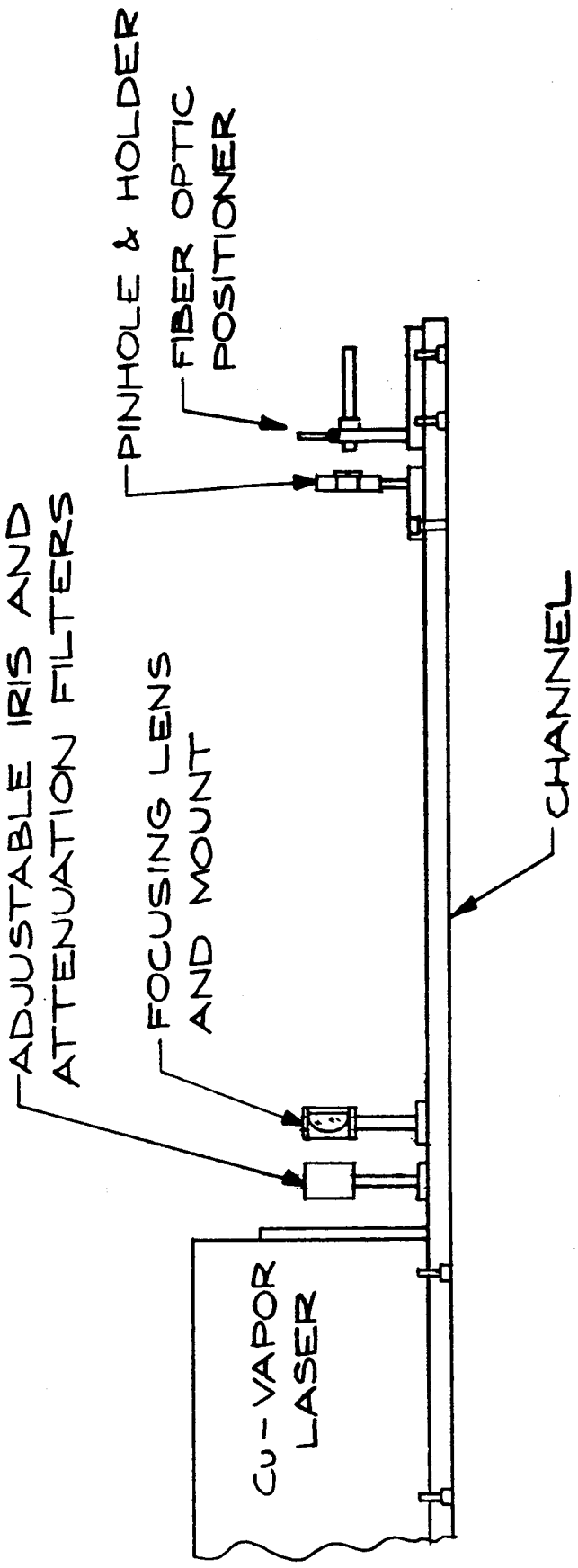

Figure 1.4 Laser/Optical Fiber Coupling Design

positioning adjustment. The pinhole blocks laser light which is emitted with a large divergence (> 3 mrad), which is roughly 60% of the total laser power. The pinhole reduces the heating of the fiber and fiber holder caused by light having too great a divergence to enter the fiber. The laser input fiber is located immediately behind the pinhole, mounted in a modified Diaguide fiber sleeve (Diaguide #SL/200) held in a Melles Griot (#07-HFO-002) fiber holder. The fiber holder is mounted on a translation stage for position adjustment along the optical axis. The fiber holder allows X-Y adjustment of the fiber position. In addition to the above components, an iris diaphragm and filter holder are mounted at the laser outlet port. The iris diaphragm and/or filters or screens can be used to attenuate the laser beam for initial alignment or for visual alignment of the probe.

The hood power monitor fiber is mounted on the pinhole holder and collects light scattered from the laser focusing lens. This fiber thus monitors the laser power before entering the input fiber, i.e., the total laser output.

The hood purge system consists of a small air pump (Air Cadet model 7530-40) with a flow rate of 0.9 CFM and a HEPA filter (Gelman #12144). A 3/8" tygon tube connects the filter outlet to the laser hood.

1.5 Detectors

Two detector assemblies are used in the RSD system. Photomultiplier tube detectors are used for the Rayleigh scattering signal, while photodiode detectors are used for the power monitor signals. The photomultiplier tubes are Hamamatsu side-on type R-1477 having a red-enhanced photocathode sensitivity. The nominal quantum efficiencies for the tube are 17% at 510 nm and 14% at 578 nm. The tubes are housed in Pacific (model #3150RF) RF-shielded tube housings. The dynode chain structure for the tube monitoring the 510 nm Rayleigh scattering signal was modified (by removing two dynodes) to provide better linearity characteristics over a wide range of gas densities. The wiring diagram for the modified dynode chain is given in Figure 1.5. With this dynode chain, the gain of the 510 nm tube at 800 V is

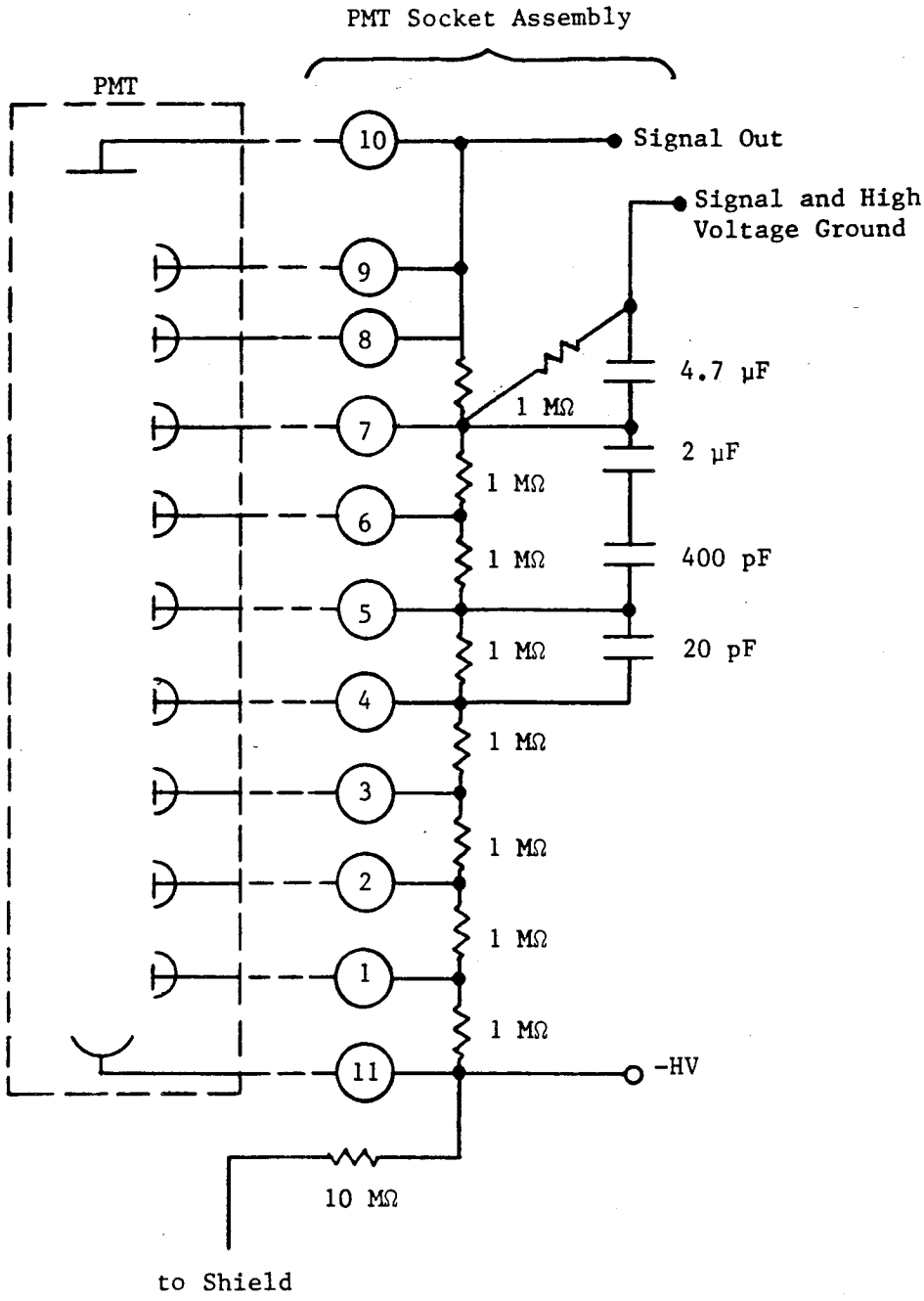

Figure 1.5 Seven Stage Dynode Chain Design

1.7×10^5 and at 1000 V is 5.5×10^5. These gains are calculated from the relation

$$\text{Gain} = \delta^n$$

and $$\delta = C_1 V^{C_2}$$

where δ = gain per dynode

n = number of dynode stages

V = dynode voltage = $V_{total}/n+1$ where V_{total} is the total PMT voltage

C_1 = tube constant (~0.177 for R1477 tubes)

C_2 = dynode voltage exponent (~0.75 for R1477 tubes)

While the dynode chain for the 578 nm tube could have been modified in the same manner, the lower signal intensity for the 578 nm line did not require the modification and the original dynode design was left unchanged. The wiring diagram for the 578 nm tube is shown in Figure 1.6. It should be noted that Hamamatsu's specification for the maximum photocathode voltage for the R1477 tubes is 125 V per stage and the design operating voltage is 100 V per stage. Thus, the maximum and design voltages for the 510 nm tube are 800 V and 1000 V, and for the 578 nm tube are 1000 V and 1250 V. An EG&G Model 556 dual output high voltage power supply is used in the RSD system. Since the outputs are not independently adjustable, the maximum setting on the supply should be 1000 V as determined by the constraint on the 510 nm tube.

The physical and optical arrangement of the photomultiplier tube detectors is shown in Figure 1.7. The detectors are enclosed in a light tight aluminum box of dimensions 24" x 23" x 11" high. The optical fibers, high voltage coaxial cables, and BNC cables enter the box through sealed apertures. The Rayleigh scattered light delivered by the collection fiber is collimated by a Melles Griot achromat lens (Melles Griot #01 LAO 001, 10 mm fl, 6 mm dia.) and split by a dichroic filter into beams containing the 510 nm and 578 nm lines. The dichroic filter is a Corion cyan subtractive filter (Corion #CS-600-S). At a 35° angle of incidence, the filter transmits 94% of the 510 nm light and reflects 99% of the 578 nm light. The vertically mounted

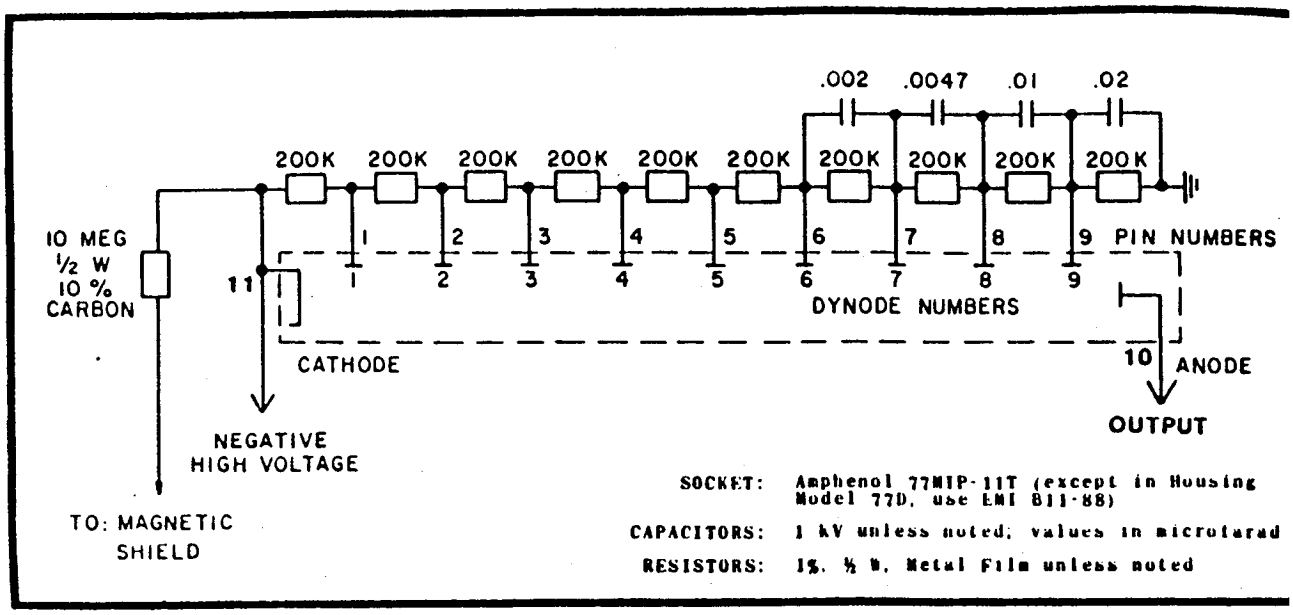

Figure 1.6 Nine Stage Dynode Chain Design

tube housings are oriented normal to the paths of the separated 510 nm and 578 nm beams, as indicated in Figure 1.7.

Photodiode detectors were selected for the power monitor signals because the intensity of the signals is too large to be adequately handled by photomultiplier tubes. Hamamatsu PIN type photovoltaic silicon detectors (model S1723-06) were selected on the basis of their fast response (15 ns rise time at 30 V reverse bias), good sensitivity (~0.3 A/W), and good linearity characteristics provided by the large detector area (100 mm^2). The photodiodes are operated with a reverse bias provided by a 45 V battery. A schematic of the photodiode housing and electrical connections is given in Figure 1.8. The optical layout of the photodiode power monitor detectors is shown in Figure 1.9. The power monitor fiber from the probe is connected to a Diaguide D-95HL collimator which produces a probe power monitor beam which is approximately 8 mm in diameter. The collimated beam is split into the 510 nm and 578 nm lines by a Corion CS-600-S dichroic filter used at a 35° angle of incidence. The photodiode detectors are oriented normal to the two beams.

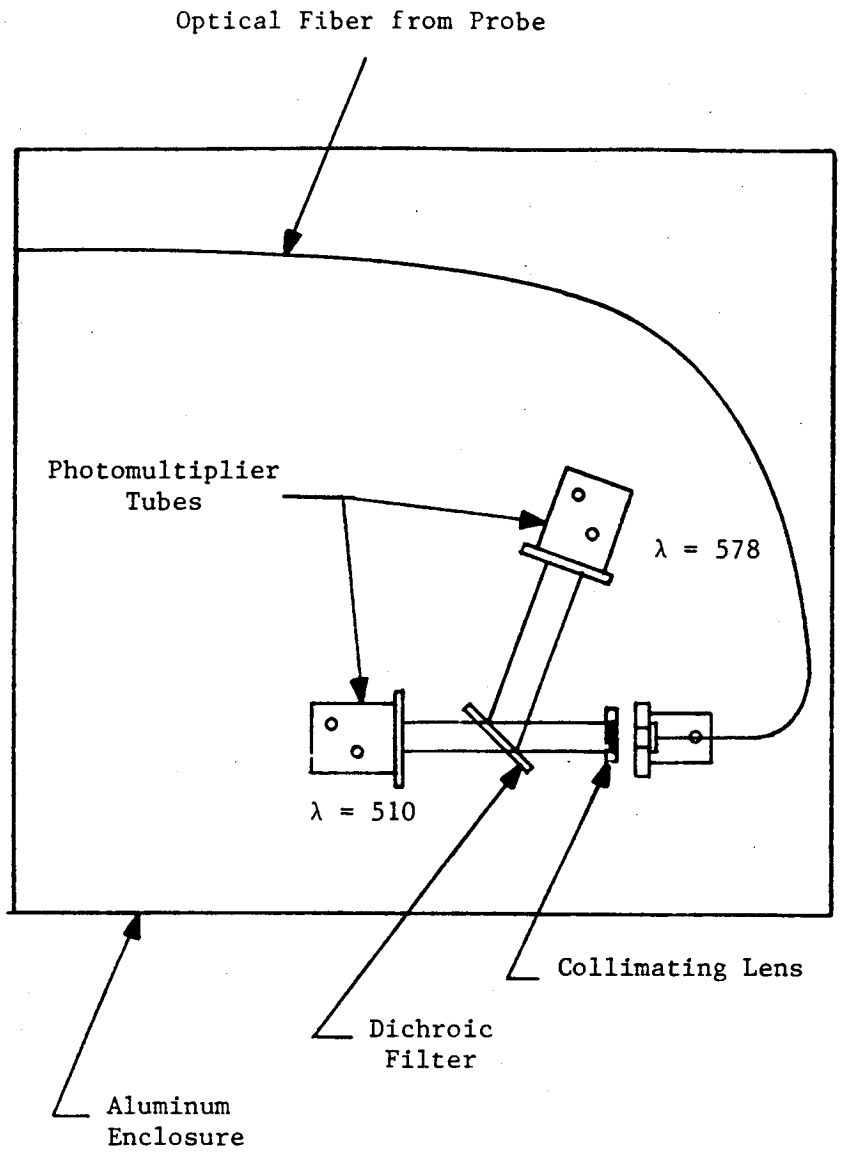

Figure 1.7 Photomultiplier Tube Detector Arrangement

The hood power monitor fiber, on the other hand, is connected to a Diaguide D-95R receptacle. The hood power monitor signal is not collimated or separated into its 510 nm and 578 nm components, but is measured directly by the third photodiode. The hood power monitor is used only as a diagnostic to give the total power emitted by the laser. It is not used in the computation of density and temperature.

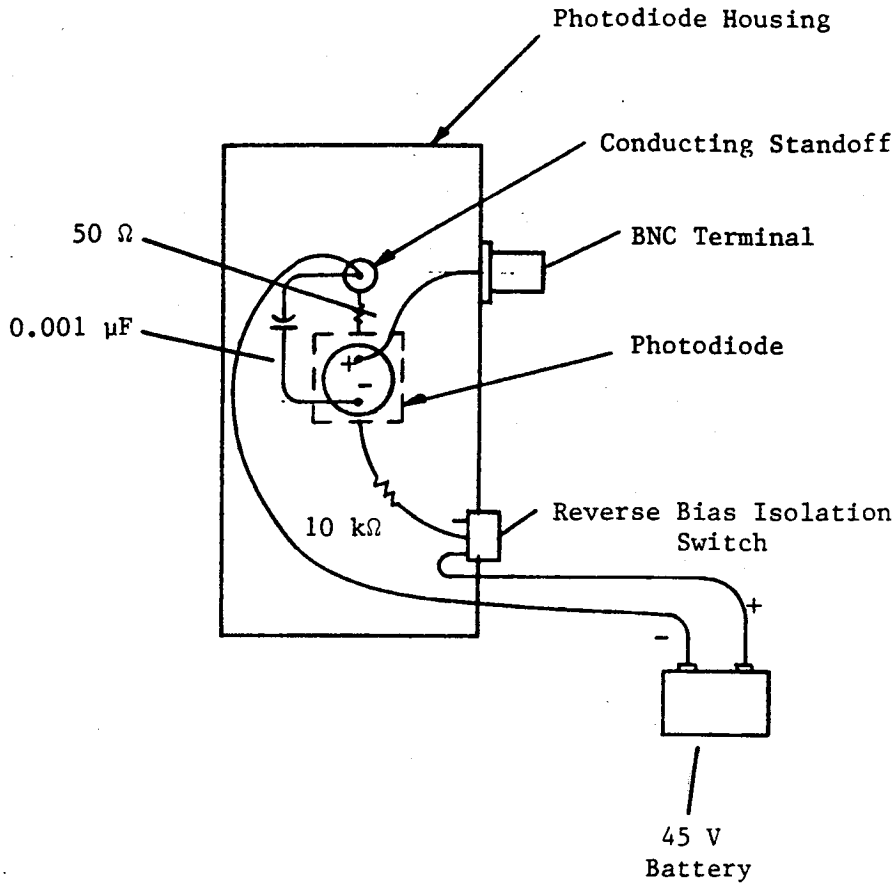

Figure 1.8a Photodiode Electrical Connections

⑧ Ultra-high speed light detection for PIN photocell

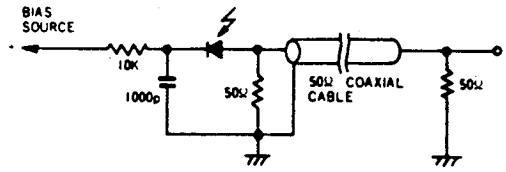

1000p: Disk ceramic capacitor 1000 pF
(Leads of the PIN photocell, ceramic capacitor and 50Ω resistor should be as short as possible.)

Figure 1.8b Photodiode Electrical Schematic

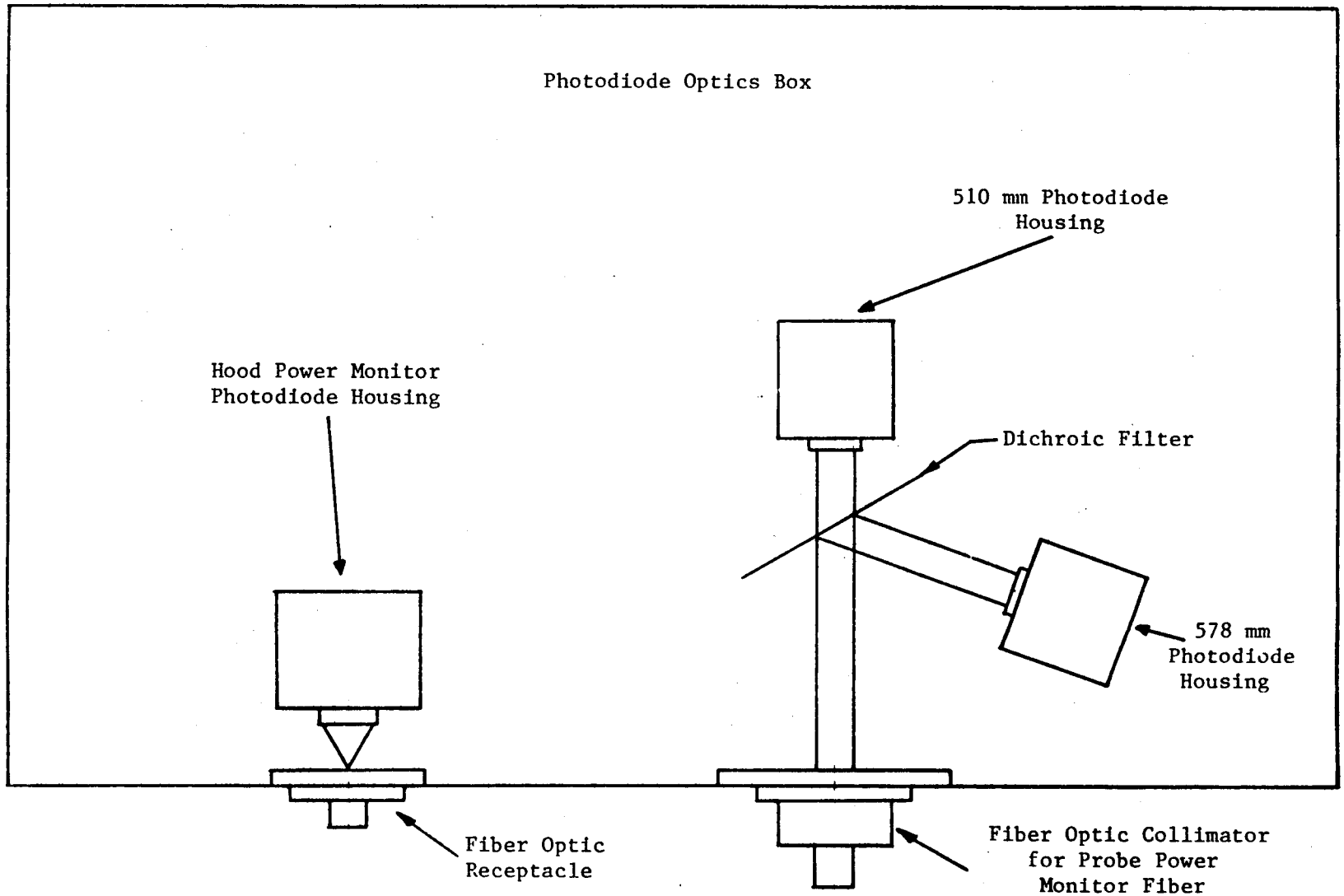

Figure 1.9 Photodiode Optical Design

1.6 Data Acquisition Electronics

The data acquisition electronics in the RSD system include the computer, clock, timing module, A/D board, and gated integrators for the Rayleigh scattering and power monitor signals. A brief overview of the interrelationship between these components was given earlier in a discussion of the data acquisition procedure in section 1.1. Since the design and operation of the timing module were determined by the characteristics of the A/D board and gated integrators, these latter components will be described first.

The two Rayleigh scattering signal gated integrators are Stanford Research Systems (SRS) Model 250 Gated Integrator and Boxcar Averager modules which are designed to be used with a NIM rack and power supply. The main features and characteristics of the SRS gated integrators are: an adjustable gate width of 2 ns to 15 μs; a gate view accuracy of 1 ns; an adjustable gate delay of 25 ns to 10 ms; a gate delay jitter of 50 ps or 0.01% of full scale; a maximum repetition rate of 20 kHz; a sensitivity range of (volts input/volts output) 1V/1V to 5 mV/1V, i.e. a gain range of 1 to 200; a maximum residual of 5% of previous output. In the RSD system, the SRS gated integrators are used primarily as single measurement integrators; the boxcar averager feature is normally not utilized. In this mode, the gated integrators acquire the signal during the "gate open" period and produce an output voltage which is proportional to the average voltage level during the gate width. The output voltage level is maintained until the next trigger signal is received from the timing module, at which time the output is cleared and the new signal acquired after the preset delay period has passed. The specification that a maximum residual of 5% of the previous output is present in the new signal refers to the ability of the gated integrator to clear the output buffer. No tests were performed in the program to determine the actual value of the residual for typical RSD operating conditions.

The NIM rack obtained for the SRS gated integrators is an EG&G model 4001C having 12 available slots. The NIM power supply is an EG&G Model 4002A. The SRS gated integrators each occupy two slots, and the high voltage power

supply for the photomultiplier tubes also occupies two slots. The remaining six slots are occupied by the timing module and the A/D connection box.

The three power monitor signal gated integrators are Evans Electronics Model 4130A gated integrator modules. The gate pulse for the modules is provided by an Evans Electronics Module 4141 programmable time delay board. These gated integrators are used in the boxcar integrator configuration with an effective time constant of 0.3 s at a measurement rate of 6 kHz. The effective time constant is given by the relation

$$\tau_{eff} = \frac{RC}{n\ \Delta t}$$

where RC = 10^{-4} s for the gated integrators, Δt is the gate width (~60 ns), and n is the measurement rate. The Model 4141 time delay board was modified by changing resistor R12 from 402 Ω to 600 Ω to allow the required delay time of 2.6 μs to be obtained. The design and operating notes for the Evans Electronics boards are included in Appendix B of this report.

The A/D board used in the RSD system is a MetraByte Dash-16 module. The characteristics of the module are: 12 bit resolution; selectable gains of 0.5, 1, 2, 5, or 10; 2 D/A output channels; 3 channel programmable interval timer; a 50 kHz throughput rate using DMA transfer; and 16 single-ended or 8 differential analog input channels. The module is used in the differential analog input configuration in the RSD system. It shall be noted that the selected gain value applies to all channels, and cannot be individually set for each channel. The A/D board occupies a full slot in the computer and is connected to the A/D connector module by a ribbon cable.

The operation of the A/D board under DMA in the RSD system is controlled partially by software commands and partially by input signals. The number and identity of the A/D channels to be scanned are set by software commands in the data acquisition program. The data acquisition rate and timing are determined by trigger pulses to the A/D board. Contrary to Metrabyte literature, the scan of a set of channels in DMA operation cannot be performed by issuing a single trigger pulse to initiate the scan. It was found that for reliable

operation, a trigger pulse was required for each channel in the scan. Thus, for an RSD system measurement rate of 6 kHz and the acquisition of three channels per measurement, the trigger rate to the A/D board would be 18 kHz. This characteristic of the A/D board had a major impact on the design of the timing module, as will be discussed shortly.

To allow for convenient electrical connections between the A/D board and external signals and electronics, an A/D connector module was constructed. The module allows BNC connectors to be used for all A/D board inputs and outputs. The module requires the analog inputs to be differential inputs. The module electrically isolates the eight analog input channels. The A/D connector module is housed in the NIM rack in a triple width blank NIM box.

The timing module coordinates and synchronizes the data acquisition and measurement processes in the RSD system. The functions of the timing module are to: issue trigger pulses to fire the laser, issue trigger pulses for the SRS gated integrators to acquire the Rayleigh scattering signals, issue trigger pulses to the Evans Electronics time delay module to acquire the power monitor signals, and issue trigger signals to the A/D board to acquire inputs from the desired channels. As mentioned earlier in the description of the laser, an optoisolator circuit in the timing module produces a trigger pulse for the laser while remaining electrically isolated from the laser. The power for the optoisolator circuit is provided by three 9 V batteries connected in parallel. The timing module contains a voltage meter to display the battery voltage on the front panel and an ON/OFF switch to disconnect the batteries from the optoisolator circuit.

The timing module contains three divider circuits to accomplish the synchronization of the components of the RSD system. The divider circuits divide the input trigger frequency from the clock to the desired frequencies for triggering the laser and the gated integrators. A diagram for the divider circuits is shown in Figure 1.10. The divider chip D1 in the middle of the diagram produces the trigger frequency for the laser, which is generally the input frequency divided by the number of A/D channels per scan. For example, for a measurement rate of 6 kHz and 3 channels per scan, the input frequency is set at 18 kHz and the divider chip D1 is set to divide by 3 to yield an

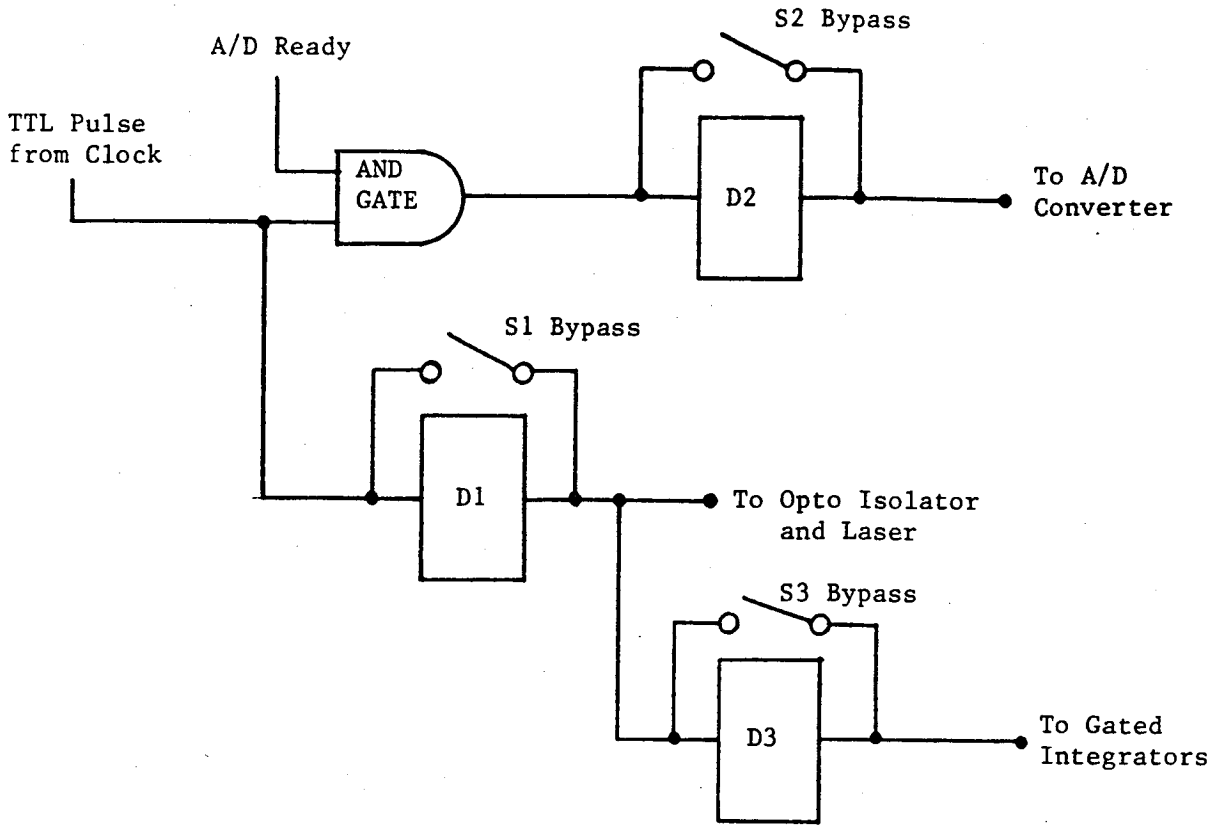

Figure 1.10 Divider Circuit Diagram for Timing Module

output frequency to the laser and gated integrators of 6 kHz. The other two divider chips are bypassed in this case by setting the S2 and S3 bypass switches.

The D2 and D3 divider chips are used if the desired measurement rate is lower than the 4 kHz operating limit of the laser. If measurements are desired at a 3 kHz rate, acquiring three A/D channels per measurement and running the laser at 6 kHz, then divider D1 is set to divide by three, the clock is set to a frequency of 3 x 6 kHz = 18 kHz, the gated integrator divider D3 is set to divide by 2, and the A/D converter is set to divide by 2. Thus, the trigger rates for the laser, A/D converter, and gated integrators are respectively 6 kHz, 9 kHz, and 3 kHz.

The clock in the RSD system is a B&K Model 3011 function generator. This unit has a digital readout to monitor the output pulse frequency. The TTL output mode is used for the measurements.

An ATT PC 6300 computer is used in the RSD system. The computer uses the 8086 processor with an 8 MHz clock speed. The computer has 640 Kbytes of memory, 20 Mbyte Tandon hard disk, and a 360 Kbyte floppy disk. Five expansion slots remain available with the A/D board installed. The original Western Digital hard disk controller was replaced with a Data Technology controller because the Western Digital controller interfered with the DMA function of the A/D board. The Data Technology controller is, however, roughly two times slower than the original controller.

1.7 Rayleigh Scattering Probe

This discussion of the Rayleigh scattering probe is separated into three sections: the probe mechanical design (including the probe body, water cooling, purge gas, and pressure transducer port details), the probe optical design including the lens holders, and the optical fiber mounting and adjustment design. Further details of selected aspects of the probe design are given in the appendices.

1.7.1 Probe Mechanical Design

1.7.1.1 Probe Construction

Two design approaches were considered for the probe. The first was a solid body construction in which the probe is formed from a single piece of material, with the necessary ports and flow passages being drilled out from the body. The second was an approach in which the probe is formed by soldering or brazing together tubes and plates to provide the needed ports and flow passages. The first design approach was selected over the second because of the simpler and more reliable manufacturing process associated with the solid body design.

The second design would consist of several pieces (front plate, probe tube body, rear plate, lens tubes, pressure measurement tube, etc.) which required brazing or soldering. One concern regarding the process of brazing or soldering is the possibility of the precise alignment of the pieces shifting due to thermal expansion during the process. A second concern regarding this design is the difficulty of machining the holes and counterbores in the front plate since the material would be soft OFHC copper. (This material is required to prevent the release of oxygen during the brazing process which would result in a joint of inferior integrity). A third concern regarding this design is the difficulty of securing the lens assemblies in the lens tubes in a manner which would permit their easy removal for cleaning, realignment, or replacement.

The solid body probe design offered a solution to all three concerns with the second design. The solid body design does not require brazing or soldering of parts which have tight alignment tolerances. Close tolerances are required in the diameter and location of the optical port holes, but these were reliably obtained. Since brazing is not required, free-machining copper was used as the solid body material. (Soft solder was adequate for all applications which required joining or sealing). Thus, the solid body design offered a more reliable method of construction. The solid body design also allowed an easy means of securing the lens assemblies in the lens ports. Set screws were inserted from the side of the probe body to lock the lens retainer rings in place. The set screws can be sealed, if necessary, with Locktite or epoxy. The solid body design offered the additional advantage that separate outer lens tubes were not required, since the lens ports functioned as outer lens tubes. This allowed the optics to have a slightly larger diameter than in the second design.

A side view of the Rayleigh scattering probe is shown in Figure 1.11. The probe consists of two pieces, the probe main body and the probe back plate. The main body consists of a 2.54 cm (1.00") diameter front section which is 10.16 cm (4.00") long and a back flange which is 7.62 cm (3.00") in diameter and 1.905 cm (0.75") thick. The front section of the probe contains ports for the two optical trains and the pressure transducer. The front section also contains water coolant passages. The back flange of the probe

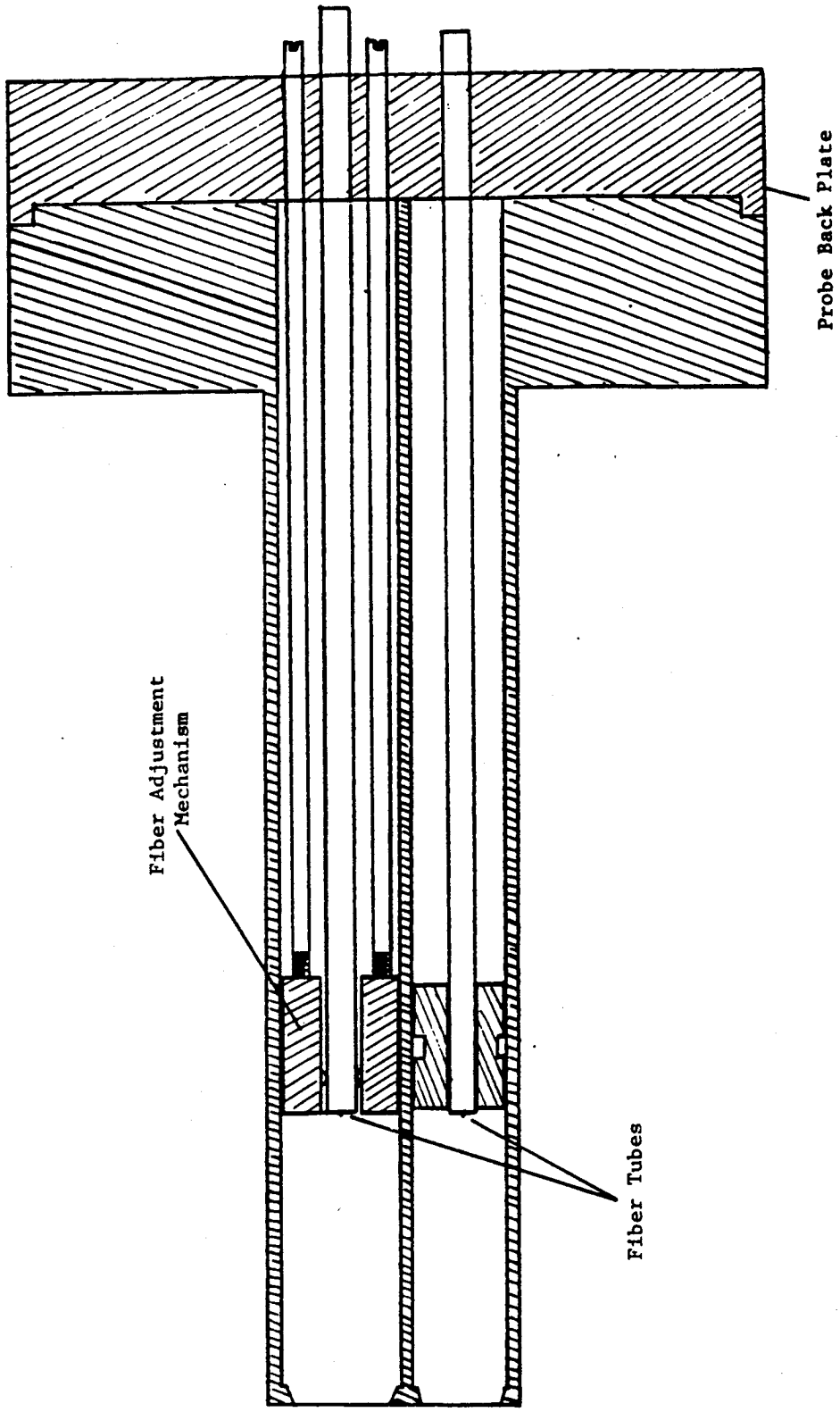

Figure 1.11 Rayleigh Scattering Probe - Side View

main body contains connections for the cooling water inlet and discharge lines and the purge gas lines. The probe back plate provides a seal for the fiber tubes (2), fiber adjustment rods (3), and the pressure transducer, all of which pass through the back plate. The back plate also provides a pressure seal for the purge gas.

The use of a back flange in the probe design, as stated above, serves two main purposes. The flange gives ample room for making cooling water and purge gas connections on its outer radius. This allows standard, inexpensive threaded fittings to be used. It also clears up the area at the back of the main probe body, allowing more room for accommodating the fiber adjustment mechanism and the fiber tubes. The second purpose of the back flange is to allow a simple pressure seal to be obtained in elevated pressure applications. In this case the back flange can be joined to a mating flange on the pressurized device, using an O-ring to provide a pressure seal. This arrangement is employed in using the probe with the calibration cell at elevated pressures. Use of the back flange as a pressure seal may not be optimal in actual elevated pressure test applications since it does not easily allow for translation or rotation of the probe for the purpose of moving the measurement location; it does, however, allow initial use of the probe at elevated pressures.

1.7.1.2 Probe Water Cooling Design

The water cooling design for the solid body probe consists of two pairs of water inlet/outlet passages which extend from the main body back flange to the front of the probe, and two passages which pass across the front of the probe 2.5 mm below the surface. Figure 1.12 illustrates the detail on the front face of the probe. The two passages which pass across the front of the probe are obtained by drilling in from the side of the probe and soldering plugs in place to seal off the holes.

Heat transfer and pressure drop calculations were performed for the water cooling design to determine the pressure level and water flow rate required for the maximum expected heat flux. A peak heat flux of 500 W/cm^2 was used in the calculations. For the purposes of the calculations, the probe front face

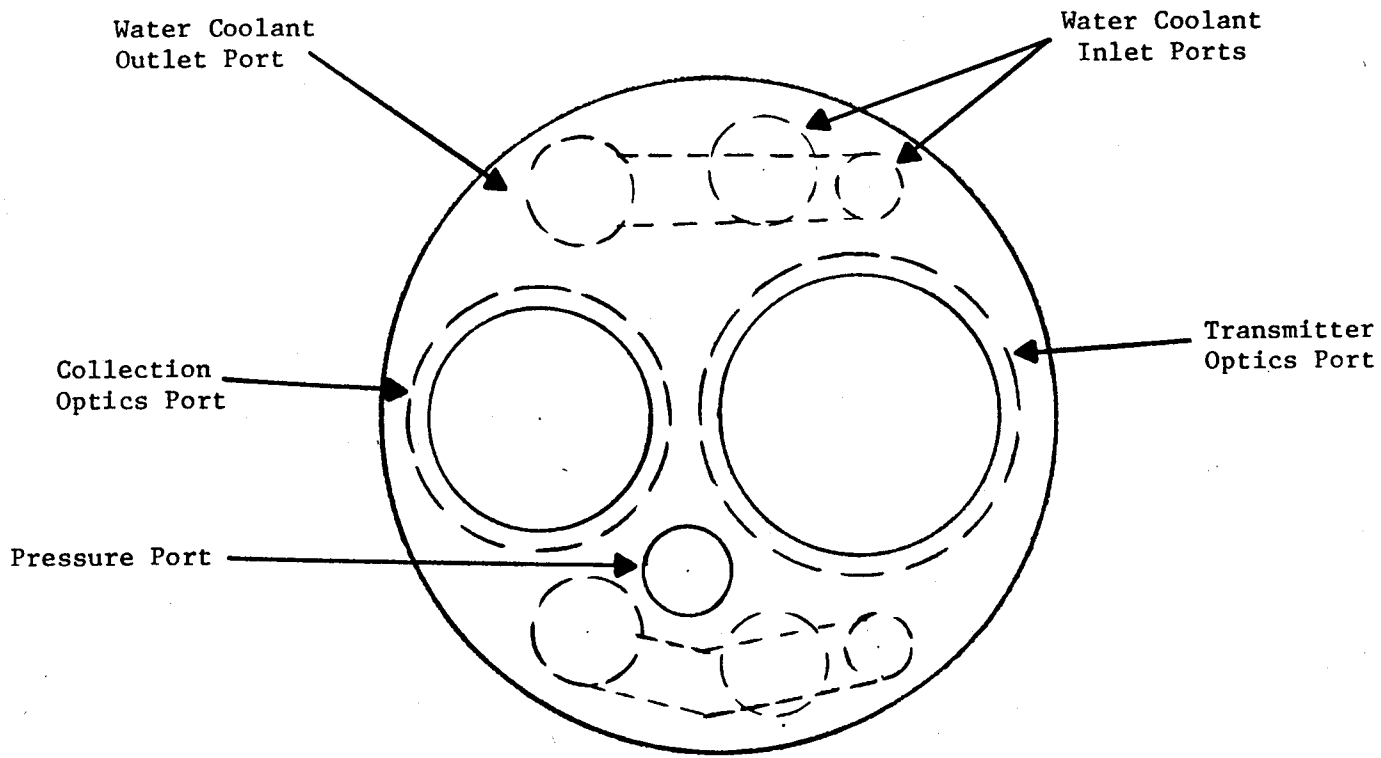

Figure 1.12 Rayleigh Scattering Probe - Front View

was divided into two segments (upper and lower), one on each side of the optics ports. For the side without the pressure port, the surface area receiving convective heat transfer is 1.49 cm^2, giving a total heat flux load of 745 W. The water passage length is 1.46 cm and the passage diameter is 0.257 cm. As an approximation, half of the water passage surface area was assumed to be effective for heat transfer, giving an effective water cooled surface area of 0.5 (3.14) (0.257 cm) (1.46 cm) = 0.589 cm^2. For a maximum design water coolant temperature of 75 °C and an inlet temperature of 15 °C, a design water coolant temperature rise of 60 °C is used. This requires a design heat transfer coefficient of $h_c = Q/(A\ T) = 750\ W/(0.589\ cm^2\ 60\ K) = 21\ W/cm^2\ K$. The water flow rate needed to obtain this value of h_c can be determined from the correlation for turbulent flow in smooth tubes

$$Nu = 0.0155\ Pr^{0.5}\ Re^{0.83} \qquad (1<Pr<20)$$

where $$Nu = \frac{h_c\ D}{k}$$

$$Re = \frac{V\ D}{\nu}$$

Pr = Prandtl Number (= 8.03 at 60 °F)

D = tube diameter (= 0.00257 m)

k = thermal conductivity (= 0.59 W/m K at 60 °F)

V = velocity

ν = kinematic viscosity (= $1.13 \times 10^{-6}\ m^2/S$ at 60 °F)

From the above equations, the required Nusselt number is Nu = 920 and the required flow velocity is 70 m/s. This yields a water flow rate of 5.75 gpm per water passage.

The pressure drop for the water coolant flow in the probe can be calculated from the flow velocity and the friction factor. A correlation for the friction factor for turbulent flow is

$$f = 0.046\ Re^{-0.2}$$

The pressure drop is then given by the expression

$$\Delta P = 0.5\ \rho V^2\ f\ (4\ L/D)$$

where ρ = density

L = water passage length

If the water inlet and outlet passages have a diameter of 0.257 cm (the same as the diameter of the passages across the front face) and the total passage length is 25 cm, a pressure drop of 4000 kPa (580 psi) is obtained. This is a very high pressure drop and would require the use of a booster pump to provide the necessary pressure level. The pressure drop in the water coolant passages can be reduced considerably if a larger diameter hole were used for the inlet and outlet passages. For an inlet and outlet passage each 12 cm in length and 0.40 cm in diameter and a 1.46 cm crossover passage of 0.257 cm diameter, the total pressure drop is reduced to 690 kPa (100 psi).

The final inlet and outlet water coolant passages in the solid body probe have a somewhat different configuration due to the space limitations of the probe. The outlet passages, which are adjacent to the smaller lens port in Figure 1.12, have a diameter of 0.40 cm (0.160"). Two passages, however, are used for each of the input lines. A passage diameter of 0.257 cm (0.101") is located as close as possible to the top of the probe while leaving a clearance of 1 mm from both the outer perimeter of the probe and the bore of the larger lens port. This passage connects with the crossover passage which cools the front face of the probe. In addition to the 0.257 cm passage, a passage of 0.40 cm diameter carries coolant to within 1 cm of the probe front face where it is then connected with the 0.257 cm passage. (This connection is not shown in Figure 1.12). The reason a single 0.40 cm passage was not used for the

inlet was that it would need to be located approximately 0.4 cm further from the top of the probe than the 0.257 cm passage. Since the region at the top of the probe (between the probe outer diameter and the larger lens port) is already further from a water coolant passage than any other region of the probe, the 0.257 cm passage was used to avoid further exacerbation of the problem. Such space constraints are not as critical for the outlet passages since they are adjacent to the smaller lens port.

1.7.1.3 Purge Gas Design

The purge gas flow serves three purposes in the probe design. The first purpose is to keep the optical elements free from soot or contamination; the second purpose is to minimize the pressure differential across the optical elements; and the third purpose is to provide cooling for the probe around the periphery of the optical elements.

The purge gas enters the probe through two inlet connections located on the back flange of the main probe body. The gas flows into the laser input optics and collection optics ports and down the length of the optics ports. At the lens assemblies, the gas flows through channels formed by slots machined in the outer periphery of the lens tube. The collection optics lens tube has eight uniformly spaced channels and the laser input option lens tube has twelve uniformly spaced channels. The design of the purge gas flow path at the point of injection into the measurement environment is based on the experience of Morey in designing a probe for combustion viewing. (W. W. Morey, "Hot Section Viewing System", UTRC, NASA CR-174773, 1984). After flowing through the slots machined in the outer periphery of the lens tube, the purge gas is deflected roughly 90° by the lip on the probe front end plate as it enters the measurement environment. Morey found that a sharp angle deflection of the purge gas across the optical element was effective in minimizing deposition on the element.

A consideration which may be important for stable optical alignment of the probe in a combustion environment, is that of matching the refractive index of the purge gas to that of the combustion gas. A perfectly matched refractive index will produce no change in the light path and no reflectance

at the purge gas-combustion gas interface. While a perfect match cannot be obtained, since it is dependent on the temperature and composition of the combustion gases which vary with time, a good match can be produced using estimated average values of the combustion gas temperature and composition. For a typical combustion gas composition at 1800 K, purge gas at 300 K consisting of 90% He and 10% N_2 will match the refractive index. If a 20% error in the ratio of combustion gas to purge gas temperatures were made, the reflectance at the interface between the two streams would be 1×10^{-7} at 30 atm. This is over two orders of magnitude less than the reflectance of 1.4×10^{-5} which would occur if pure N_2 were used as the purge gas. The effect on beamsteering at the interface is similar.

The pressure differential between the measurement environment and the interior of the lens tubes is determined by the purge gas flow rate for a fixed flow passage design. The purge gas flow areas of 1.2 mm^2 and 1.8 mm^2 (8 and 12 slots, 0.2 mm x 0.75 mm) for the collection and input lens tubes respectively give purge gas flow rates which are similar to those used by Morey. The pressure differential is composed of contributions from flow contraction losses at the entrance to the lens retainer ring passages, friction losses within the passages, and a flow acceleration pressure drop which is not recovered at the purge gas outlet. Table 1.1 summarizes these pressure drop contributions for a range of mass flow rates at 30 atm and 1 atm. A mixture of 90% He and 10% N_2 is used in the calculations. For a flow rate at 30 atm of 7 kg/hr (the flow rate used by Morey) per lens tube, a pressure differential of approximately 5% is obtained.

For the same relative pressure differentials at different measurement environment pressures, the flow rate needs to be adjusted. Thus, an active means of controlling the flow rate is needed if the relative pressure differential across the optical components were to remain constant for an application such as a gas turbine engine. A computer controlled flow metering valve, which adjusts the flow based on the pressure level sensed by the pressure transducer in the probe would fill this need, although a system which maintains a constant pressure differential between the purge gas and the measurement environment for a varying measurement environment would also

satisfy this need. This system, which does not require electronic controllers, is discussed further in Appendix C.

TABLE 1.1

Summary of Pressure Drop Calculations

Mass Flow Rate, kg/hr	Total Pressure, atm	$\frac{\Delta P}{P}$ Contraction	$\frac{\Delta P}{P}$ Friction	$\frac{\Delta P}{P}$ Flow Acceleration	$\frac{\Delta P}{P}$ Total
6.70	30	0.010	0.015	0.018	0.043
9.00	30	0.018	0.025	0.032	0.078
11.20	30	0.029	0.037	0.050	0.116
13.40	30	0.041	0.050	0.070	0.162
0.22	1	0.010	0.035	0.018	0.063
0.30	1	0.018	0.058	0.032	0.108
0.37	1	0.029	0.086	0.050	0.165
0.45	1	0.041	0.118	0.070	0.229

The purge gas flow also plays an important function in cooling the probe front flange in the vicinity of the edge of the probe. Water cooling is least effective in this region due to the long conduction paths to the coolant passages, as discussed earlier. For a purge gas flow rate of 11 kg/hr, the convective heat transfer coefficient in the flow passage along the lens retainer ring is 2.9 W/cm^2 K (for a 90% He, 10% H_2 mixture). If a 6 mm^2 area located in the narrow region of the front end plate between the large lens tube and the edge of the probe is considered, a heat flux of (0.06 cm^2) (500 W/cm^2) = 30 W would be received by this area. The effective flow passage area for heat transfer is approximately (1.25 + 0.2 + 0.2 mm) (10 mm) = 16.5 mm^2, for a purge gas passage 1 cm in length. This assumes that heat transfer efficiently occurs through three sides of the flow passage, since the side facing the lens will not be very effective in removing heat from the probe front end plate. For one flow passage to remove all of the heat input to the 6 mm^2 area, a temperature differential between the purge gas and the flow passage walls of (30 W)/(0.165 cm^2) (2.9 W/cm^2 K) = 63 K would be required. For an effective conduction heat transfer path length between the probe front

face and the purge gas passage walls of 0.5 cm, an additional temperature differential of roughly 30 W/[(3.68 W/cmK) (0.06 cm^2)/(0.5 cm)] = 68 K would exist. Thus, the front face of the copper will be roughly 130 K higher than the purge gas temperature if heat transfer to the purge gas were the only heat removal mechanism. This is comparable to the peak temperatures calculated for the probe of Morey, and is well within the constraints of the material.

1.7.1.4 Lens Stress and Temperature Calculations

The optical components in the Rayleigh scattering probe will be subjected to bending stresses due to pressure differentials and elevated temperatures due to radiative heating when the probe is used in a high temperature, high pressure environment. Calculations were performed for the lens stress and radiative heating effects to roughly assess their severity. These calculations, which are given in Appendix D, assumed the use of fused silica optics, which were anticipated to be used in the final probe design. However, only BK-7 optics were able to be obtained in this effort, so all of the quantitative results in Appendix D are not applicable to the current optics.

The use of BK-7 does not have a significant effect on the ability of the lenses to withstand the maximum anticipated pressure differential of 50 psi. The tensile strength of BK-7 is approximately 4000 psi, which is still much larger than the conservative estimate of the maximum stress of 1500 psi.

The use of BK-7, however, does adversely affect the lens heating problem. BK-7 does not transmit as far in the infrared spectral region as fused silica or sapphire. It is strongly recommended that optics made of IR grade fused silica or sapphire be used if the probe is to be used in an environment having a high temperature blackbody background.

1.7.1.5 Probe Pressure Measurement

The pressure transducer configuration in the Rayleigh scattering probe was designed to allow a high frequency response while not subjecting the transducer to a severe operating environment. The transducer selected for the probe is a modified version of the Kulite XT-140 series silicon diaphragm

transducer. The transducer barrel has been extended to a length of 11.9 cm (4.7 in) so that the front of the transducer is located 1 cm from the front face of the probe in the pressure port, as shown in Figure 1.13. Purge gas from the laser input optics port flows through a small channel in the probe back flange to the pressure port and then flows down the small annular passage between the port wall and the transducer. The purge gas prevents the transducer from being exposed to combustion products, and in the case where a 90% He/10% N_2 purge gas mixture is used, increases the frequency response of the pressure measurement.

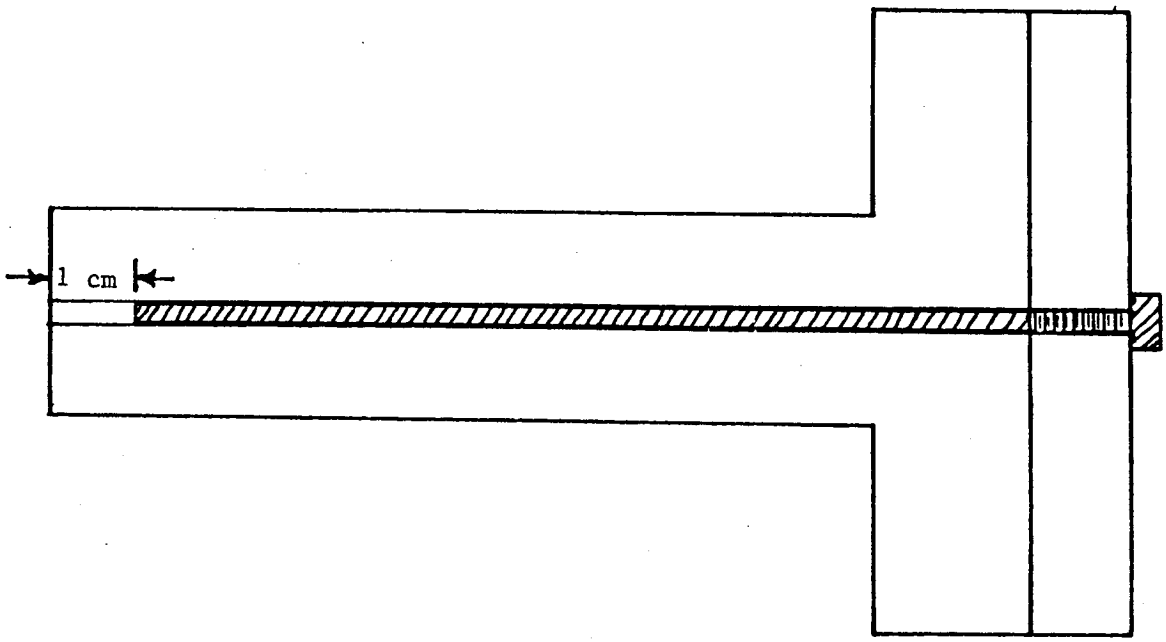

Figure 1.13 Pressure Transducer Mounting Design

The transducer is designed for the measurement of differential pressures. The transducer is rated for a full scale differential of 25 psig, and for a maximum differential of 50 psig. A small tube allows the transducer to be supplied with a reference pressure for the differential measurement. This feature allows the differential pressure measurement to be used in conjunction

with a purge gas control system of the type described in Appendix C. In this case, the reference tube would be connected to a damped source of either the measurement environment pressure or the purge gas pressure. While the reference pressures would also need to be measured, this can be easily and accurately done since it will be a slowly varying signal. The advantage of using the probe pressure transducer in this manner is that the transducer can be used over a large range of measurement environment pressures and operate at maximum sensitivity at all times.

An analysis of the frequency response of the pressure measurement is given in Appendix E. For a purge gas of 90% He/10% N_2, the resonant frequency of the transducer port is 20 kHz. A 5% deviation from unity gain is experienced at a frequency of 4.4 kHz.

1.7.2 Probe Optical Design

Three critical considerations played a major role in the optical design of the Rayleigh scattering probe. The three considerations are: 1) the need to minimize the diameter of the probe; 2) the need to minimize the size of the measurement volume so as to reduce the adverse effect of particles in the measurement environment; and 3) the need to minimize the collection of laser light scattered off of surfaces. To a significant extent, these three considerations are related and competing. The third consideration requires that separate optics be used for focusing the laser light and collecting the Rayleigh scattered light. Any common optical element would result in the collection of surface scattered light far in excess of the Rayleigh scattering signal. Colinear optics would, however, allow the probe diameter to be minimized. Thus, the third consideration competes against the first. The third consideration also competes against the second, since for a fixed diameter probe, colinear optics would allow the measurement volume size to be minimized. For the same reason, the first and second considerations are competing - since the size of the measurement volume can be reduced by using larger optics, resulting in a larger probe diameter.

The Rayleigh scattering probe optical design reflects an attempt to achieve the best compromise among the three considerations. A probe diameter

of 2.54 cm (1.00") was selected as a difficult but feasible design specification. Separate optical trains were used - a necessary (though not sufficient) requirement for limiting the interference from surface scattering to acceptable levels. Multiple element optical systems were used both for the laser input and collection optics to reduce spherical abberations and minimize the measurement volume size. These multiple element systems can be seen in Figure 1.14 which illustrates the optical design of the probe. An optical standoff distance, defined as the distance between the measurement volume location and the front end of the probe, of 2.5 cm (1.00") was selected. This value represented a compromise between the additional flexibility and usefulness which would be obtained with an increased standoff distance, and the increased interference due to particle scattering which would also occur as the measurement volume size increased with standoff distance.

The discussion of the probe optical design will now continue by first considering the design of the input and collection optics, followed by a brief discussion of the mounting hardware for the optics.

1.7.2.1 Probe Optical Components

The greatest number of compromises in the optical design of the probe concerned the design of the laser input optics. In general, these compromises directly affected the performance of the probe and measurement system as a whole. While the detailed design of the collection optics was actually more complicated due to the need to turn the rays of collected light, the laser input optical design was the more critical of the two.

The probe specifications are summarized in Table 1.2, with the parameters in the table referring to Figure 1.15. Further discussion of the design now follows.

1.7.2.1.1 Laser Input (Transmitter) Optics

A complete discussion of the tradeoffs involved in the laser input optical design is given in Appendix A. In the present discussion, only limited mention will be made of the details of these tradeoffs. The diameter

of the input optical components was selected primarily on the basis of the requirements imposed by a standard fiber numerical aperture of 0.20 and a unity conjugate ratio of the optics. (The value of 0.20 for the fiber NA was the lowest available for standard fibers. Lower NA fibers could be obtained, but generally only on a special basis and at a greatly increased cost). For a 2.5 cm nominal standoff distance, a spot diameter of 10 mm on the input optics is obtained. The input optical components were designed to have a diameter of 11.6 mm (0.457"). A 200 μm core diameter optical fiber was selected as the laser input fiber. This selection was based on tests with short (3 - 4m) lengths of fiber in which 200 μm fibers transmitted nearly all of the low divergence power of the copper vapor laser with only occasional occurrences of

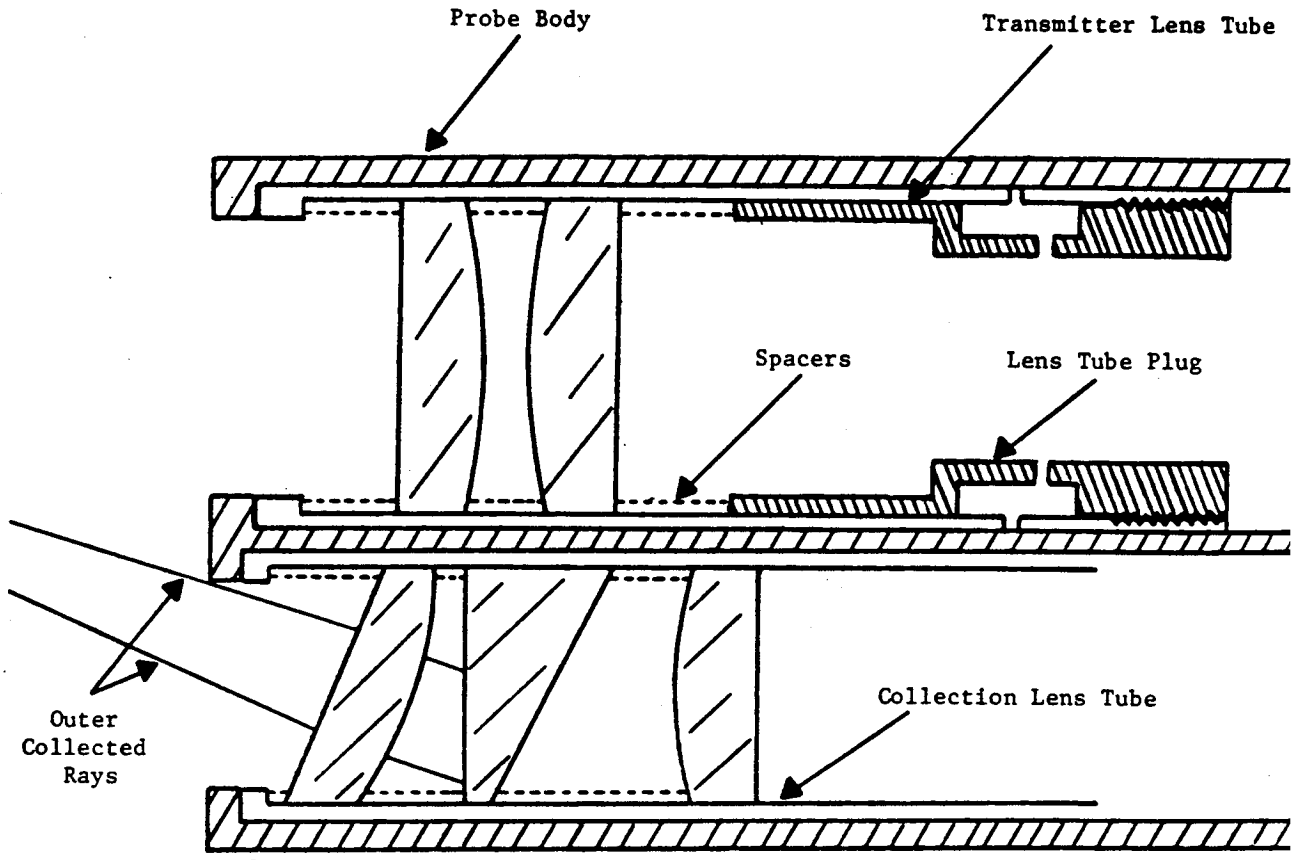

Figure 1.14 Probe Optical Design

TABLE 1.2

Probe Optical Design Parameters

(Refer to Figure 1.15)

Collection Optics		Laser Input (Transmission) Optics	
D_{LENS}	8.84 mm	D_{LENS}	11.61 mm
Clear Aperture	7.82 mm	Clear Aperture	10.57 mm
D_{FIB} (core)	0.20 mm	D_{FIB} (core)	0.20 mm
Lens 1:		**Lens 1 and 2:**	
Back Focal Length	32.80 mm	Back Focal Length	32.80 mm
Index of Refraction	1.523	Index of Refraction	1.523
Radius of Curvature	18.20 mm	Radius of Curvature	18.20 mm
Center Thickness	3.10 mm	Center Thickness	3.10 mm
Edge Thickness t_{L_1}	2.55 mm	Edge Thickness t_L	2.15 mm
L_1	32.30 mm	L_1	30.80 mm
d_1	6.731	d_L	2.79 mm
		Distance to Probe Face	6.604 mm
Wedge:		X_{FOC}	32.298 mm
θ_W	23°58'21"	Standoff Distance	26.202 mm
n_W	1.8632	Spot Size	0.428 mm
t_W	1.016 mm		
d_2	3.581		
Lens 2:			
Back Focal Length	32.80 mm		
Index of Refraction	1.523		
Radius of Curvature	18.20 mm		
θ_L	21°35'15"		
t_{L_2}	2.921 mm		
Distance to Probe Face	2.540 mm		
X_{FOC}	32.80 mm		
Standoff Distance	26.202 mm (1.032")		
Spot Size (x-axis Projection)	0.63 mm		

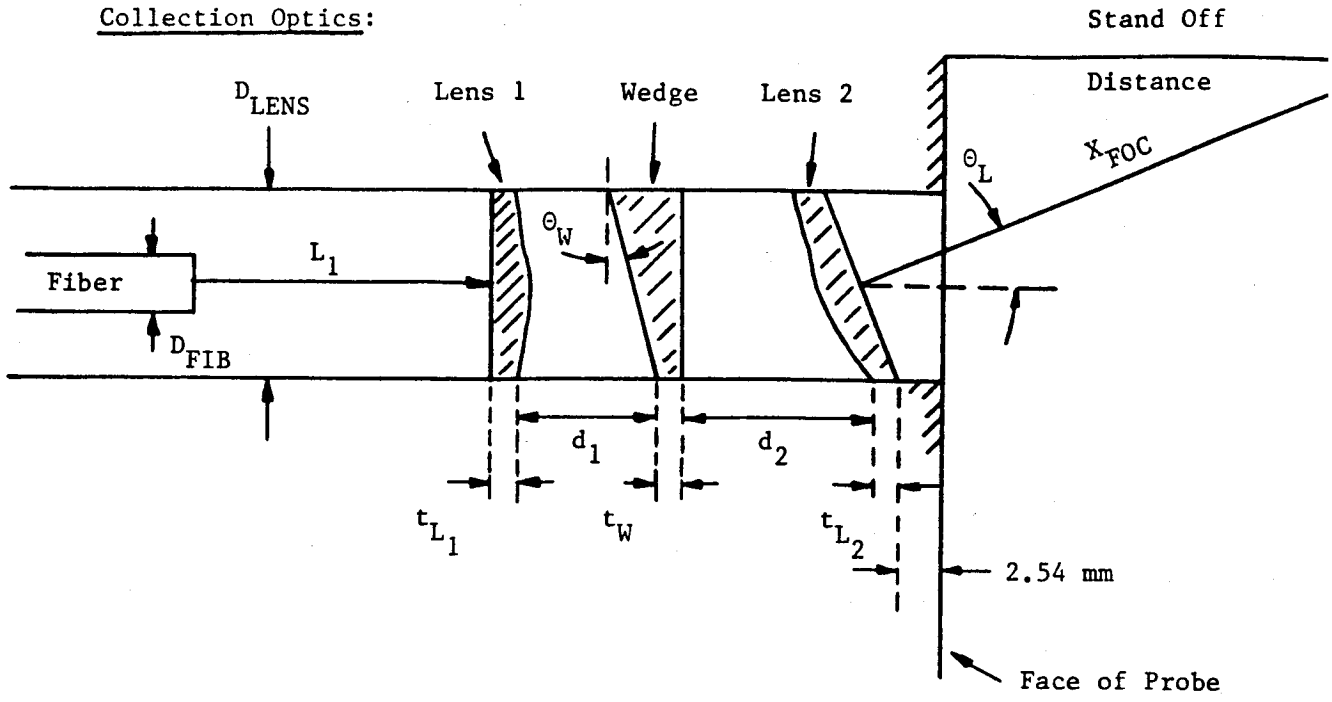

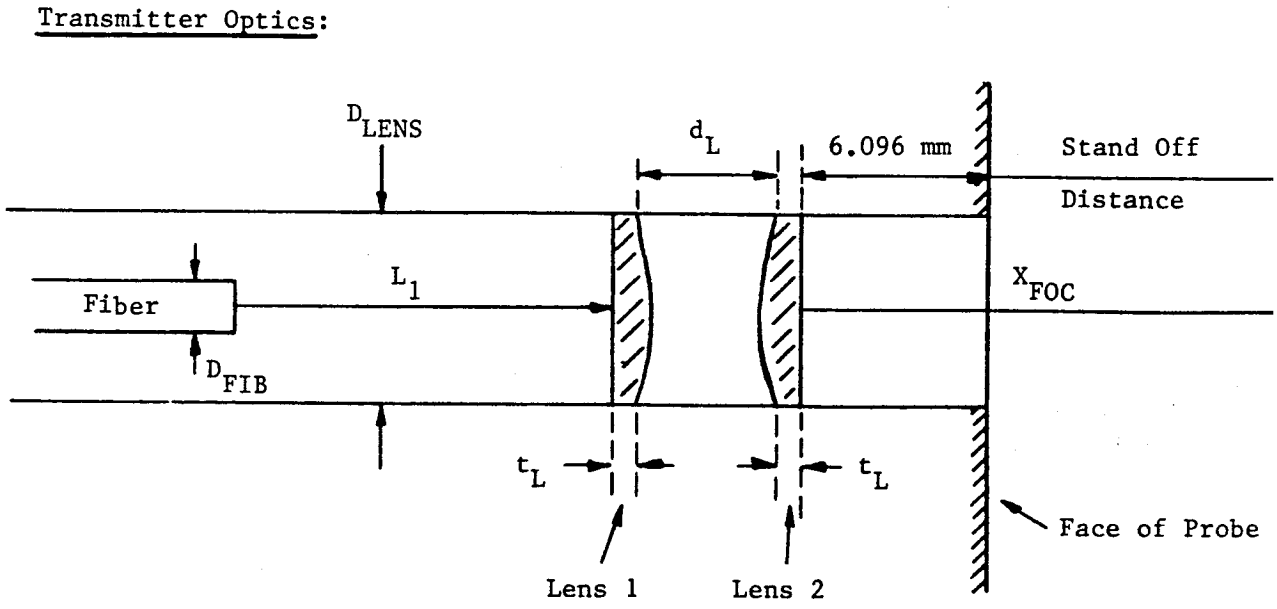

Figure 1.15 Probe Optical Specifications (Refer to Table 1.2)

substantial laser damage. Thus, in the interest of minimizing the measurement volume diameter, the 200 μm diameter fiber was used instead of larger fibers.

The laser input fiber, as mentioned previously in section 1.3, is General Fiber Optics fiber (obtained through a special, one-time purchase) designed for high power lasers and has an NA of 0.13. The NA of this fiber is lower than the value assumed in the design of the input lenses, and therefore the laser spot diameter on the input lenses is less than the lens clear aperture. This allows a future modification to be made to take advantage of the lower fiber NA. This modification will be discussed shortly.

The laser input optics consist of two plano-convex, BK-7 lenses having a back focal length of 32.8 mm and a nominal focal length of 35 mm (Ealing #30-6878). The diameter of the lenses, originally 15 mm, was ground down to 11.61 mm. The edge and center thicknesses are respectively 3.1 mm and 2.15 mm. The edge spacing between the lenses is 2.79 mm (0.110"). The lenses are coated with an MgF_2 antireflection coating optimized for a wavelength of 550 nm. The use of two plano-convex lenses instead of a single biconvex lens was chosen because the plano-convex pair had much lower spherical abberations. A discussion of the ray tracing analysis for the input optics appears in Appendix F.

The major disadvantage of this design is that it theoretically produces a six-fold increase in the amount of stray laser light which enters the measurement environment. This would not be a problem if the lenses had an effective antireflection coating; however, the MgF_2 coating presently on the lenses did not appear to reduce the stray light level significantly below the level produced by uncoated lenses.

1.7.2.1.2 Collection (Receiver) Optics

The collection optics consist of two plano-convex lenses and a wedge. The wedge turns the light scattered from the measurement volume, which is in line with the axis of the laser input optics, into the optical axis of the collection optics and fiber. The limited diameter of the probe did not allow the optical axis of the collection optics to be directly in line with the

measurement volume, thus requiring the use of a wedge. While the wedge complicates the optical design, it gives the probe greater flexibility in that the standoff distance of the measurement volume can be changed by using different optical components - a new probe body is not required. The use of two plano-convex lenses in the collection optical system instead of a single biconvex lens was selected to minimize spherical aberrations. (A ray tracing analysis of the collection system is presented in Appendix F). The use of two plano-convex lenses is even more important for the collection optics than for the laser input optics, since the wedge will introduce even further aberrations if the light entering it is not collimated. To provide collimated light for the wedge, the collection lens nearest the measurement volume must be canted, as shown in Figure 1.14, so that a normal through its center passes through the measurement volume.

The lenses in the collection optical system are plano-convex, BK-7 lenses having a back focal length of 32.8 mm and a nominal focal length of 35 mm, i.e. the same as the input lenses (Ealing #30-6878). The lens closest to the fiber was ground to a diameter of 8.84 mm (0.348") and had center and edge thicknesses of 3.1 mm and 2.56 mm, respectively. The canted lens was ground so that the edge formed an angle of 0.3768 rad (21°35'15") with the plane face. The wedge was constructed of Schott LaSF9 glass. It was ground to a diameter of 8.84 mm (0.348") and a wedge angle of 0.4184 rad (23°58'21"). Its maximum edge thickness is 4.95 mm (0.195") and its minimum edge thickness is 1.016 mm (0.040"). An average value of the refractive index of LaSF9 over the 510 nm and 578 nm copper vapor laser wavelengths is 1.8632.

The collection optics were coated with an MgF_2 antireflection coating to minimize the collection of stray light. In the course of assembling and deassembling the collection optics, the wedge and canted lenses were chipped along the narrowest edges. To prevent these chips from reflecting stray light into the collection fiber, the chips were coated with black paint. While this significantly reduced the amount of surface scattered light collected by the optics, it also somewhat reduced the amount of Rayleigh scattered light which was collected.

1.7.2.2 Probe Optical Component Mounting Arrangement

The basic scheme for mounting the laser input (transmitter) and collection optics is indicated in Figure 1.14.

Separate lens tubes hold the laser input lenses and the collection lenses and wedge. The optical components are positioned within each lens tube by spacers and held in place by lens tube plugs. (The collection lens tube plug is not shown in Figure 1.14, since the arrangement is identical to the laser input assembly). The laser input assembly is axisymmetric and therefore does not have a required rotational orientation. The collection assembly, however, has both a required orientation of the canted lens and wedge with respect to each other and a required rotational orientation of the assembly with respect to the probe. The primary requirement for the positioning of the collection optics is that the image of the collection fiber at the measurement volume coincides with the image of the laser input fiber at the measurement volume. Since the position of the laser input fiber can be adjusted to a small degree, the orientation of the collection optics assembly need not be perfect for the images of the two fibers to coincide. However, the resolution of the images is not optimum unless the orientation is exact. Scribe marks have been placed on the spacers, wedge, and the canted lens to assist in properly orientating these components with respect to each other. Two small notches have been placed at the end of the collection lens tube to allow a special, dual pin tool to be used in rotating the lens tube to achieve proper alignment with respect to the probe body and the laser input optics.

The optical mounting hardware serves one additional purpose - that of providing flow passages for the purge gas, as mentioned previously in section 1.7.1. The sectional view of the lens tube plug in Figure 1.14 indicates that a plenum for the purge gas is formed between the plug and the lens tube with inlets provided by four 1.5 mm (0.060") diameter holes in the lens tube plug. Outlet holes from the plenum are located in the lens tube, eight in the collection lens tube and twelve in the laser input lens tube. The holes, 0.75 mm (0.030") in diameter, are located at the end of the slots which have been machined lengthwise into the outer periphery of the lens tube. The purge gas enters the slots through the holes in the lens tube, flows down the length

of the lens tube, and exits at the end of the probe through passages located between the lens tube and probe body. The purge gas arrangement is the same for both the laser input and collection lens tubes, with the exception that the former has twelve flow passages while the latter has eight.

1.7.2.3 Probe Fiber Optics

The laser input, power monitor, and collection optical fibers are contained in stainless steel "fiber tubes" in the probe. The fiber tubes serve to protect the fibers, permit a pressure seal to be made at the back of the probe, and allow the position of the laser input fiber to be both adjusted and firmly secured. The fiber tubes are made of stainless steel, have an outer diameter of 3.0 mm (0.120"), wall thickness of 0.33 mm (0.013"), and are nominally 15 cm (6") long. The laser input and power monitor fibers are contained in one fiber tube, while the collection optical fiber is contained in the other fiber tube. Ferrules, such as shown in Figure 1.16, are used to position the optical fibers at the ends of the tubes. The front ferrule for the laser input fiber tube has a center hole for the laser input fiber and an off-center hole for the power monitor fiber. The ends of the fibers are positioned in the front ferrules to be slightly recessed from the end of the ferrule so that the ferrule sides offer some physical protection for the fibers. The fibers are sealed in place in both the front and back ferrules with a cyanoacrylate glue. This glue provides a pressure seal at low pressures (~2 atm), but was not tested at higher pressures.

The ends of the fiber tubes are secured inside the probe body by fiber tube plugs. The plug for the collection optics centers the collection fiber tube and does not allow any adjustment of its position, except in the axial direction. The plug for the laser input fiber tube, on the other hand, functions as the body of the fiber position adjustment mechanism. This mechanism is shown in Figure 1.17. The mechanism allows a maximum position adjustment of 0.5 mm from its center position, or 1.0 mm total adjustment. Since the laser input optics have a unity conjugate ratio, this corresponds to a maximum adjustment of the focused laser beam location of 1 mm. The fiber tube position is adjusted by means of three threaded stainless steel rods. The rods have a conical tip and a slot in the back end which extends out the

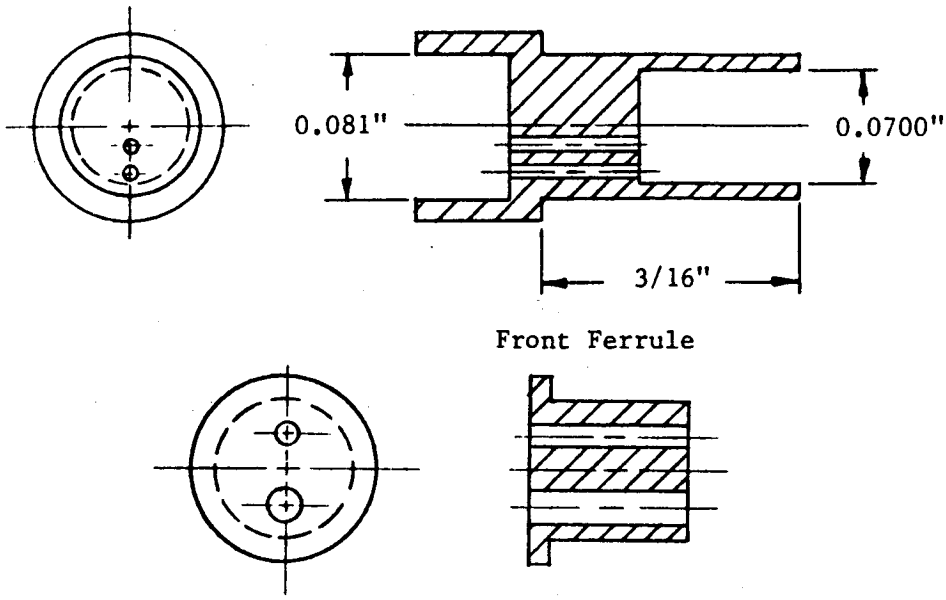

Front Ferrule

Back Ferrule

Figure 1.16a Ferrules Laser Input for Laser Input Fiber Tube

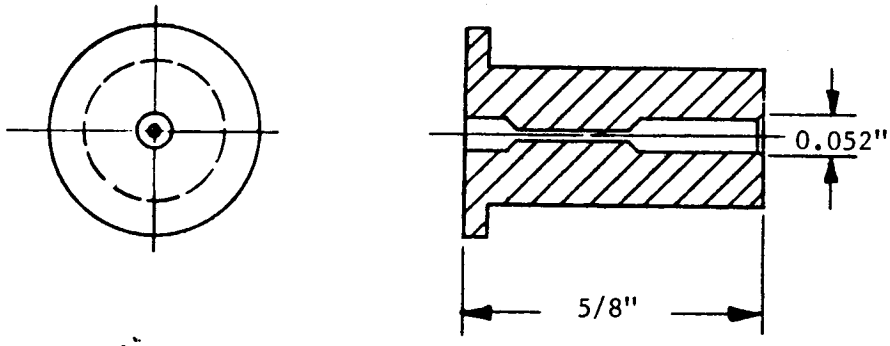

Front Ferrule

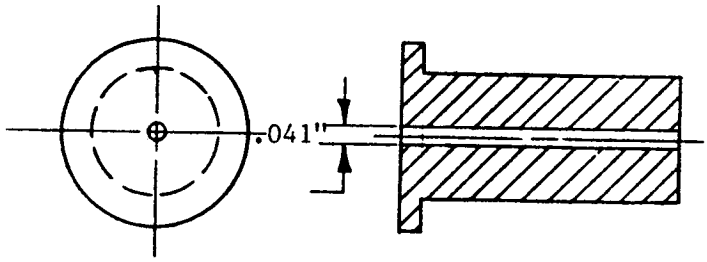

Back Ferrule

Figure 1.16b Ferrules for Collection Fiber Tube

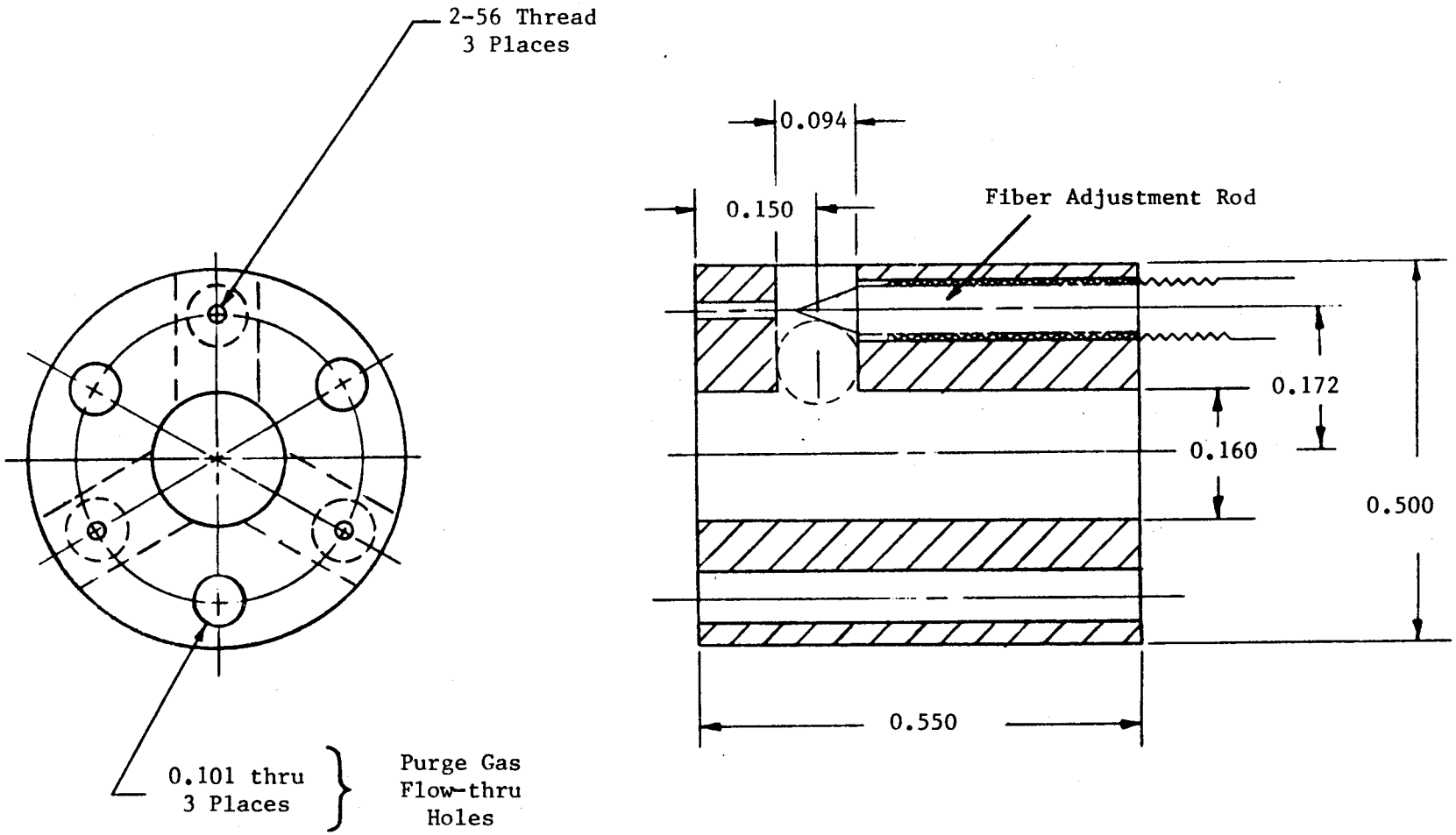

Figure 1.17 Fiber Adjustment Mechanism

back of the probe. Turning an adjustment rod advances or retracts the conical tip which is in contact with a stainless steel ball. The other end of the stainless steel ball is in contact with the fiber tube. By properly adjusting the three rods, the balls can securely position the fiber tube anywhere within the central bore of the fiber adjustment body (fiber plug). The fiber adjustment body is itself secured within the probe body by means of set screws.

The fiber tubes and fiber adjustment rods require a separate pressure seal arrangement at the back of the probe. This requirement is satisfied by the probe back plate which is attached to the probe back flange and contains O-ring grooves for sealing the fiber tubes and fiber adjustment rods. After the fiber tubes and fiber adjustment rods are properly positioned, the O-rings are compressed and a pressure seal formed by screwing the back plate firmly to the back flange. The probe back flange, back plate, fiber tubes, fiber tube centering plugs, and adjustment rods, therefore, form a unit which can be removed from and inserted into the probe body during assembly or to replace an optical fiber.

A safety feature which is provided with the probe for use at elevated pressures is a clamp assembly for the fiber tubes. While the tubes are designed to be held in place by O-ring seals, the clamp assembly can be used to prevent a fiber tube from being ejected from the probe if an O-ring seal fails.

1.8 Rayleigh Scattering Calibration Cell

The Rayleigh scattering calibration cell is used to obtain the calibration constants required for absolute measurements of density and pressure with the RSD system. The cell consists of an MDC Corp. stainless steel 3" 6-way cross with an extension tube, which contains a water-cooled light trap, fastened to one arm of the cross. The cell is shown in Figure 1.18. Aluminum flanges, containing fittings for a gas inlet line, a pressure transducer, and an exhaust line are used to seal the top and bottom arms. For use with the calibration cell, the probe requires an adapter flange. This flange matches the bolt circles of the calibration cell flange and the probe,

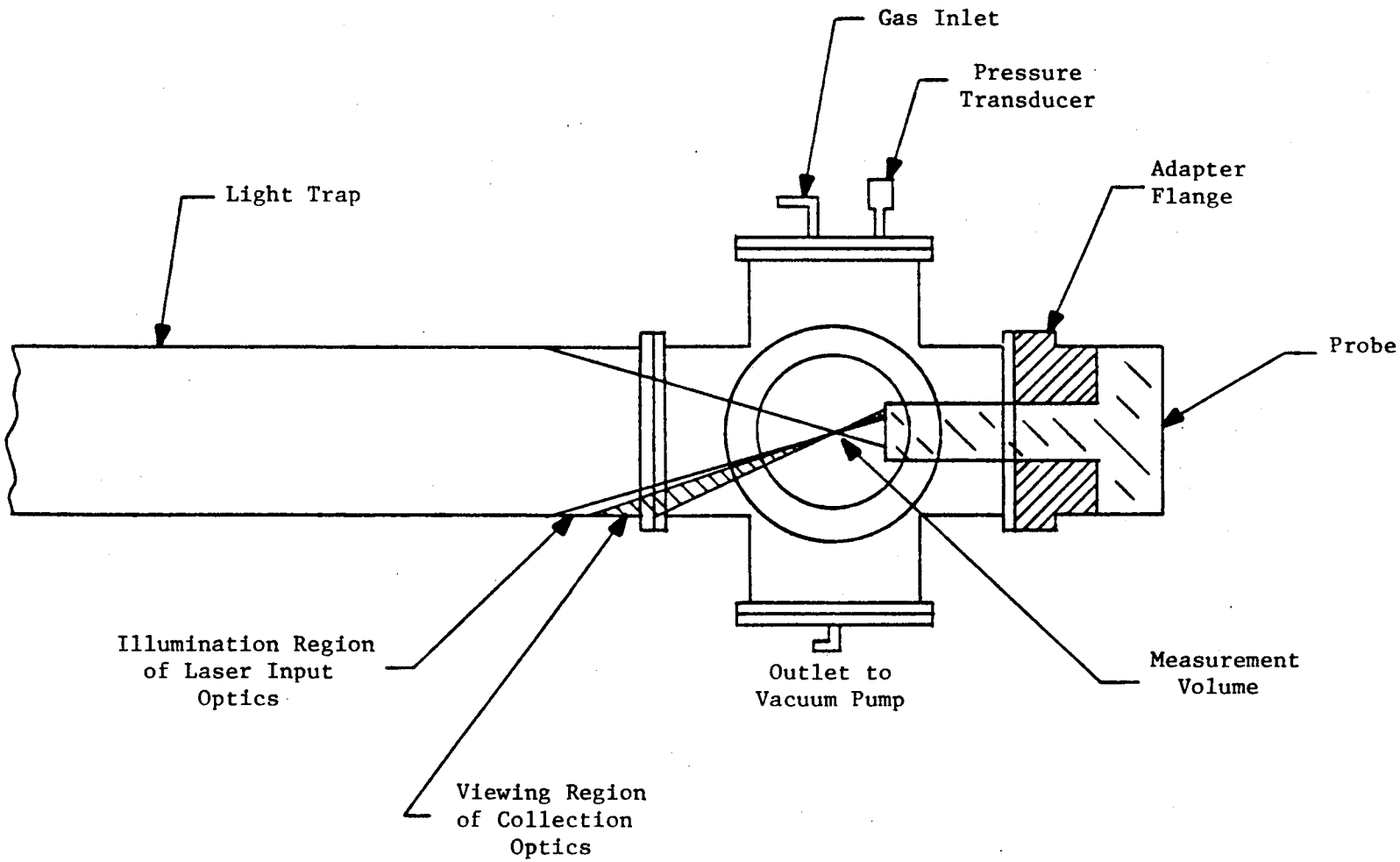

Figure 1.18 Standard Calibration Cell Configuration

and positions the probe such that the measurement volume is in the center of the cell. The flanges of the calibration cell are sealed with rubber gaskets for either vacuum or moderate pressure operation. The probe is sealed to the adapter flange by an O-ring.

The viewing path of the collection optical fiber and the illumination path of the laser input fiber are shown in Figure 1.18. Ideally, the two paths intersect only in the measurement volume. However, as mentioned previously in the discussion of the probe optics, the collection fiber views a substantial amount of surface scattered laser light. It has been experimentally determined that most of this light is due to stray light coming from the laser input optics, and not due to reflections from the light trap (see section 3.2).

The calibration cell can also be used without the probe or with an additional Rayleigh scattering detector at 90°. For the former case, the beam from the laser is focused directly into the calibration cell, as shown in Figure 1.19. Flanges with windows are used for the arms transmitting the laser beam and the Rayleigh scattered light. In this configuration, the cell has an operating pressure range of 1 torr to approximately 2 atm. Safety considerations limit the maximum pressure. Standard window thickness, 0.5" for 2" diameter and 0.75" for 3" diameter, would provide a safety factor of 2 at 30 atm. A higher factor of safety is recommended, even if surrounding equipment and personnel are shielded against the failure of a cell window.

Use of the calibration cell with the probe and an additional Rayleigh scattering detector at 90° may be useful in testing the laser/fiber delivery system and the probe power monitor. This configuration is similar to that shown in Figure 1.19 with the exception that the probe is used instead of directly focusing the beam from the laser. The 90° scattering signal should be relatively free from interference by surface scattered light, and therefore will provide an accurate measure of the laser power in the measurement volume. This signal can be used to determine the temporal fluctuation of the laser power at the measurement volume which, combined with direct measurements of the laser output, can determine the effect of the fiber on the stability of the laser power. This signal can also be used to check the accuracy of the

laser power monitor signal and the power monitor gated integrators/long term averagers.

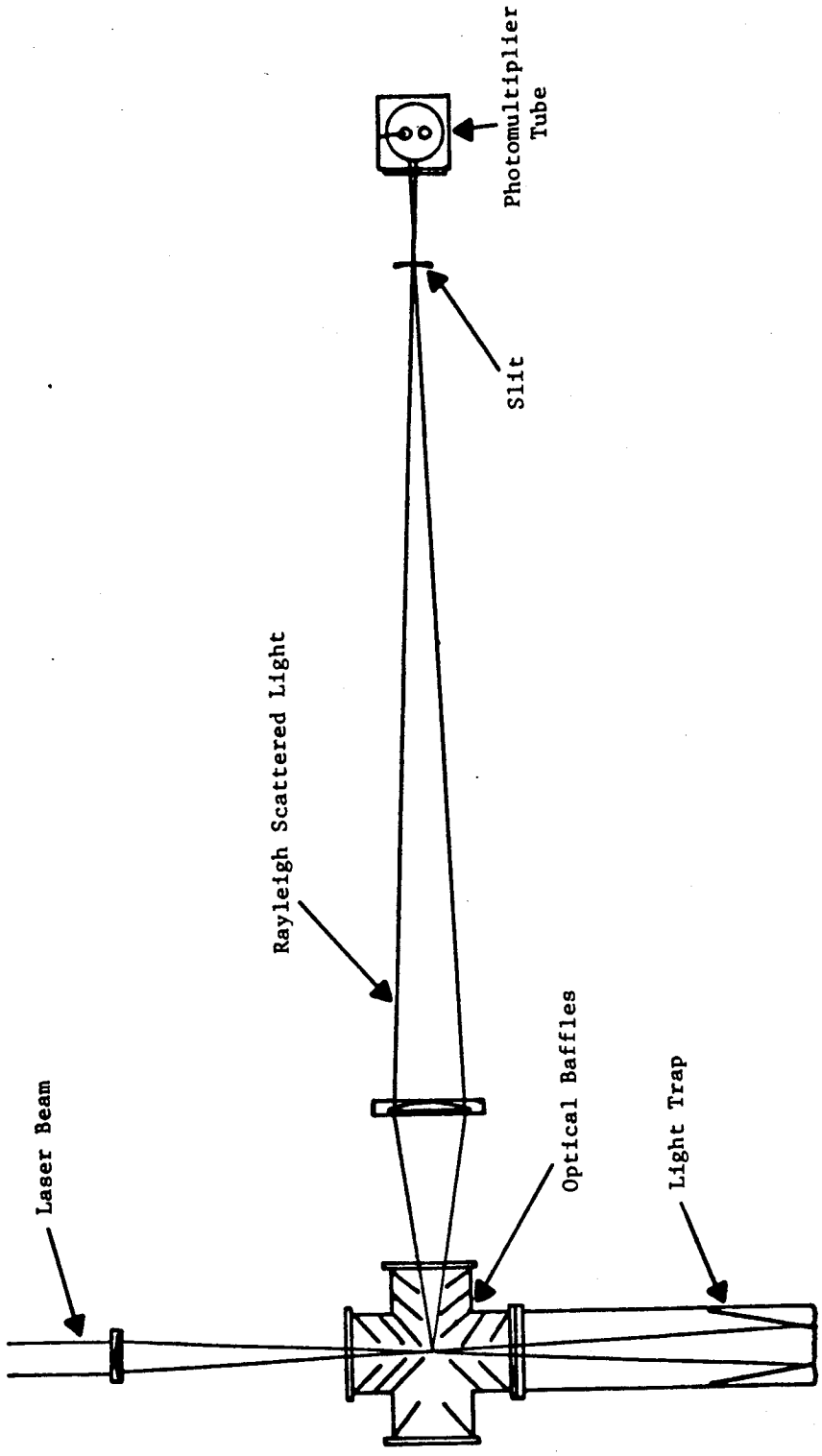

Figure 1.19 Calibration Cell Configuration without Probe

II. SYSTEM OPERATION

2.1 Copper Vapor Laser

The operating instructions for the Plasma Kinetics Model 251 copper vapor laser are contained in the laser manual. The operating instructions will not be repeated in this section. Instead, this section is intended to supplement the laser manual with suggestions received from Plasma Kinetics engineers and derived from our experience in operating the laser.

The Model 251 copper vapor laser requires 3 phase, 30 A power at a voltage between 208 V and 240 V and cooling water at a flow rate of 1 gpm at standard pressure (~50 psi). The laser has two interlocks which can trip the power supply: a high voltage interlock which is tripped when the laser cover is opened or a power supply side panel is removed, and a low water flow rate interlock which is tripped if the rate falls much below 1 gpm. A third optional interlock is provided which closes the shutter of the laser outlet if a switch, such as a sensor on a room entrance door, is opened.

After the power supply and the high voltage to the laser are turned on, the laser requires between 45 and 60 minutes for the lasing action to begin. This occurs when the laser tube is at operating temperature and the copper in the tube vaporizes. The laser is typically run at an input power of 3.5 kW as determined from the voltmeter/ammeter on the power supply. For a pulse rate frequency of 6 kHz, which is the frequency of the internal trigger source in the laser power supply, the voltage should be on the order of 7.5 kV. The voltage setting is adjusted by the rheostat on the front of the power supply. While the voltage is set in the process of turning on the high voltage to the laser, the voltage needs to be reset several minutes later since the voltage level will fall off 10 - 20% from the initial setting. The voltage should also be checked periodically during the laser operation since it will drift as much as 10% over a period of 30 minutes. This voltage drift also affects the laser output power.

The pressure in the laser tube is normally maintained between 20 - 40 torr during laser operation. The lower end of the pressure range results in

an increase in the ratio of 510 nm radiation to the 578 nm radiation. The higher end of the range has a lower ratio of 510 nm to 578 nm power, although the total power output is higher at the higher pressures. The laser was typically operated at 30 torr during the development and testing of the RSD system. The pressure in the tube is adjusted by means of a throttle valve at the vacuum pump inlet. The neon flow rate is not substantially affected by the tube pressure setting, but is primarily controlled by a needle valve in the laser head. This needle valve is not normally adjusted and cannot be accessed while the laser is operating.

In shutting down the laser, the cooling water must flow through the laser for 1 hour after the high voltage has been turned off. This is required to remove the heat stored in the laser during operation. If the laser is not properly cooled down, connections to the plastic water and vacuum lines will likely be damaged. More severe damage to the laser tube is also possible. Part of the laser shutdown procedure is to close the neon and vacuum line shutoff valves at the back end of the laser. In addition to these valves, we closed the shutoff valve for the vacuum line adjacent to the front end of the laser tube. This was done to prevent air, which may leak into the vacuum line at connections with the vacuum gauge, from entering and contaminating the laser tube. Since this valve is inside the laser enclosure, the power to the laser must be off before access to the valve can be gained.

Due to the long startup and shutdown time required by the laser, we turned the laser off only when it was not going to be used for the remainder of the day. In between periods of use on the same day, the laser was run with the shutter closed.

The Model 251 copper vapor laser can be triggered using either the 6 kHz internal source or by an external source. The voltage of the external pulse should nominally be 10 V, although a voltage as low as 5 V will usually work. Plasma Kinetics specifies the required trigger pulse characteristics to be a pulse width of 300 ns and a rise time of 50 ns. We have found that a square wave from a function generator will also be acceptable. The laser can be switched from internal to external trigger sources, or vice versa, while the laser is operating if the switch is performed quickly. The main constraint is

that the laser not be off for a long enough time so that the laser tube cools. Using a function or pulse generator as an external trigger source, the laser pulse rate can be varied. The pulse rate range of the laser as specified by Plasma Kinetics is 4 kHz - 10 kHz.

The laser is not, however, designed to permit easy and quick changes in its repetition rate. One important point is that the number of capacitors in the laser firing circuit must be changed if the pulse rate is to be changed significantly. For operation between 7 and 10 kHz, Plasma Kinetics specifies that 4 nF capacitance (two capacitors) be used, while for operation between 4 kHz and 6 kHz, 6 nF (three capacitors) should be used. In switching between the ranges, a capacitor must be added or removed. The capacitors are located inside the laser enclosure near the back (high voltage) end of the tube. The capacitors cannot be altered, therefore, unless the laser is not operating. As an additional safety precaution, the capacitors should also be checked to ensure that they are discharged before they are altered.

A second note regarding the variation of the laser repetition rate is that the voltage-current characteristics of the laser change with the repetition rate. In general, the laser input power will not remain constant as the pulse frequency is changed. The laser voltage will have to be adjusted to maintain the desired input power.

The laser appeared to exhibit good pulse-to-pulse power stability. This conclusion was drawn from the fact that the Rayleigh scattering signal did not show signs of amplitude fluctuation when displayed on an oscilloscope. The laser also exhibited very low jitter based on the same observations. The laser did exhibit short term (~1 s) and long term (~30 minute) variations in laser power. The short term variations were characterized by 3 - 5% changes in laser power as measured by a calorimeter-type laser power meter. The variations were accompanied by a change in the intensity of the glow coming from the laser tube which can be detected on the walls of the laser hood when laser goggles are worn. This suggests that the short term power variation may be due to an instability in the electrical discharge in the tube or a switch of lasing modes. The longer term variation is usually correlated with a drift in the laser voltage. This can be minimized, if necessary, by closely

monitoring this voltage. Plasma Kinetics, at additional cost, also offers a voltage regulation system which can prevent the long term drift in voltage.

Towards the end of the testing of the RSD system, adjustments in the thyratron reservoir voltage setting were required to keep the laser operating properly. On several occasions it was necessary to increase the resorvoir setting (at the back of the power supply) to maintain or increase the laser power. On one occasion, the reservoir voltage needed to be increased before the trigger pulses would produce a discharge in the tube during the startup of the laser. If the thyratron reservoir voltage setting is too high, however, the laser will "thump" and/or "motorboat". If this occurs, the reservoir setting must be reduced until the "thumping" or "motorboating" stops. It may be necessary on some days to increase the setting and on other days to reduce the setting.

The RF radiation generated by the laser is a function of the thyratron reservoir voltage setting. The RF radiation was found to occasionally interfere with the normal operation of the A/D board. Specifically, the A/D board would alter the sequence with which it reads the A/D input channels during data acquisition using DMA transfer to the computer. This alteration of the data sequence prevented proper interpretation of the data and thus produced an invalid data set. Lowering the reservoir voltage removed this problem, but also decreased the laser power.

Maintenance on the laser may need to be performed when the laser power falls off and the cause cannot be attributed to a lower reservoir voltage setting or misaligned mirrors. Two possible causes of low power that can be addressed without a Plasma Kinetics service call are a low amount of copper and a dirty tube. The laser manual gives instructions on loading new copper into the tube. It should be remarked that the copper bead towards the back of the laser is the one which is critical to good laser operation. If a bead of copper is still present at the front of the laser while none is present at the back, copper should be added to the laser. Since, however, it is a relatively simple matter to blow out the tube while preparing to load copper into the laser tube, this procedure should also be considered.

Alumina dust in the laser tube, which is lined with alumina insulation, can cause a decrease in laser power. "Blowing out" the laser tube to remove the dust can be tried if no other obvious reasons for low laser power are evident. To blow out the tube, the tube must be brought up to ambient pressure and the windows removed in the same manner as is performed for loading copper into the laser. It is also recommended that the laser mirrors be removed since they will most likely get dirty in the process. A source of clean compressed gas is needed to blow out the tube. A compressed air line is not recommended since it usually is contaminated with oil. A piece of plastic tubing attached to a bottle of N_2 was used previously. Care must be taken to avoid scratching the inside of the tube when directing the jet of compressed gas into the tube. A damp towel or cloth should be placed outside the tube at the other end to collect the dust being blown from the tube. After the tube has been blown out, the window O-rings and O-ring grooves should be inspected and cleaned before replacing the windows. Plasma Kinetics does not recommend the use of vacuum grease on these seals.

2.2 Optical Fibers

Three types of fibers are used in the RSD system. The most critical fiber is the laser input fiber which is a special, low numerical aperture fiber manufactured by General Fiber Optics and designed for high power (pulsed Nd-YAG) lasers. The probe power monitor fiber and Rayleigh scattering collection fiber are standard fibers manufactured by Diaguide. Both of these types of fibers are silica core/silica clad and have core/cladding diameters of 200/250 μm. A third type of fiber is a plastic fiber used for monitoring the laser power in the laser hood.

Fiber Termination

The preferred method of terminating fibers which transmit high levels of power, such as the laser input fiber, is cleaving. A properly cleaved fiber has a perfectly smooth end, whereas a ground and polished end contains small scratches. Since any defect on the face of a fiber can concentrate the laser power and cause laser damage, a fiber with a ground and polished end has a lower laser damage threshold than a fiber with a properly cleaved end. While

the Diaguide fibers did not require cleaved ends since they did not carry large amounts of power, these ends were also cleaved. If fiber connectors were used with these fibers, a ground and polished end would be preferred since this termination method can regularly produce a face at 90° to the fiber axis - an important consideration for a low loss connection. Since a single length of fiber was used both for the probe power monitor signal and the collection signal, grinding and polishing were not necessary.

A Precomp sapphire fiber cleaver was used in cleaving the silica fibers. It was found that a good cleave could be easily and regularly obtained with a fiber cleaver in good condition. On the other hand, a worn fiber cleaver rarely produced an acceptable cleave. The condition of a cleaver can be checked by inspecting the knife edge under a microscope. Other equipment needed in cleaving a fiber are a sharp X-acto knife or razor blade and two small pieces (~3" x 4") of aluminum (between 1/4" and 1/2" thick). The first step in cleaving a fiber is to strip the plastic secondary coating from the fiber with the X-acto knife. The secondary coating should be removed from the last 3 - 4 cm of the fiber. The primary buffer coating, a thin layer of silicone-type material, should then be gently removed as best as possible with one's fingernails, being careful not to break the fiber. The fiber is then taped across the middle of the two pieces of aluminum, which are placed on a flat, smooth surface, such that approximately 2 cm of the stripped fiber is on each piece. On the piece opposite the fiber end, the tape is placed on the unstripped portion of the fiber. A slight tension is then applied to the fiber by gently separating the pieces of aluminum, and the fiber is carefully scribed with the cleaver about 1.5 cm from the end of the primary and secondary coatings. The scribing action consists of carefully pressing the knife edge of the cleaver on the fiber, using only light to moderate force. The desired result is a small, shallow scribe mark (not usually visible) on the fiber. Slow, steady force is then applied to separate the pieces of aluminum so that the fiber will break in tension. The fiber must not be bent as tension is applied since this usually leaves a lip or a chip on the newly cleaved fiber end. If the fiber does not break under moderate tension the usual reason is that the fiber was not properly scribed. The best procedure to follow in this case is to apply heavier tension until the fiber breaks and to start over if the resulting fiber surface has defects.

After the fiber has been cleaved, the end of the fiber must be inspected with a microscope. A 20X magnification will allow observation of the smallest defects. A lower power microscope, such as the Fotec portable fiber inspection microscope, is adequate, however. The detection of defects with lower power microscopes can be aided by examining the fiber not only with top illumination, but also by illuminating the other end of the fiber. If dirt appears to be present on the end of the fiber, it can be removed by wiping the end of the fiber with lens tissue wetted with methanol. The fiber should be supported near the tip when this is done.

The plastic fiber cannot be terminated by cleaving. The recommended termination procedure is to grind and polish the fiber end. We have obtained acceptable results, however, by simply "chopping" the end of the unstripped fiber with a razor blade and then stripping back the plastic protective coating. While this does not produce a high quality surface, it is sufficient for the purpose of monitoring the laser power in the hood.

Laser Input Fiber Preparation

The laser input fiber is held in a modified Diaguide fiber sleeve (#SL/200) at the laser/fiber coupling end and in the fiber tube at the probe end. The fiber sleeve consists of two pieces - the main body and a short (~1 cm) barrel which fits tightly over the end of the fiber. For the fiber to be easily inserted into the barrel, the primary buffer coating must be completely removed. This can be done with special solvents, although we had good success with charring the coating by rapidly passing the stripped end through the flame of a propane torch. The charred coating can then be removed with lens tissue wetted with methanol. The fiber sleeve is assembled by first passing the fiber through the sleeve main body so that the stripped end extends beyond the end of the sleeve. The stripped end is then inserted into the barrel and the barrel gently pushed down over the stripped end until the bare fiber protrudes from the barrel by about 1 mm. The barrel and fiber are then carefully pushed back into the main body of the sleeve. While the fiber can then be glued to the back end of the fiber sleeve, we did not find it necessary to permanently secure the fiber.

The probe end of the fiber is held in the fiber tube, together with the power monitor fiber, by ferrules at the front and back of the tube. The laser input and power monitor fibers are therefore installed in the fiber tube at the same time. The first step of this installation process is to pass both fibers through the back ferrule. (Both fibers should have the secondary coating stripped 2 cm from the end). Refer to Figure 1.16 for schematics for the fiber tube ferrules. The two holes of different diameter, 0.57 mm (0.0225") and 1.04 mm (0.041"), are for the General Fiber Optics laser input fiber and Diaguide power monitor fiber, respectively. The back ferrule should be slid back roughly 20 cm from the ends of the fibers. The fibers are then inserted through the fiber tube.

The second step of the installation process is to slide the front ferrule over the fibers. First, insert the power monitor fiber into the central hole of the front ferrule. Next, insert the power monitor fiber through the side hole. This is complicated by the fact that the fiber cannot be directly observed while searching for the side hole; the hole can be found, however, by gently probing along the side wall with the fiber in the vicinity of the hole.

The third step of the process is to insert the front ferrule into the fiber tube, pushing it gently but firmly into the fiber tube until it seats against the tube. Match the fiber lengths as the fibers protrude about 1 cm beyond the front of the ferrule. Then carefully place a very small amount of cyanoacrylate adhesive into the bottom of the recessed area at the front of the ferrule and immediately pull both fibers back together until they are flush with or just barely protrude from the front of the ferrule. The tips of the fibers should be checked for cleanliness with a microscope. If glue covers the end of a fiber, it can be removed by gently rubbing the tip with a tissue wetted with acetone.

The fourth and final step of the installation process is to slide the back ferrule into the fiber tube, being careful not to push or pull on the fiber inside the tube. For elevated pressure application, it is recommended to apply cyanoacrylate adhesive to the outer surface of the ferrule which is in contact with the fiber tube. After the back ferrule is in place, cyanoacrylate glue is applied to the back of the ferrule to create a vacuum or

pressure seal around the two fibers. If desired, a fillet of epoxy adhesive can be applied to the ridge formed between the back ferrule and the end of the fiber tube. We did not find this necessary for vacuum operation since the back ferrule fits snugly in the tube.

Preparation of Remaining Fibers

A similar process as described above is performed for the probe end of the collection fiber. The process is somewhat simpler, however, since only one fiber is being installed. The basic four steps described above are used for the installation of the collection fiber into the fiber tube.

A necessity, at least for the General Fiber Optics laser input fiber, is the use of a tube to protect the 10 m lengths of fibers from damage. The laser input fiber has a very thin plastic coating which offers minimal protection for the fiber. For this reason, this fiber was inserted into a small diameter Tygon tube for additional protection. The Diaguide fibers were protected by a vinyl jacket in addition to the tough nylon secondary coating and did not require additional protection. However, since handling separate collection and power monitor fibers was found to be awkward, these Diaguide fibers were inserted into a larger diameter Tygon tube so that they could be handled as a single piece in travelling between the probe and the detector assemblies. These Tygon tubes, however, complicate the process of installing the fibers into the fiber tubes. It is recommended that they be stripped sufficiently far back from the ends of the fibers so that they do not increase the difficulty in installing the fibers in the fiber tubes. Particular care must be taken in stripping back the small Tygon tube from the laser input fiber, for it is fairly easy to inadvertently slice into the fiber and damage it.

The detector ends of the Diaguide collection and power monitor fibers are inserted into Diaguide D95P/250 plugs. We did not wish to permanently attach the plugs during the development and testing, so the fibers were simply taped at the ends of the plugs. A permanent installation is recommended for use in actual tests. Epoxy adhesive can be used for this purpose. Additional plugs

should be obtained, however, when a permanent installation is made since they cannot then be reused if a new termination is required.

The General Fiber Optics plastic fiber for the hood power monitor is inserted into a modified Diaguide fiber sleeve (#SL/400) at the laser hood and into a Diaguide D95P/500 plug at the detector end. In the laser hood, the fiber sleeve is inserted into a mount in the pinhole holder. The same remarks in the above paragraph regarding the permanent installation of the fibers in the plugs apply to the hood power monitor fiber.

2.3 Laser/Fiber Coupling

The design of the laser/fiber coupling system has two main purposes - to maximize the amount of power coupled into the fiber and to minimize the potential for laser damage occurring to the fiber. The laser hood which covers the focusing optics and optical fiber positioners is intended to reduce the dust level in the vicinity of the laser/fiber coupling region. The hood is used in conjunction with a filtered air purge which keeps the laser hood under a slight positive pressure. The laser hood also serves as an additional safety measure in blocking any stray laser light. During alignment of the pinhole and optical fiber, the top cover of the laser hood is partially slid back or removed. The side panels of the hood can remain in place during alignment. All alignment should be performed only when laser goggles are being worn.

The first step in aligning the laser/fiber coupling system is to align the pinhole. The pinhole, as stated in section 1.4, blocks the weakly focused laser light and thus reduces the heat load on the fiber holder. The Melles Griot rod-mounted fiber holder must be removed for this procedure. A laser power detector is placed behind the pinhole to measure the power transmitted by the pinhole. In the initial positioning of the pinhole, it is recommended that several screens be placed in the filter holder mounted on the front of the laser to reduce the intensity of the focused beam. An unattenuated beam can burn the pinhole. After the pinhole is positioned so that the laser beam is transmitted, the screens should be removed. The pinhole position should first be optimized in the plane transverse to the laser axis. Then the axial

position of the pinhole should be optimized. The best axial position of the pinhole is at the forward edge (closest of the laser) of the region where the power transmitted is a maximum.

After adjusting the location of the pinhole, the optical fiber must next be positioned. The Melles Griot fiber holder should be located 1 - 2 cm behind the pinhole and the laser input fiber inserted into the fiber holder. (The laser shutter is closed). The coarse positioning of the fiber can be performed by carefully moving the end of the fiber close to the pinhole and aligning the tip of the fiber with the pinhole. The remainder of the alignment procedure requires that some quantitative measure of the laser power being transmitted through the fiber be obtained. If possible, a power meter should be placed in front of the probe to directly measure the laser power. If this is inconvenient or not possible, then the probe power monitor signal or Rayleigh scattering signal should be observed to obtain a relative measure of the laser power. This can be done by displaying the signals on an oscilloscope. Screens to attenuate the laser beam should be used in the initial adjustment of the fiber. This will reduce the possibility of damage to the fiber or fiber sleeve by a misaligned, focused laser beam. Initially, it is recommended that the fiber position be optimized after each screen is removed. The best axial position of the fiber was usually ~1 mm behind the pinhole, although this distance may vary depending on how the axial position of the pinhole was set.

The maximum power transmitted through either a Diaguide or General Fiber Optics 200 μm core, 10 m long fiber was on the order of 1 W. If the maximum power transmitted through the laser input fiber is much less than this value with the laser operating at a power of 15 W or greater, the most likely problems are that either the fiber is fractured, or the laser mirrors are misaligned. If the fiber is fractured at some point between the two ends, a "hot spot" should be visible in the fiber when the laser is coupled into the fiber, unless the fracture is at a point within the Diaguide sleeve or within the fiber tube at the probe. With the unstable resonator optics, the mirrors can be misaligned to a point where the laser beam cannot couple efficiently into the fiber, and yet both the total laser power and the fractional power transmitted through the 600 μm pinhole appears nearly normal. If this may be

the case, then the alignment should be checked and, if necessary, realigned following the procedures in the laser manual.

2.4 Detectors and Detector Assemblies

In this section the optical alignment and electronic setup procedures will be discussed, starting with the photomultiplier tube detectors for the Rayleigh scattering signal and followed by the photodiode detectors for the laser power monitor signals.

2.4.1 Photomultiplier Tube Detectors

The photomultiplier tube (PMT) detectors and associated optics are housed in an aluminum box which is designed to provide a light-tight environment for the highly sensitive PMT detectors and to reduce interference which may be caused by RF emission from the laser. The PMT detector arrangement was shown in Figure 1.7. It should be noted again that the PMT housings for the 510 nm and 578 nm signals are currently different in that the 510 nm housing has a seven stage dynode chain while the 578 nm housing has a standard nine stage dynode chain.

The initial alignment of the PMT optics requires adjusting the Rayleigh scattering signal collimation optics, the angle of the dichroic filter mount, and the positions of the 510 nm and 578 nm PMT housings. This alignment can be performed using several light sources. The best source is copper vapor laser light which can be obtained by putting the collection optics fiber tube, if available, in the unfocused laser beam. An alternate light source could be obtained by using a spare piece of fiber terminated in a Diaguide D95P/250 plug in a manner identical to the collection fiber. As with the first method, the other end is placed in the unfocused copper vapor laser beam. The first step in the alignment is to adjust the distance between the detector fiber mount and the collimating lens. The light source is connected to the receptacle in the fiber mount, ensuring that the key on the plug slides into the slot on the receptacle and the plug is fully inserted. The distance between the fiber mount and lens should then be adjusted so that the beam is as nearly collimated as possible. The collimated beam diameter will be ~4 mm

at the 510 mm tube housing and ~5 mm at the 578 mm tube housing. Next, the lateral and vertical positions of the lens must be adjusted so that the height of the beam remains constant and that the beam is centered on the 510 nm PMT photocathode. It is recommended that the beam be very weak so that the PMT photocathode is not saturated. The proper lateral position of the beam can be determined by maximizing the output of the 510 nm PMT. This adjustment must be performed in a dark room with the cover removed from the aluminum box and with a very low voltage level on the PMT so that the tube is not saturated. It is advised that the peak PMT current be held to 1 mA or lower. After the best beam position is found for the 510 nm beam, the collimating lens mount should be firmly secured.

The next step in the alignment is to adjust the angle of the dichroic filter. A mark on the aluminum base at the side of the box indicates the spot over which the collimated beam passes for the proper angle of incidence (35°) on the dichroic filter. With the 578 nm PMT housing temporarily removed, the dichroic filter mount is rotated so that the collimated beam passes over this mark. When the proper position is found, the filter mount is firmly secured and the 578 nm PMT housing put back into place.

The final step in the alignment is to position the 578 nm tube housing so that the PMT produces the maximum signal. This is done in the same manner as for the 510 nm tube, except the position of the tube housing is rather than the beam position. The translation stage for the 578 nm PMT is locked into position after the signal has been maximized.

After the initial alignment of the optics has been performed, it does not need to be redone unless an optical component has been moved out of position or unless there is a reason to suspect misalignment. The positioning of the collection fiber in the receptacle is very reproducible.

The alignment procedure is performed with the cover off of the aluminum box which allows the light source fiber to enter the box through the open sides. For an actual measurement, the collection fiber must be brought into the box through the sealed opening provided for this purpose. To pass the collection fiber with the D95P/250 plug through the opening, the split plate

and grommet must be removed. The plug can then be passed through the hole in the side of the box. The rubber grommet is then put over the fiber jacket and the split plate installed over the grommet. The collection fiber plug is then inserted into the receptacle. At this point the box can be closed up.

The signals for the 510 nm and 578 nm photomultiplier tubes should be observed as the voltage level on the high voltage power supply is turned up. This precaution is recommended since the PMT tube could be desensitized or damaged if high voltage were applied while the collection optics were observing an erroneously high signal such as that caused by a reflection.

Due to the different dynode chain structures for the two tubes, the maximum voltage which can be applied to each is different. The 578 nm tube is rated for a maximum voltage of 1250 V, while the 510 nm tube is rated for a maximum voltage of 1000 V. Since the dual outputs on the high voltage power supply are not independently controlled, the maximum voltage setting used for the RSD system should be 1000 V.

2.4.2 Photodiode Detectors

The photodiode detectors and associated optics are housed in a BUD aluminum box, mounted on an aluminum base which also holds the electronics for the power monitor signals. The optical layout of the photodiodes was shown in Figure 1.9. A Diaguide D-95HL collimator which is mounted on the side of the BUD box collimates the power monitor beam to a diameter of 8 mm. The dichroic filter is mounted at a 35° angle of incidence with respect to the collimated beam axis and reflects the 578 nm portion of the beam onto the 578 nm photodiode assembly. Alignment of the optics consists of setting the dichroic filter at a 35° angle to the beam axis by using a protractor, and then adjusting the position of the photodiodes so that the collimated spot is centered on the photosensitive surface. In a dimly lit or dark room, the power monitor signal from the probe is strong enough to detect by eye. If the power monitor signal is not available, the same light source used for the alignment of the PMT detectors can be used for the photodiodes.

Alignment is normally not necessary for the hood power monitor signal. No collimating or focusing optics are used. The fiber is simply plugged into the receptacle mounted on the side of the box. The light from the fiber then impinges directly on the photosensitive surface of the photodiode.

The electrical setup of the photodiodes simply consists in providing the photodiodes with a reverse bias voltage. The terminal cap is placed on a 45 V battery located inside the BUD box. Then the switch on each photodiode is set to the "ON" position. If any photodiode will not be used, the switch should be left in the "OFF" position. Hamamatsu does not recommend applying a high reverse bias to the photodiodes for extended periods of time. After applying a bias voltage to the photodiodes, the signals should be inspected on an oscilloscope to verify that the photodiodes are operating properly. The cover of the BUD box should be replaced after the photodiodes are set for operation.

2.5 Data Acquisition Electronics

The essential features of the data acquisition electronics have been described in section 1.6. In this section, the configuration of the Metrabyte A/D board for the RSD system and a description of the electrical connections will be given.

The Metrabyte DASH-16 I/O lines that are used by the RSD system are the following: A/D channels 0 through 4, DIG 0 OUT, and IPO/TRIG 0. The A/D input range is set to -5 to +5 volts by switches on the board (see the Metrabyte manual). The line assignments are:

A/D 0:	Pressure Signal
A/D 1:	510 nm Rayleigh Signal
A/D 2:	578 nm Rayleigh Signal
A/D 3:	510 nm Laser Reference (Power Monitor) Signal
A/D 4:	578 nm Laser Reference (Power Monitor) Signal
DIG 0 OUT:	Timing Gate Signal (TTL) (out)
IPO/TRIG 0:	A/D Trigger Signal (TTL) (in)

The DASH-16 uses a single A/D-converter that is multiplexed to the 8 input lines. After each data conversion the multiplexer increments to the next input channel. The user may select through software the lowest and highest channel numbers to be sampled, and the multiplexer then continuously cycles between these limits. For example, for the 5 channel Rayleigh scattering apparatus, the channels to be scanned are 0 - 4, thus the A/D sequence is 0-1-2-3-4-0-1-2-3-4-0-1 ..... .

When data are acquired in the DMA modes, a separate trigger signal is required for each data conversion. Thus, for each laser shot 5 A/D triggers are required in order to sample the 5 input signals. It is this consideration that made the timing module necessary

The connections to the A/D are shown schematically in Figure 2.1, which shows all the connections between the A/D, timing module, and gated integrators. The "Comp Trig" output from the timing module goes to the A/D trigger input (IP0/TRIG 0) and the A/D DIG 0 OUT goes to the "GATE IN" connector on the timing module. The "gate in" signal is used to inhibit the trigger signal to the A/D when the software is interacting with the A/D registers. The "integrator out" or "INT TRIG" from the timing module is connected to the SRS gated integrator "trigger" inputs and the power monitor electronics box "trigger" input. The "laser out" is connected to the laser "external trigger" input on the laser power supply rear panel. (Note: the "laser out" BNC connector on the timing module panel should have a floating or isolated ground, which it does not have at present. This should be corrected).

The signal outputs from the photomultipliers (used to detect the Rayleigh scattered light) are connected to the inputs at the two SRS gated integrators. Both "signal output" connectors are terminated to 50 Ω. (For set-up the PMT signals are fed to a scope via a T-connector before entering the integrators). The "gate" signals from the SRS integrators should also be connected to the scope for alignment purposes (terminated in 50 Ω). Finally, the "Last Sample" outputs from the integrators are connected to the A/D 1 and 2 input channels.

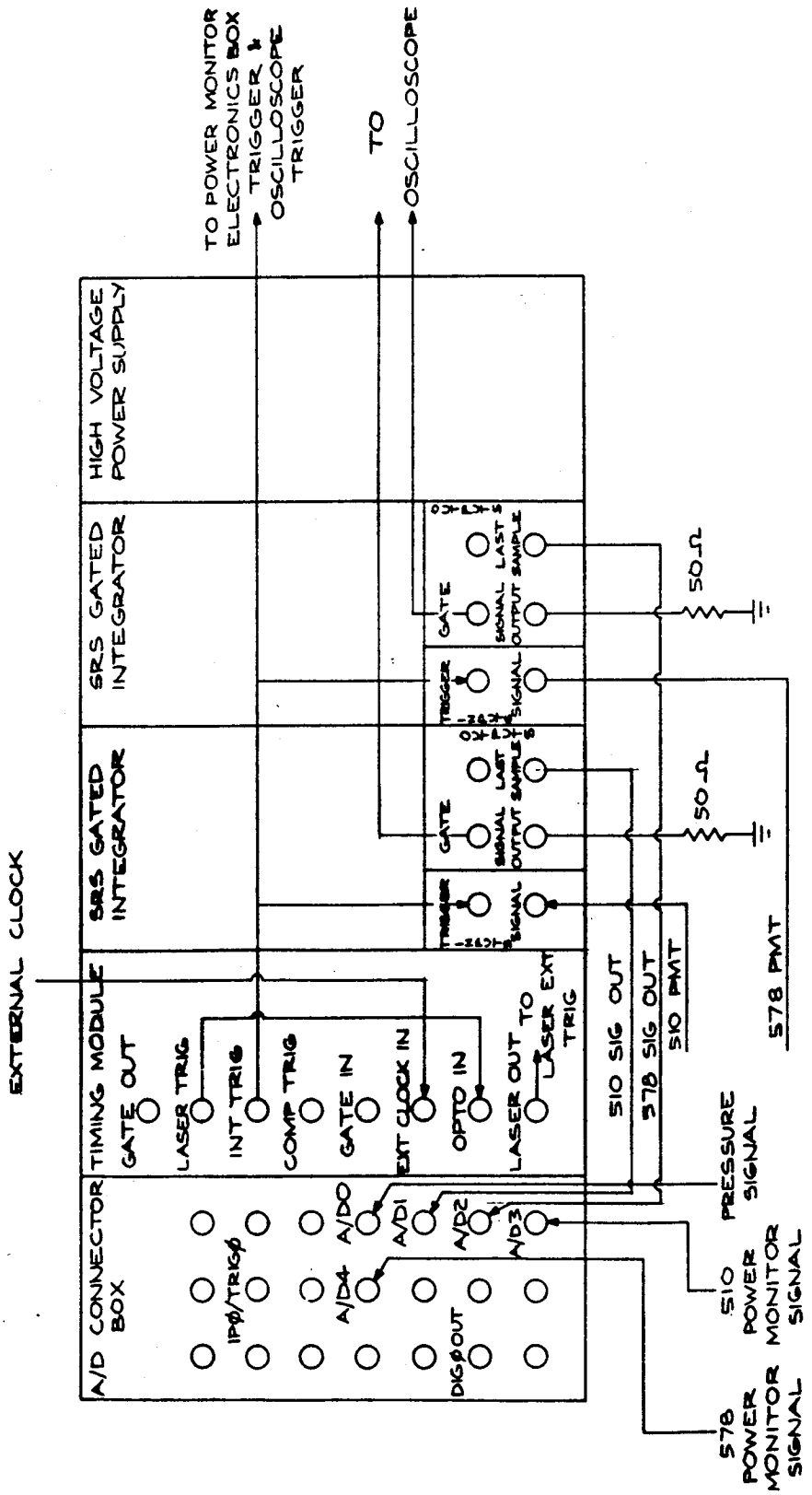

Figure 2.1 NIM Rack Components and Electrical Connections

The SRS gated integrators should be set in the non-averaging mode, and the sensitivity should be set so that the integrator output is consistent with the -5 to +5 V range of the A/D. The offset setting is not important in that the computer samples the no light condition and subtracts that from the actual signal (thus reading the difference, not the absolute signals). However, if the maximum signal is between 5 and 10 V, e.g. then the offset can be used to reset it to the proper -5 to +5 V range. The gate width and delay should be set by superimposing the gate-out signal over the PMT signal on the scope. Since the integrator output reflects the average signal over the gate interval, narrowing the gate increases the output. However, too narrow a gate width increases sensitivity to timing jitter. The best setting can be found by also observing the integrator output on the scope.

The power monitor electronics consist of three Evans Electronics Gated Integrators and one Evans Electronics Time Delay Module. The manuals for these boards appear in Appendix B. While gated integrators are provided for the 510 nm and 578 nm probe power monitor signals and the hood power monitor signal, only the first two are used to obtain quantitative results in the RSD system. Setting up the power monitor electronics involves setting the proper gate delay and gate widths. Setting the proper offset of the output signals is optional since the data acquisition procedure subtracts off the background levels, but it produces more meaningful raw data. The gate delay and width are observed by using a probe to obtain the signal on pin 3 of the time delay module (the DEL pulse output as shown in Appendix B) and displaying the signal on an oscilloscope. The required delay is approximately 2.6 μs. The delay can be set by adjusting the R1 and R11 potentiometers on the time delay board. The delay width can be set by adjusting the R15 potentiometer labeled "DW". The gate pulse should coincide with the power monitor signal obtained from the photodiodes. The best settings can be found by maximizing the signal out of the gated integrators. The DC offset level of the gated integrators is adjusted by adjusting the R66 potentiometer on the gated integrator board. To zero out the DC offset level, close the shutter on the laser and adjust each gated integrator so that it produces a zero voltage level.

Apart from setting up the SRS and Evans gated integrators as described above, the timing module settings must be selected. The software displays the

correct choice of settings for desired laser rep rate, data rate, and number of sampled channels, which should then be set by the operator. The operator must also turn on the battery power to the optical isolator circuit. If the battery voltage falls too low, the laser will not trigger and the 9 V batteries must be replaced. The PMT supply voltage must also be selected for best signal without tube saturation. Once the electronics have been set up and a calibration begun, no setting may be altered. Changing any setting ruins the calibration or invalidates a calibration already completed.

Calibrations and data acquisition are carried out under software control. The programs provide the necessary instructions to the operator. Invalid results (seen by inspecting program output on the screen) can sometimes be caused by RF interference from the thyratron in the laser. This problem has exhibited itself by altering the sequence of A/D channels acquired by the computer. This can be verified by inspecting the data file. Three courses of action are possible in such an event: 1) reduce thyratron driver voltage (which also reduces laser power), 2) increase distance between electronics and laser, and 3) shield laser or electronics. In all previous occurrences, the problem has been solved by option 1 - the easiest but least permanent solution.

A Kulite modified XT-140 high frequency pressure transducer was acquired but never used. Therefore, two tasks must be carried out in order to integrate it into the apparatus. First, signal conditioning must be provided to ensure that the output range is between -5 and 5 V, and second, the gauge plus conditioning plus A/D must be calibrated. The calibration must then be incorporated in the software.

2.6 Data Acquisition and Data Reduction Software

Introduction

There are three main tasks to be handled by the software package. These are: 1) calibration, 2) experimental data acquisition, and 3) data reduction. Calibration involves obtaining and reducing a set of data at known conditions, and then calculating the system calibration constants from that data. Data

acquisition involves taking and recording data during the actual experiment of interest, and providing limited calculational and graphical support for immediate data verification. Data reduction is the process by which the system calibration constants are used to convert the raw data to the quantity of interest, in this case temperature. Corrections for surface scattering and particle interference are performed in this last step.

The approach we have taken is to handle each one of these tasks with a separate program, communication between the programs occurring through a series of files. Thus, the calibration program writes a file containing the calibration data and calibration constants. This file is then read by both the data acquisition and reduction programs. The data acquisition program writes files containing the raw data which are read by the reduction program (along with the calibration file). The reduced data are then written out to a file which can be read and processed in any way desired. Presently these files are all written in ASCII format, although to save space the programs could be modified so that they are written in binary.

The calibration and data acquisition programs are interfaced to the experiment through the METRABYTE DASH-16 A/D board. The required connections were shown in the previous section. The timing of the experiment is controlled by a variable rate function generator which triggers the laser, gated integrators, and the A/D board. When triggered, the A/D board samples the 5 data channels sequentially, beginning with channel 0. The Rayleigh signal values associated with each laser pulse (Channels 1 - 2) are acquired and held for the A/D by the gated integrators and therefore represent simultaneous data. The power monitor gated integrators, while not having this "sample and hold" capability, produce an output which represents an average of the power monitor signal over a time period which is much longer than the acquisition time between A/D channels. Thus, the values (Channels 3 - 4) also represent simultaneous data. The pressure is read first on each scan of the A/D directly from the analog transducer signal while the gated integrators are acquiring the other 4 signals. Thus, there is a time offset between the pressure data and the other 4 channels of data equal to the difference between the A/D trigger delay and the laser trigger delay. The timing of the data acquisition process is shown in Figure 2.2. When all 5 channels are read by

the A/D board the maximum data rate is 10 kHz. If the laser power monitor signals are steady enough not to require shot to shot monitoring, then only 3 channels need be read and the maximum data rate rises to ~16 kHz.

Rayleigh Scattering Calibration (RSC)

The calibration procedure establishes the calibration constants of the RSD system, relating the system inputs to the output for a particular probe, optics, and electronic configuration. Thus, any adjustment to these components, including the gated integrator settings, invalidates the previous calibration.

The calibration is carried out by taking measurements at a set of conditions for which the temperature, pressure, and composition are known. The ambient temperature calibration cell and the Rayleigh Scattering Calibration program (RSC) are used for this purpose. The cell is filled to several different pressures with gas from a cylinder (typically N_2 or CO_2), and RSC is used to measure the resultant signal (temperature is ambient, and therefore both a constant and known). A detailed description of RSC now follows.

RSC is a command driven program consisting of several levels. At each level a list of options and explanations, where necessary, can be obtained by typing "he" (help). The overall structure of the program is shown in Figure 2.3. In the "set" level the various parameters needed to control the program, take the data, and reduce the data are adjusted. Each parameter has a reasonable default value, and so it need only be set if a change is desired. The parameters are:

- a flag to allow the pressure at each condition to be entered from the keyboard and substituted for the value read from channel 0. (default = not set)

- the number of data points (scans of the input channels) to take at each condition. (default = 1000)

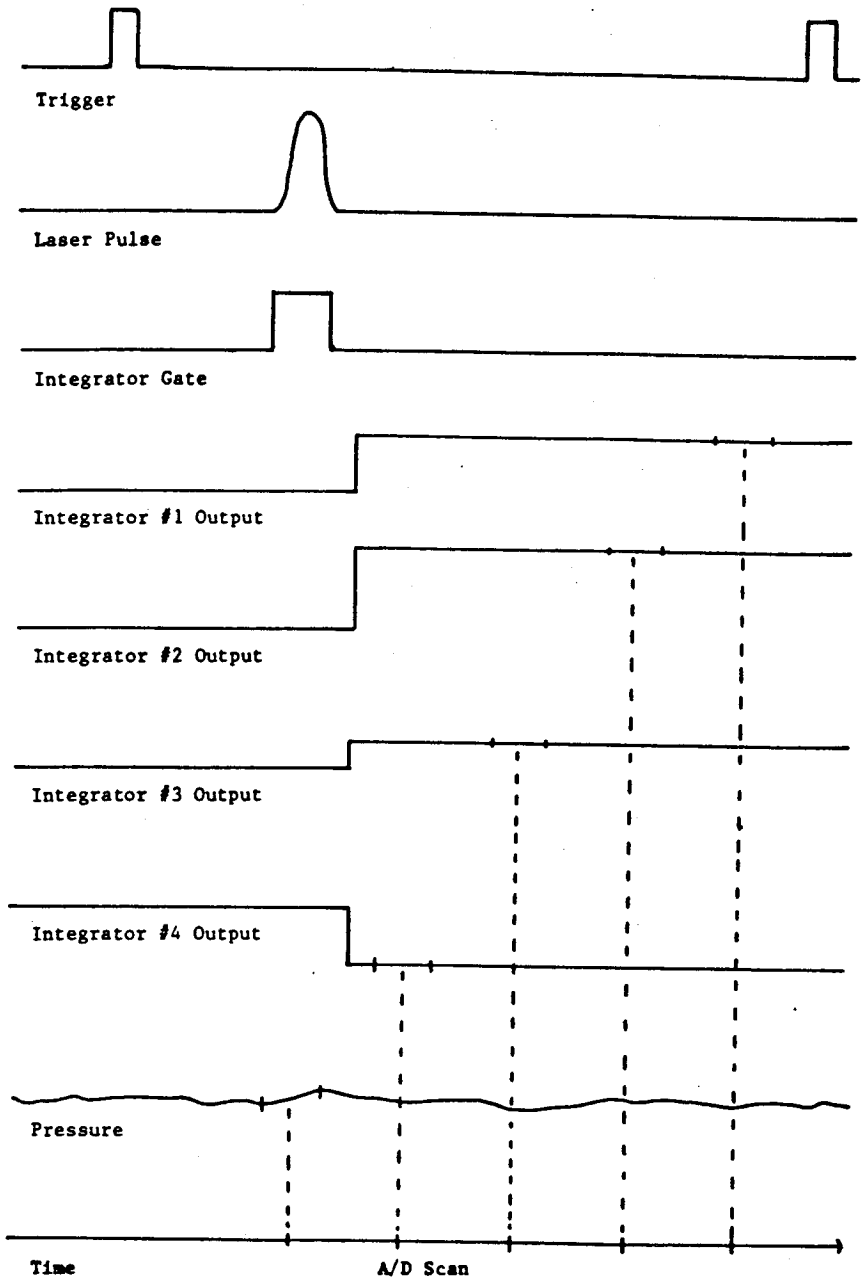

Figure 2.2 Data Acquisition Timing

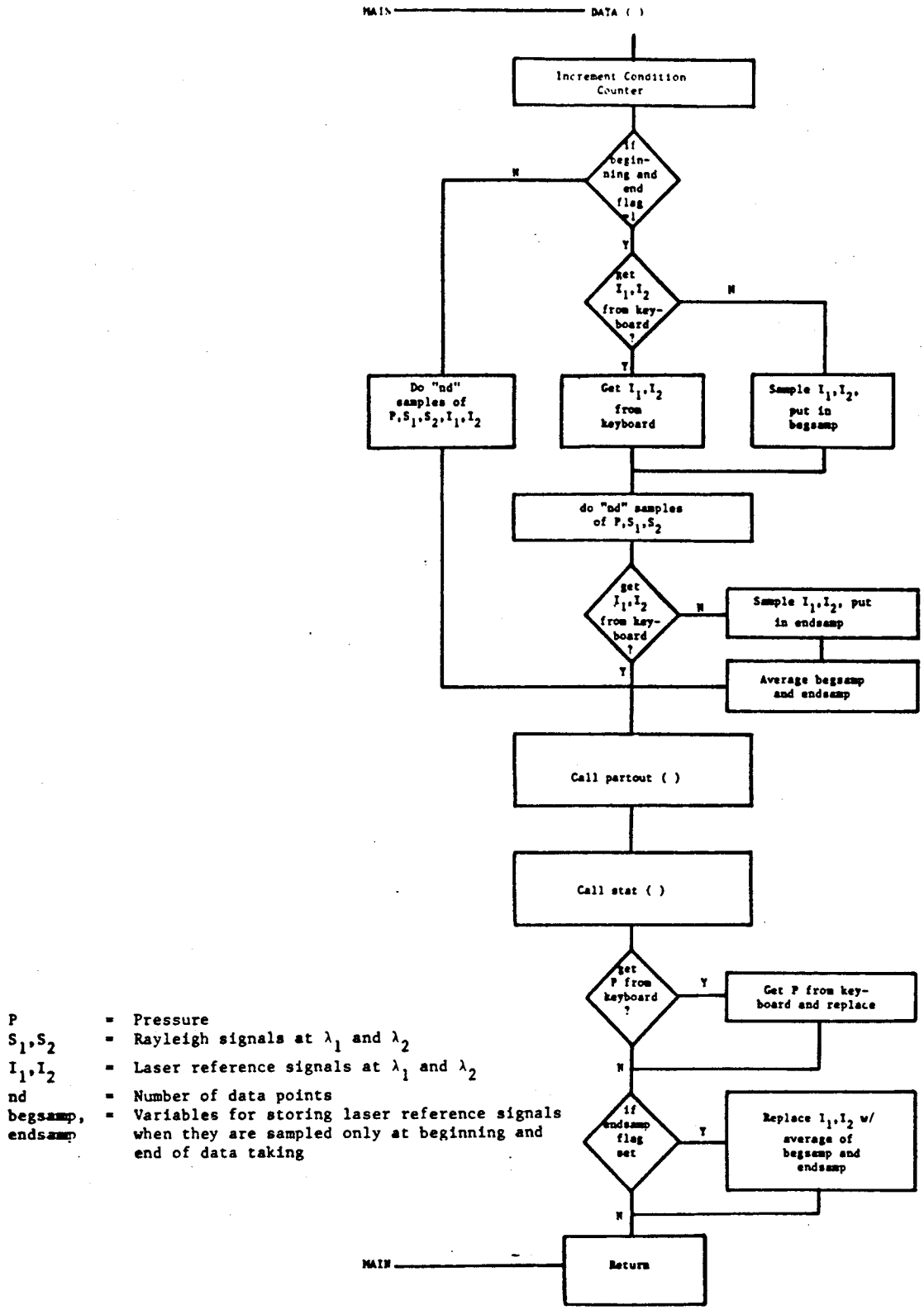

P = Pressure

S_1, S_2 = Rayleigh signals at λ_1 and λ_2

I_1, I_2 = Laser reference signals at λ_1 and λ_2

nd = Number of data points

begsamp, endsamp = Variables for storing laser reference signals when they are sampled only at beginning and end of data taking

Figure 2.3 Flowchart of the Rayleigh Scattering Calibration Program

- the number of the current calibration condition. This value is incremented automatically each time data are taken, and should be changed only when retaking data. When reset, old data at higher numbered conditions are overwritten.

- the threshold value (0 to 4096) for particle detection. Discontinuities larger than this value in the data are used to identify the presence of particles. (default = 1.5 x avg signal)

- the gas composition is specified by entering the mole fractions of the species present in the mixture. Currently 14 species are included in the program. (default = 100% N_2)

- the angle between the laser beam and the collection optics. (default = 158.4° as determined by probe optics)

- the laser wavelengths (default = the two copper vapor lines at 510 and 578 nm)

- a flag signaling to the data taking routine that only channels 0, 1, 2 should be scanned. Channels 3 and 4 (laser references) are then read before and after data taking. (default = not set)

- an additional flag indicating that the laser references should be obtained from the keyboard rather than the A/D. Setting this flag automatically sets the one described in the preceding item. (default = not set)

At each calibration condition data are then taken in one of the modes specified in "set". Particles are identified and discarded by scanning through both channels 1 and 2. (An earlier version of the program scanned only channel 1, and was found to be inadequate). For each condition the mean values of the data from each channel (and their standard deviations) are then stored.

When data at each calibration condition have been obtained, the stored averages are reduced. The reduction procedure is predicated upon the following analysis.

The signal measured at each wavelength is made up of a Rayleigh scattered component (S) and a surface scattered background (B),

$$Sig = S + B \tag{1}$$

The Rayleigh scattered component is given by:

$$S = CIN\sigma \tag{2}$$

where I is the laser intensity, N the number density of scatter, σ the effective Rayleigh scattering cross section, and C a system dependent constant. The background is given by:

$$B = CC'I \tag{3}$$

where C' is a constant. Thus:

$$\frac{Sig}{I} = CN\sigma + C'C \tag{4}$$

The expected response is therefore linear, and a least squares fit to the stored data with y = Sig/I and x = Nσ yields the slope, C, and intercept CC'. The least squares fit is done according to:

$$\text{slope} = C = \frac{n\Sigma xy - \Sigma x\Sigma y}{n\Sigma x^2 - (\Sigma x)^2} \tag{5}$$

$$\text{intercept} = CC' = \frac{\Sigma y\Sigma x^2 - \Sigma x\Sigma xy}{n\Sigma x^2 - (\Sigma x)^2}$$

where n is the number of conditions. The Rayleigh cross section is found from:

$$\sigma = \Sigma X_i \sigma_i$$

$$\sigma_i(\theta) = \frac{2}{3}\left(\frac{2\pi}{\lambda}\right)^4 \alpha^2 \frac{6 + 3p_n}{6 - 7p_n} P(\theta).$$

The expressions for α and $P(\theta)$ are given in the Phase I final report and are repeated in Appendix G, as are values for p_n. The angle between the laser and collection optics is θ. Number density is calculated from the ideal gas law since P and T are known.

Since the fit gives the background term in equation (1), it is also used to check the accuracy of the two color background subtraction calculation:

$$B_{\lambda 1} = \frac{Sig_{\lambda 1} - Sig_{\lambda 2} \dfrac{I_1 \sigma_1 C_1}{I_2 \sigma_2 C_2}}{1 - \dfrac{C_2' \sigma_1}{C_1' \sigma_2}}$$

The results of the calculations are written to the screen, and, when the "write" command is given, also written to the file specified both for record keeping purposes and for use by the other programs. The raw data obtained at each condition may also be called up on the screen and written to a file.

Rayleigh Scattering Data Acquisition (RDA)

The main purpose of the data acquisition program is to obtain and record the required amount of data as quickly as possible. Two approaches to attaining this objective were considered. In one, data would be taken until a segment of memory was filled. That segment would then be written to the hard disk and the process repeated. For sampling 3 channels, a segment holds 10,900 data points; 5 channels, 6,540 points. In the other approach, the entire memory of the computer would be filled (6 available segments) before

the data would be written to the disk. There would be short gaps in the data between segments, and the process of writing to the disk would take longer in this approach.

In the current version of RDA, only the first approach has been taken. This choice was made for the following reasons:

i) typically 2,000 points or more are ample for obtaining statistics in a turbulent flow field, thus ~10,000 points are easily adequate;

ii) to take data over longer periods of time, one would reduce the data rate rather than take more points;

iii) to monitor the flow periodically over long periods of time, the first approach works well;

iv) taking 6 segments vs. 1 is not a particular advantage, especially as those 6 segments do not form a temporally continuous record;

v) the write time at the end of 6 segments of data taking is ~6 times longer than it is for 1 segment.

The general architecture of RDA is the same as that of RSC. On command the program will take as many "frames" of "ndp" data points as specified (each "frame" is a set of data points up to 1 segment long separated by a write to the disk). If requested, between frames the data can be reduced according to parameters given in "SET". To minimize the time between frames, this option should not be exercised. However, the reduction procedure can be performed on the last frame of data (in memory) by command from the "MAIN" level. The program will sample from 1 to 5 channels (sequentially) per data point, with the unsampled channels read before and after the frame if desired. A flowchart of the main features of the program is shown in Figure 2.4.

The parameters to control the data acquisition and reduction are specified in "SET". They are:

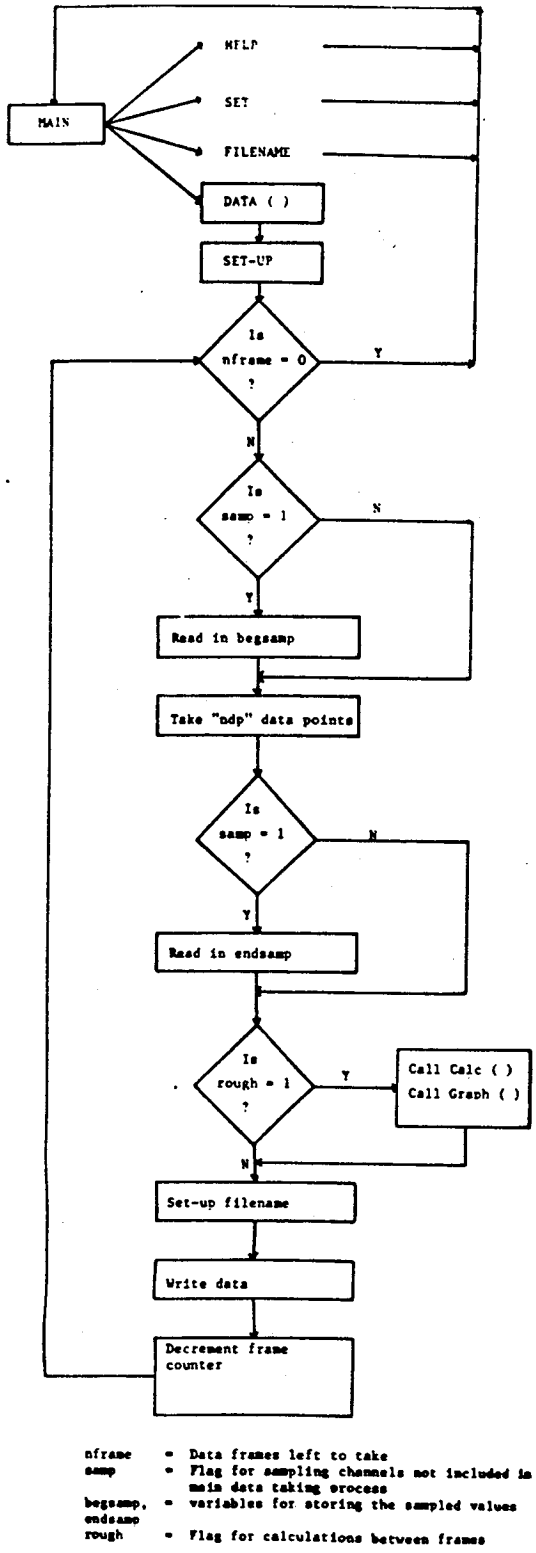

Figure 2.4 Flowchart of the Rayleigh Data Acquisition Program

- number of channels to sample at each data point. (default = 1)

- sample flag: controls whether the remaining channels will be sampled before and after each frame. (default = not set)

- number of data points per frame. (default = 1000)

- number of frames. (default = 1)

- flag for reduction between frames. (default = not set)

- flag for graphing between frames. (default = not set)

- write every N data points (default = 1)

- laser repetition rate. (default = 10 kHz)

- gas composition. (default = 100% N_2)

- collection angle. (default = 158.4° as determined by probe optics)

- laser wavelengths. (default = 578, 510 nm)

- particle detection threshold. (default = 1.5 x signal average)

- data rate. (default = laser rep rate, 10 kHz)

Additional inputs required at the "main" level are the calibration data and output filenames. On output, each frame of data is written to a separate file. The filenames are formed automatically from a root specified by the user. Specifically, the filenames are of the form rootxxx.dat, where xxx is replaced by a number, starting with 001, which is incremented automatically. When disk space is used up no more data taking is allowed.

The rough calculations serve to aid the user in determining the validity of the data. The gas composition is specified manually in "SET". Particles

in the data are identified and ignored, and values of $\langle N \rangle$, σ_n and $\langle T \rangle$ are calculated and written to the screen. The number of points the calculations are based on can be set by the user, and controls how much time the process takes. Only the raw data (including particles) are saved.

2.7 Rayleigh Scattering Probe Optical Assembly and Alignment

The details of the optical design procedure were detailed in Section 1.7.2 and in Appendices A and F. The overall configuration is shown in Figure 2.5. The collection and transmission optics are held inside two separate lens tubes or barrels that slide down the two parallel port holes in the probe until firmly against the lips at the front end. The barrels are held in place by set screws. The optics in each lens tube are separated by spacer rings inserted between the elements, the assembly held in place by a threaded plug that exerts a light compressive force when tightened.

The assembly of the transmitter optics is straightforward. After painting all the surfaces which will form the wall of the light passages flat black to minimize surface light scattering (such as the inside of the spacer rings), the spacers and lenses are slid down the transmitter lens tube in the order shown in Figure 2.5 (making sure that the curved surfaces of the lenses face each other). The lens tube plug is next inserted and tightened. The whole assembly is then pushed into the probe body firmly against the lip at the end. The set screws are then tightened to hold the barrel in place. Several Delrin mandrels have been provided to help push the elements into the barrel, and the barrel into the probe.

Assembly of the collection optics proceeds in a similar manner. However, the orientation of the wedge relative to the first lens is important. To obtain correct alignment, spacer 2 and the wedge should be glued together (we found that Locktite works well) prior to insertion in the lens tube barrel. The correct orientation of the spacer and wedge is such that the thinnest part of the wedge is aligned with the thickest part of the spacer. The various elements are then inserted in order, tapping lightly after each element is added to ensure that the elements fall into the correct orientation (although they should be inserted in as close to the correct orientation as possible).

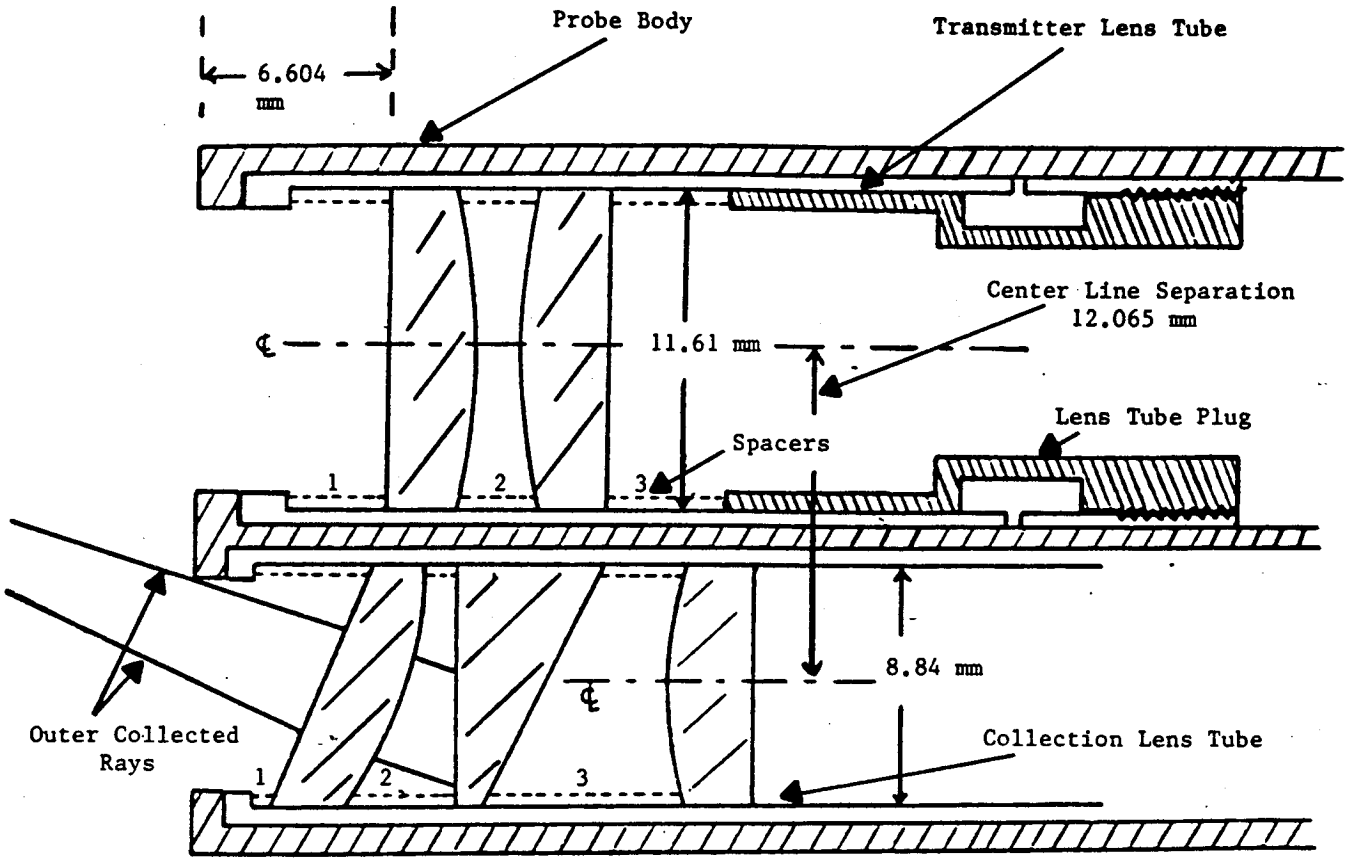

Figure 2.5 Rayleigh Scattering Probe Optical Design

The edges of the wedge and first lens have been chipped by repeated handling in the early stages of learning how to best assemble the probe. The chips should be painted black to prevent them from steering or reflecting stray light into the collection systems. Additionally, the parts of lens 1 that are vignetted should also be painted. The assembled collection lens barrel is then inserted into the probe and pushed to the end, but should not be locked in place at this point. The final assembly step is to bolt the back-plate of the probe (with the fiber tubes) into place.

Optical alignment of the probe is best accomplished by passing weak laser light through both transmitter and collection fibers and into the probe. This may be accomplished by placing the other ends of the fibers in the unfocused Cu-vapor laser beam (thus using the correct wavelengths). A screen (a sheet of paper will do) should be mounted on a micrometer stage and placed at exactly the stand-off distance in front of the probe, and a microscope positioned behind the screen to view the spots produced by the probe (see Figure 2.6). Coarse alignment is obtained by inserting the wire tool for rotating the collection lens tube into the two holes in the inside lip of the lens tube and rotating the tube to bring the laser input and collection spots into the best overlap possible. Focus of the spots is achieved by sliding the fiber tubes in or out as appropriate. When coarse alignment is achieved the collection lens tube set screws can be tightened. Fine alignment is accomplished by turning the 3 adjustment rods surrounding the laser input fiber tube, and can be observed by viewing through the microscope. The collection and laser input spots should be superimposed and the focus adjusted so that their size is minimized at the crossover point. Additional fine alignments to maximize the Rayleigh scattered signal can be made later.

Using the apparatus shown in Figure 2.6 we measured spot sizes of about 250 μm for both the laser input and collection systems. The collection spot displays partial resolution into green and yellow portions, indicating that the two copper vapor wavelengths (510 and 578 nm) will be imaged from slightly different locations by the collection systems. Thus, particles passing through the collection volume will not necessarily show up on both Rayleigh scattering channels. Correct handling of particles therefore requires the detection algorithm to inspect the data from both channels.

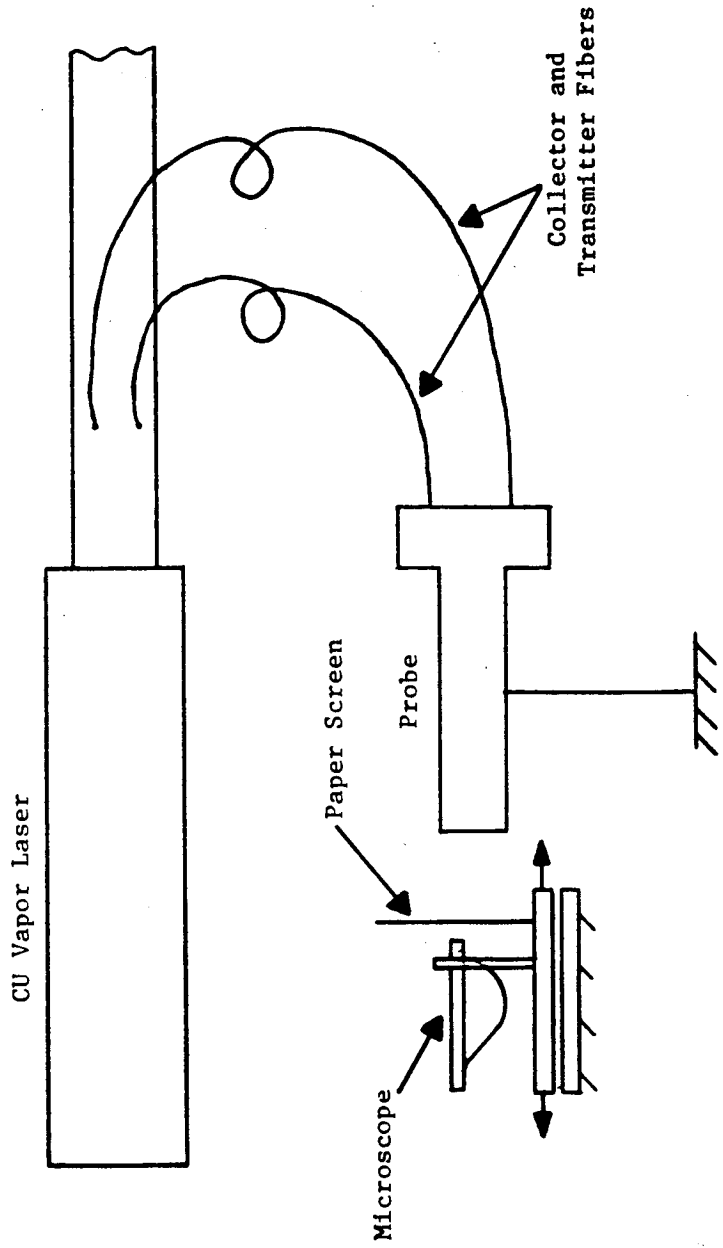

Figure 2.6 Setup for Optical Alignment of Probe

2.8 System Calibration and Data Acquisition

System calibration and data acquisition are both carried out under software control and guidance. Once the laser and electronics are operating properly and a good Rayleigh signal has been obtained, one takes data or calibrates by using the "RDA" or "RSC" programs, respectively. It is important to note that once a calibration has begun, no setting on the electronics can be adjusted without invalidating the calibration. Likewise, after a calibration is finished, any adjustments to the electronics, for example, while taking data, make it necessary to recalibrate.

The calibration procedure is straightforward. First, the calibration cell is evacuated and then filled to several pressures with gas of a known composition and temperature (e.g., room temperature nitrogen). At each pressure, RSC is used to take data. RSC then computes the system calibration constants and places them in a file to be read by the data acquisition and reduction programs. The larger the number of pressures used, the more accurate the calibration will be. An example of a calibration run output is shown in Figure 2.7.

```
# Rayleigh Calibration File 327nm Rayleigh channels 1 & 2 are:
#      C1             C2              B1             B2
   2.236124E+09  3.108372E+09    7.15387        22.2986
# Pressure from keyboard (1=YES) : 1
# No. of data points specified : 1000
# No. of calibration conditions :  13
# Particle detection threshold : 1000
# Calibration gas composition :
# Species     Mole Fraction
      1          1.0000
      2           .0000
      3           .0000
      4           .0000
      5           .0000
      6           .0000
      7           .0000
      8           .0000
      9           .0000
     10           .0000
     11           .0000
     12           .0000
     13           .0000
# Calibration temperature [K] :  298.00
# Collection angle [deg] :   22.00
# Laser wavelengths : 5100.00    5780.00
# p     psigma  s1    s1sigma s2    s2sigm   i1    i1sigma i2  i2sigma part num
  163.6    .0  598.3  42.1 1048.6  61.3   65.5    .0   43.0    .0      0.  1000
  202.2    .0  644.4  41.8 1086.5  65.4   65.4    .0   43.5    .0      0.  1000
  242.6    .0  698.2  42.8 1135.7  68.2   69.7    .0   45.9    .0      0.  1000
  284.7    .0  739.2  44.8 1174.7  64.1   66.3    .0   45.4    .0      0.  1000
  332.1    .0  760.2  46.7 1191.2  64.9   66.5    .0   46.3    .0      0.  1000
  365.4    .0  777.0  44.6 1197.8  64.2   66.8    .0   46.5    .0      0.  1000
  412.8    .0  843.9  45.6 1249.3  62.6   66.8    .0   47.4    .0      0.  1000
  465.4    .0  872.9  45.3 1273.4  65.0   66.2    .0   47.5    .0      0.  1000
  518.0    .0  925.7  49.0 1304.4  61.2   66.6    .0   48.5    .0      0.  1000
  583.0    .0  960.3  45.9 1340.5  61.4   63.7    .0   46.2    .0      0.  1000
  642.6    .0 1011.2  49.1 1370.0  65.0   65.5    .0   47.7    .0      0.  1000
  698.8    .0 1034.5  47.8 1392.0  58.5   64.9    .0   46.0    .0      0.  1000
  763.7    .0 1082.9  46.2 1418.5  59.6   64.5    .0   45.5    .0      0.  1000
# Rayleigh cross-sections :  .1777E-27     .1067E-27
# Avg background error :     -.11
# Error of fit at 95% confidence:
# error c1 = .15318E+09     error b1 =     .41882
# error c2 = .58709E+09      error b2 =     .96418
```

Figure 2.7 Sample Calibration Program Output

III. COMPONENT AND SYSTEM TESTING

3.1 System Characterization and Calibration

The performance of the Rayleigh scattering system utilizing the probe was evaluated by making calibration and data runs using primarily 100% N_2 (filtered) in the calibration cell. These studies served to identify problems in operating the system and the necessary remedies to characterize the performance of the data acquisition system, and to evaluate the capability of the apparatus to make accurate density and temperature measurements.

Several problems arose during the checkout phase of the experiments. 60 cycle interference was an early problem that was mostly eliminated by being careful to tie all the electronics to a common ground (i.e., plug into some multiple outlet). Even after this step there was however some residual 60 cycle noise present that we were unable to eliminate completely. We also found that the Evans Electronics gated integrators used to amplify the laser monitor signals had fairly lengthy time constants. Thus, it is necessary to wait at least 3 seconds after opening or closing the laser shutter before allowing data to be taken. Finally, we found that thyratron reservoir voltage settings greater than 56 on the laser power supply caused the A/D board to malfunction. When this occurred, the thyratron voltage had to be reduced until proper computer operation resumed (unfortunately the laser output increases with thyratron voltage).

Tests of the electronics showed that the signal processing train of PMT, SRS gated integrator, and A/D operated with a precision of ~1%. Observation of Rayleigh scattering signals with the same apparatus had a precision of ~10% based on 1000 measurements. Comparisons of signals obtained with different N_2 pressures showed that the precision scaled in the manner expected of a Poisson distribution, thus indicating that photon statistics are responsible for the level of precision attained by the measurements at pressures of 1 atm or below.

The laser power monitor signals, amplified by the Evans Electronics gated integrators, also showed a precision of ~10% (over 1000 points) as well as

significant variability between measurements. Since the hood power monitor signal showed no detectable pulse to pulse variation, we checked the probe power monitor signals with the SRS integrators and found just the residual 1% precision of the electronics. Thus, the power monitor electronics are not performing well, and are in fact the limiting factor in the current apparatus. We recommend that two more SRS integrators be added to the system to replace the Evans.

Performance of the probe optics was measured by observing the surface scattering background to total signal ratio. This was obtained by measuring the signal level at 1 atm and 0 atm (when only background is present). Background varied between 60 and 75% of the total signal as the probe was repeatedly reassembled. Even AR coating the optics made no difference to this figure.

Examples of complete calibrations are shown in Figures 3.1a - 3.1c and graphically in Figures 3.2a - 3.2f. Although the calibrations look quite good, the calculated error in the calibration constants for channels 1 and 2 are about 10% and 20%, respectively. The first two calibrations are for 100% N_2, the third for a mixture of CO_2 and air. The calibration constants all fall within the error bars. Note that the average background error, which is the difference between the background determined at each calibration point by the two color algorithms and the background determined by the fit to the data, is less than the error of fitted background value. This indicates that the background subtraction algorithm works quite well.

Data acquired using the RDA program were used to calculate temperatures based on 1000 points. On two successive days, using room temperature N_2, we measured T = 317 K (σ = 14.75), and T = 290 K (σ = 8.95). These two data sets were reduced with different calibrations, thus illustrating how the uncertainty in calibration constants affects the results. The precision of the two measurements is a result of the uncertainty in the Rayleigh and monitor signals themselves. Thus, given the previous characterization of system performance, these temperature results are expected.

```
# Rayleigh Calibration File 22761.cal
# Constants and Intercepts of Rayleigh Channels 1 & 2 are:
#      C1            C2                B1            B2
  2.236124E+09  3.188372E+09    7.15387       22.2986
# Pressure from keyboard (1=YES) : 1
# No. of data points specified : 1000
# No. of calibration conditions :  13
# Particle detection threshold : 1000
# Calibration gas composition :
# Species     Mole Fraction
      1          1.0000
      2           .0000
      3           .0000
      4           .0000
      5           .0000
      6           .0000
      7           .0000
      8           .0000
      9           .0000
     10           .0000
     11           .0000
     12           .0000
     13           .0000
# Calibration temperature [K] :  298.00
# Collection angle [deg] :   22.00
# Laser wavelengths : 5100.00    5780.00
# p     psigma  s1   s1sigma s2     s2sigm   i1    i1sigma i2   i2sigma part num
  163.6    .0  598.3  42.1 1048.6  61.3   65.5    .0   43.0    .0      0.  10
  202.2    .0  644.4  41.8 1086.5  65.4   65.4    .0   43.5    .0      0.  10
  242.6    .0  690.2  42.8 1135.7  68.2   69.7    .0   45.9    .0      0.  10
  284.7    .0  739.2  44.8 1174.7  64.1   66.3    .0   45.4    .0      0.  10
  332.1    .0  760.2  46.7 1191.2  64.9   66.5    .0   46.3    .0      0.  10
  365.4    .0  777.0  44.6 1197.8  64.2   66.8    .0   46.5    .0      0.  10
  412.8    .0  843.9  45.6 1249.3  62.6   66.8    .0   47.4    .0      0.  10
  465.4    .0  872.9  45.3 1273.4  65.0   66.2    .0   47.5    .0      0.  10
  518.0    .0  925.7  49.0 1304.4  61.2   66.6    .0   48.5    .0      0.  10
  583.0    .0  960.3  45.9 1340.5  61.4   63.7    .0   46.2    .0      0.  10
  642.6    .0 1011.2  49.1 1370.0  65.0   65.5    .0   47.7    .0      0.  10
  698.8    .0 1034.5  47.8 1392.0  58.5   64.9    .0   46.0    .0      0.  10
  763.7    .0 1082.9  46.2 1418.5  59.6   64.5    .0   45.5    .0      0.  10
# Rayleigh cross-sections :   .1777E-27     .1067E-27
# Avg background error :     -.11
# Error of fit at 95% confidence:
# error c1 = .15318E+09     error b1 =     .41882
# error c2 = .58709E+09     error b2 =     .96418
```

Figure 3.1a Rayleigh Scattering Calibration Output for Test #1 with 100% N_2

```
# Rayleigh Calibration File 325r2.cal
# Slopes and intercepts of Rayleigh channels 1 & 2 are:
#      C1              C2              B1              B2
  2.289294E+09  3.923423E+09    8.50803        23.2537
# Pressure from keyboard (1=YES) : 1
# No. of data points specified : 1000
# No. of calibration conditions :  14
# Particle detection threshold : 1000
# Calibration gas composition :
# Species     Mole Fraction
      1          1.0000
      2           .0000
      3           .0000
      4           .0000
      5           .0000
      6           .0000
      7           .0000
      8           .0000
      9           .0000
     10           .0000
     11           .0000
     12           .0000
     13           .0000
# Calibration temperature [K] :  298.00
# Collection angle [deg] :    22.00
# Laser wavelengths : 5100.00    5780.00
# p     psigma   s1    s1sigma s2     s2sigm   i1    i1sigma i2   i2sigma part num
  126.8     .0  587.1   38.9 1093.5   62.0    58.0     .0    43.0     .0      0.   1000.
  193.4     .0  635.2   41.2 1127.7   62.1    57.1     .0    43.3     .0      0.   1000.
  237.3     .0  668.7   43.3 1158.4   59.6    57.4     .0    43.2     .0      0.   1000.
  277.7     .0  699.3   42.1 1179.9   60.5    59.0     .0    44.4     .0      0.   1000.
  323.3     .0  723.9   41.7 1192.8   57.9    57.4     .0    43.8     .0      0.   1000.
  367.1     .0  758.0   42.3 1220.5   59.4    56.6     .0    43.9     .0      0.   1000.
  411.0     .0  778.3   44.5 1225.7   58.3    57.0     .0    44.0     .0      0.   1000.
  449.6     .0  825.8   46.6 1277.0   59.3    55.1     .0    43.2     .0      0.   1000.
  495.2     .0  842.7   45.7 1286.7   60.7    53.6     .0    41.8     .0      0.   1000.
  540.8     .0  847.5   45.1 1290.2   59.1    54.3     .0    41.4     .0      0.   1000.
  586.5     .0  899.4   44.6 1333.9   58.4    56.9     .0    43.3     .0      0.   1000.
  644.4     .0  916.9   46.3 1347.6   59.0    52.4     .0    41.6     .0      0.   1000.
  698.8     .0  927.1   44.6 1353.5   57.7    54.3     .0    42.4     .0      0.   1000.
  761.9     .0  991.0   47.4 1400.2   60.5    53.3     .0    41.1     .0      0.   1000.
# Rayleigh cross-sections :  .1777E-27     .1067E-27
# Avg background error :     -.06
# Error of fit at 95% confidence:
# error c1 = .24175E+09    error b1 =     .66167
# error c2 = .60049E+09     error b2 =     .98722
```

Figure 3.1b Rayleigh Scattering Calibration Output for Test #2 with 100% N_2

```
# Rayleigh Calibration File 325r3.cal
# Slopes and intercepts of Rayleigh channels 1 & 2 are:
#      C1             C2              B1             B2
  2.669493E+09  3.872659E+09    10.4238        28.4402
# Pressure from keyboard (1=YES) : 1
# No. of data points specified : 1000
# No. of calibration conditions :  15
# Particle detection threshold : 1000
# Calibration gas composition :
# Species     Mole Fraction
      1            .5500
      2            .0000
      3            .3000
      4            .0000
      5            .0000
      6            .0000
      7            .0000
      8            .0000
      9            .0000
     10            .0000
     11            .0000
     12            .0000
     13            .1500
# Calibration temperature [K] :  298.00
# Collection angle [deg] :   22.00
# Laser wavelengths : 5100.00    5780.00
# p     psigma  s1    s1sigma s2     s2sigm   i1    i1sigma i2   i2sigma part nu
  139.1     .0  532.7  39.0 1071.4  59.6   41.9     .0    36.1     .0      0.   1
  189.9     .0  571.6  38.7 1107.5  59.8   40.9     .0    35.9     .0      0.   1
  235.6     .0  606.5  40.3 1135.3  57.6   40.5     .0    35.1     .0      0.   1
  277.7     .0  638.8  40.7 1171.4  58.5   39.8     .0    34.8     .0      0.   1
  321.5     .0  675.8  40.3 1199.2  57.1   38.6     .0    33.9     .0      0.   1
  363.6     .0  696.1  39.6 1211.7  55.7   36.6     .0    34.0     .0      0.   1
  411.0     .0  705.5  39.3 1224.7  56.8   35.8     .0    33.8     .0      0.   1
  449.6     .0  740.0  42.4 1254.3  61.0   34.6     .0    32.7     .0      0.   1
  495.2     .0  772.7  41.1 1290.9  54.2   35.2     .0    33.5     .0      0.   1
  540.8     .0  770.8  41.2 1289.1  57.5   34.1     .0    32.0     .0      0.   1
  583.0     .0  773.1  40.8 1296.7  56.2   33.7     .0    32.1     .0      0.   1
  626.8     .0  797.9  39.6 1322.0  55.8   32.8     .0    32.6     .0      0.   1
  670.7     .0  797.6  38.8 1318.8  55.4   33.9     .0    33.1     .0      0.   1
  719.8     .0  833.7  39.3 1363.3  56.1   32.2     .0    33.2     .0      0.   1
  776.0     .0  851.5  40.0 1368.6  55.0   32.3     .0    33.2     .0      0.   1
# Rayleigh cross-sections :  .2494E-27     .1496E-27
# Avg background error :     -.13
# Error of fit at 95% confidence:
# error c1 = .30965E+09     error b1 =    1.23185
# error c2 = .78859E+09     error b2 =    1.88178
```

Figure 3.1c Rayleigh Scattering Calibration Output for Test #3 with 70% Air and 30% CO_2

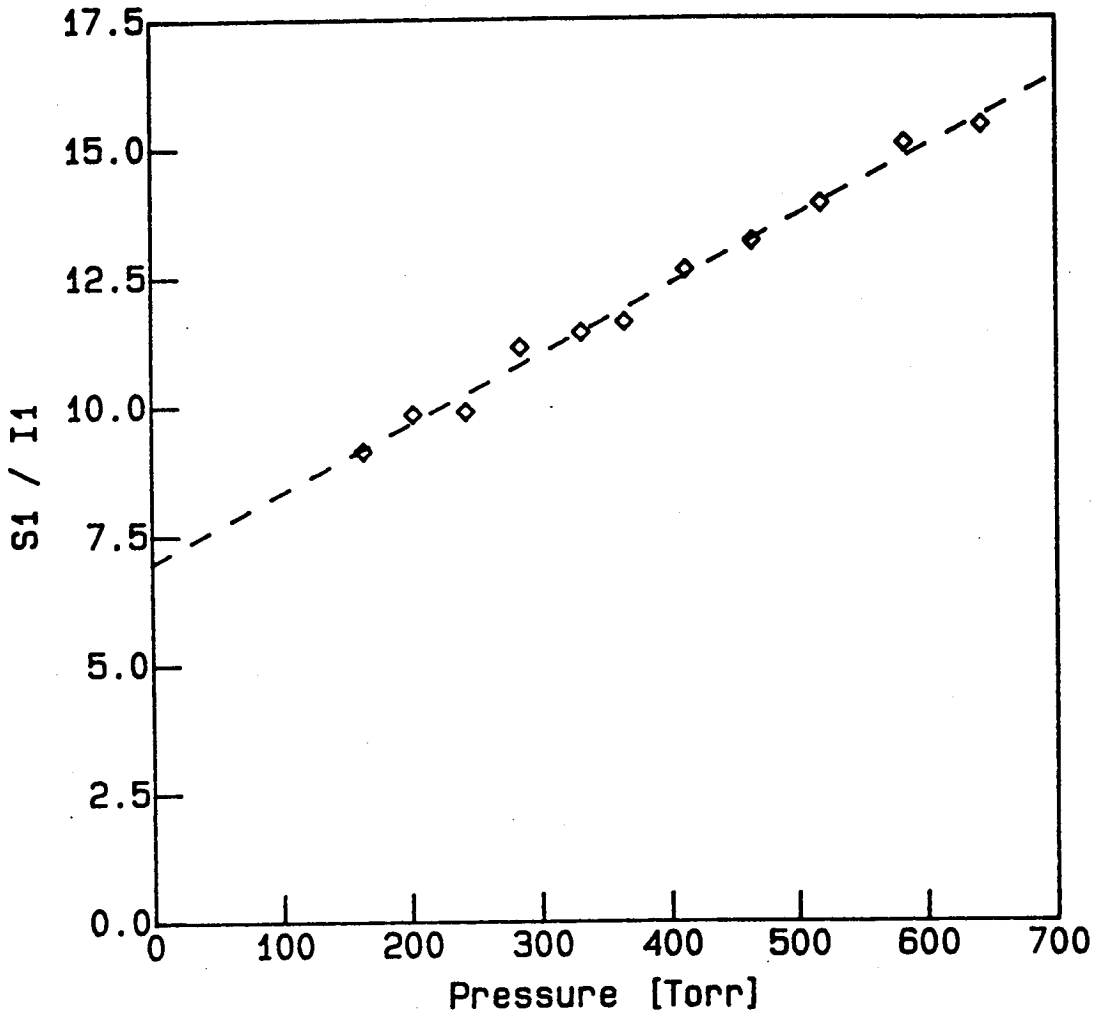

Figure 3.2a Calibration Plot of 510 nm Signal for Test #1

C-2

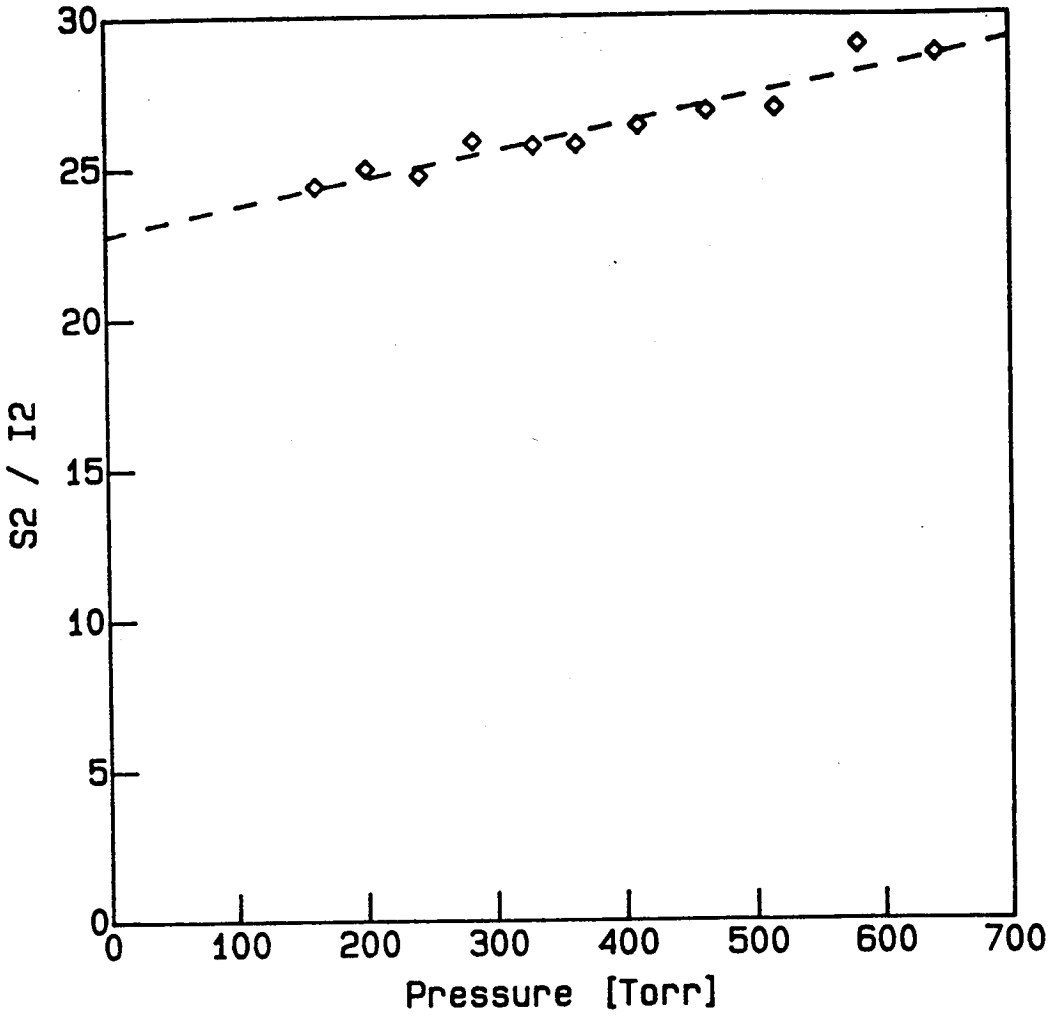

Figure 3.2b Calibration Plot of 578 nm Signal for Test #1

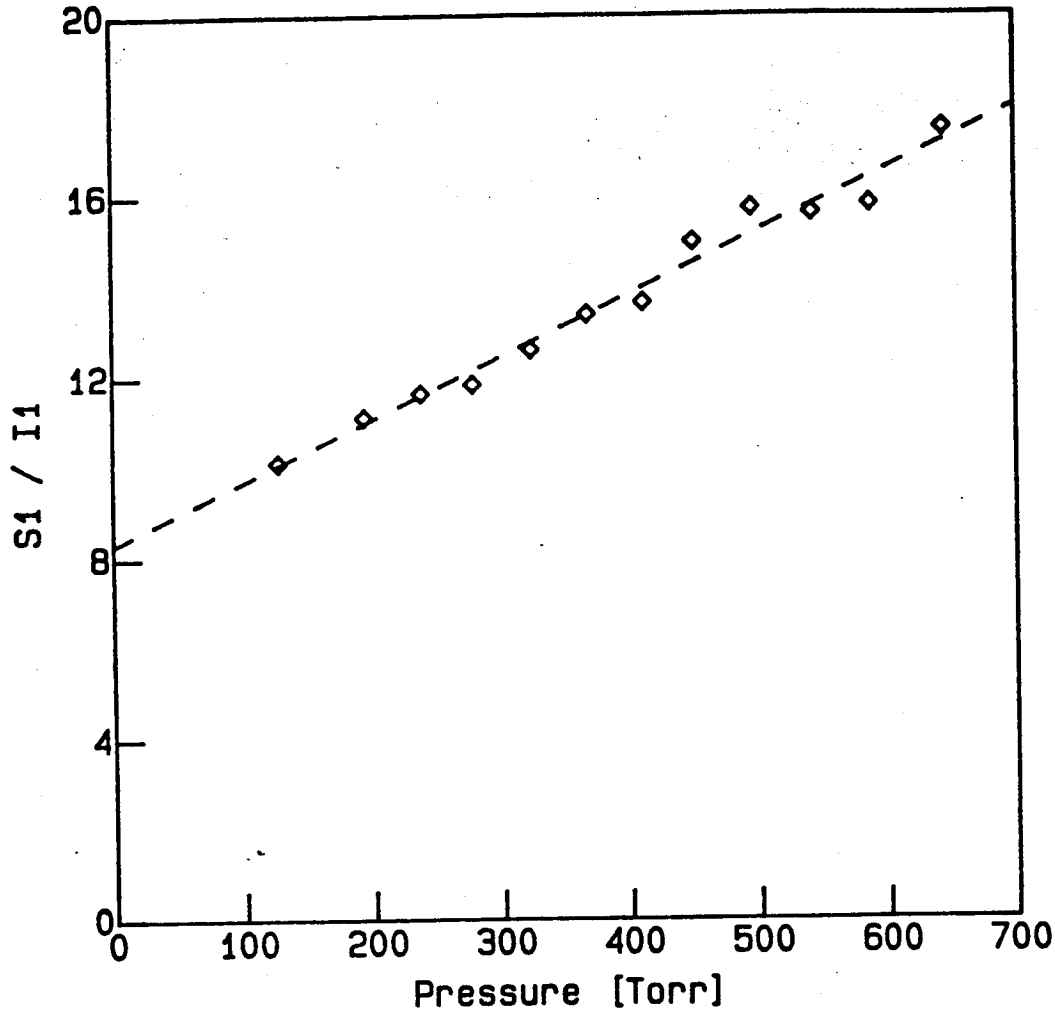

Calibration Data File 325r2.cal

Figure 3.2c Calibration Plot of 510 nm Signal for Test #2

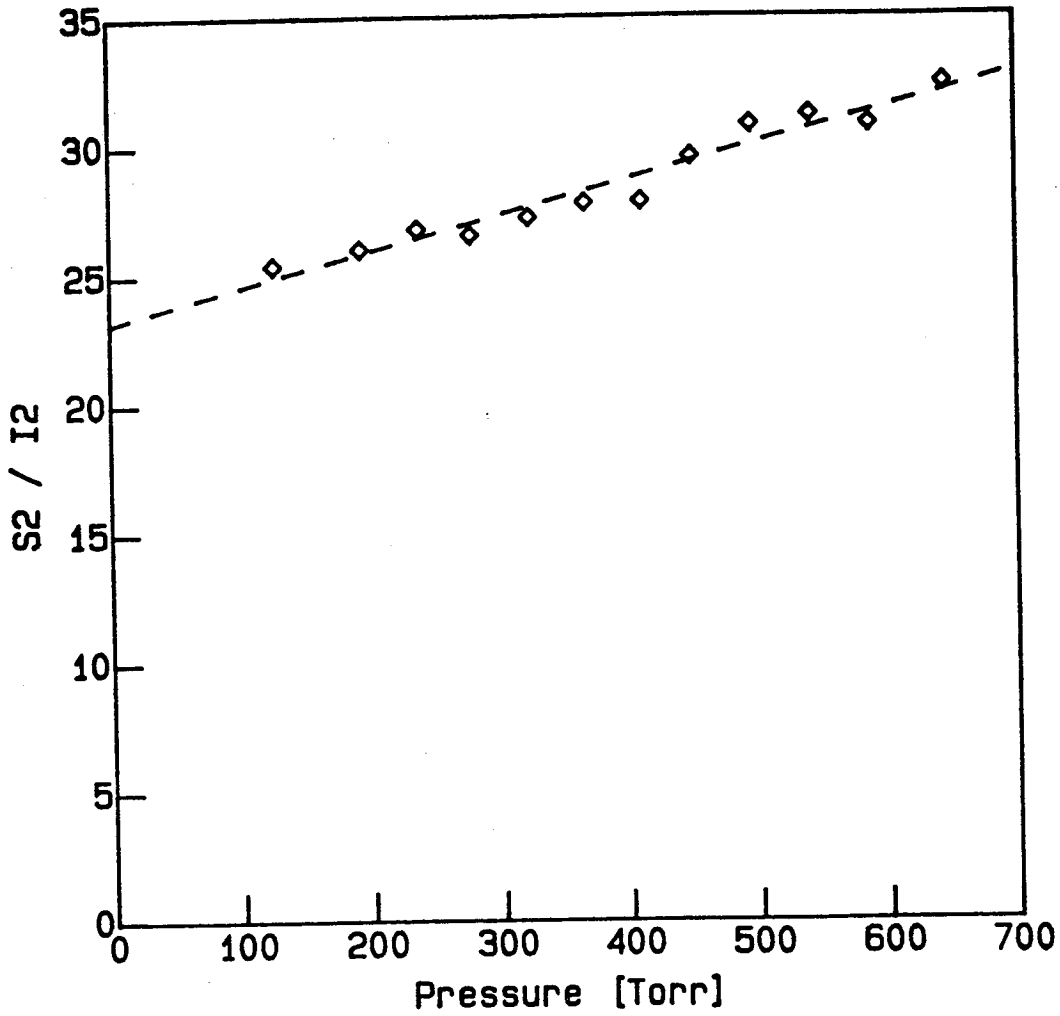

Figure 3.2d Calibration Plot of 578 nm Signal for Test #2

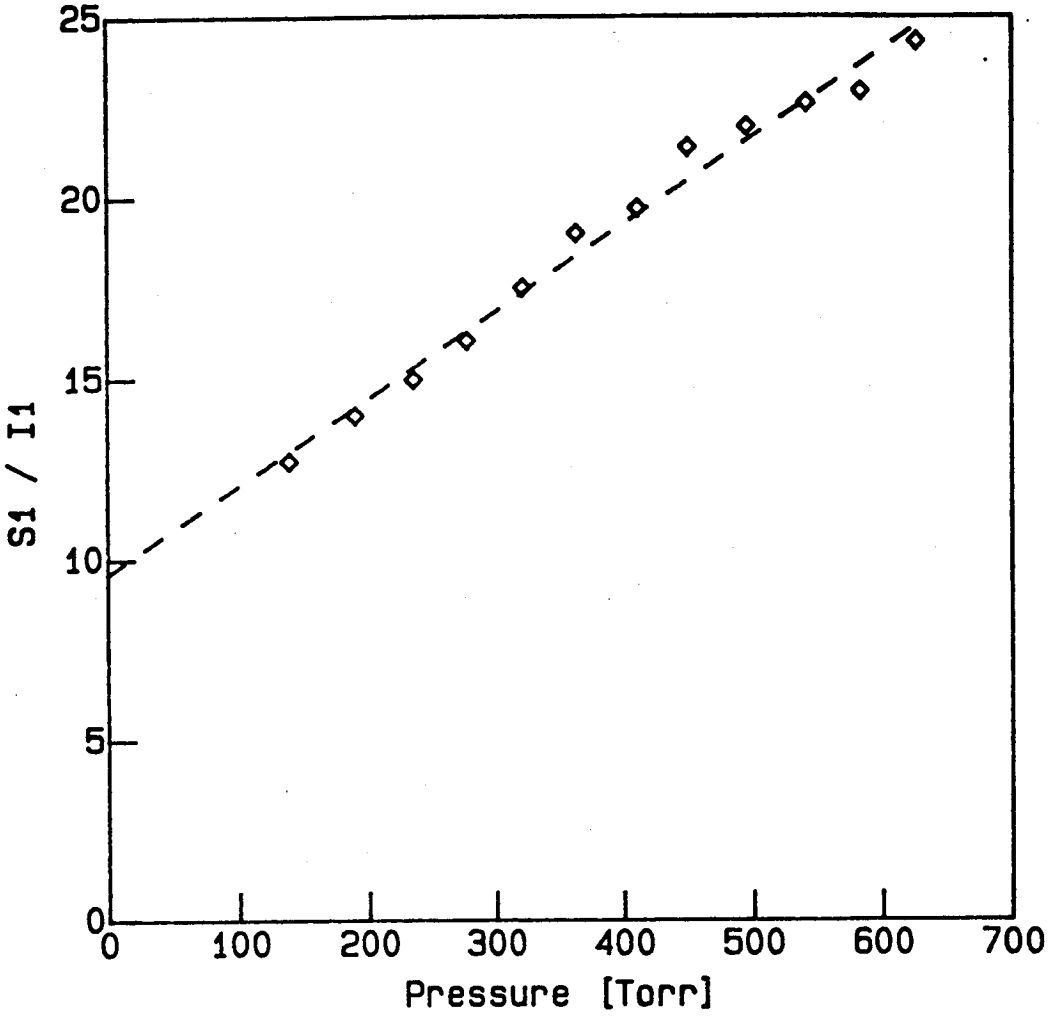

Figure 3.2e Calibration Plot of 510 nm Signal for Test #3

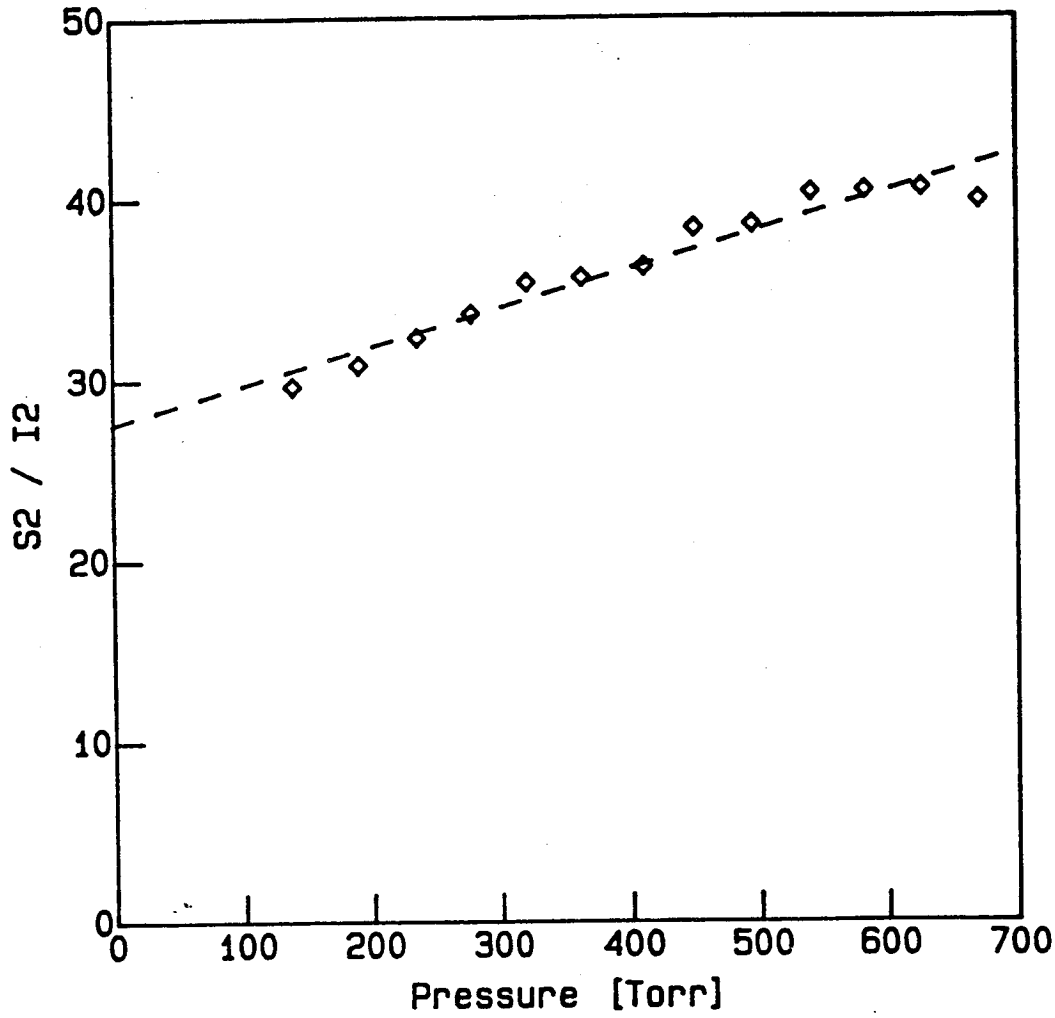

Figure 3.2f Calibration Plot of 578 nm Signal for Test #3

Tests in which particles were blown through the probe volume were also conducted. We found that, in general, particles were detected at the two wavelengths independently, thus requiring the software to examine both signal channels. The software was modified to do this, but an actual experiment testing the algorithm was never carried out. We also found that the computer would not operate with data sets larger than 3000 points. This is a limitation of the Fortran data routine library supplied with the A/D board, and has supposedly been fixed in the new release of the software that is included with this report. The programs must be relinked with the new library in order to fix the problem.

3.2 Surface Scattering Test

The purpose of the surface scattering test, which was conducted in the final days of the RSD system testing, was to characterize the principal sources of surface scattering in the calibration cell. With this information, it could then be determined whether improvements in the probe optics would substantially reduce the level of surface scattering interference and what these improvements may be. The tests consisted of repeated measurements of the Rayleigh scattering and surface scattering signal levels with baffles being inserted and adjusted in the calibration cell to remove possible sources of surface scattered light viewed by the collection optics. This process allowed the major source of surface scattering interference to be identified.

The configuration of the calibration cell for the tests is shown in Figure 3.3 and the results of the surface scattering tests are presented in Table 3.1. The tests started with only the back baffle in place. The purpose of this baffle was to reduce the amount of light scattered from the light trap which illuminates the region of the cell viewed by the collection optics. Rayleigh scattering measurements in the calibration cell performed before the surface scattering test showed roughly the same level of surface scattering, indicating that the back baffle did not initially produce a significant change in the surface scattering level. Adjustments to the position of the back baffle were then made. The only adjustment which produced a reduction in the background level was that of tilting the baffle upwards. As can be determined from Figure 3.3, this would increase the shielding effect of the baffle in

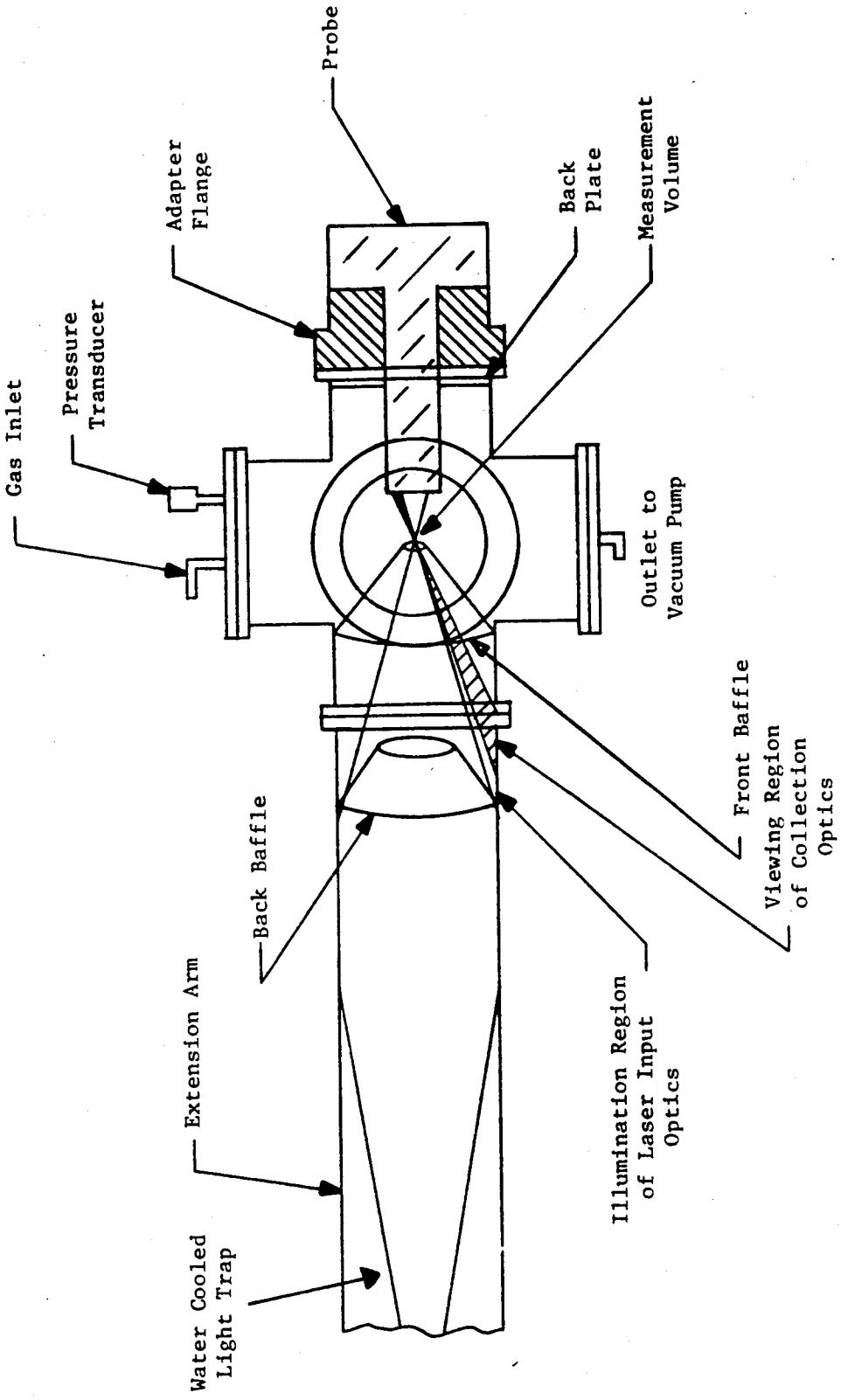

Figure 3.3 Calibration Cell Configuration for Surface Scattering Test

TABLE 3.1

Surface Scattering Characterization Test Summary

Run #	Total Signal mV	Surface Scattering mV	Surface Scattering %	Rayleigh Scattering mV	Rayleigh Scattering %	Rayleigh Surface	Comments
1	140	80	58	60	42	0.75	Back Baffle initially placed
2	140	76	54	64	46	0.84	Back Baffle tilted up
3	136	84	61	52	39	0.62	Back Baffle tilted down
4	138	80	58	58	42	0.73	Back Baffle tilted sideways
5	136	78	57	58	43	0.74	Black Backplate
6	128	64	50	64	50	1.00	Added Front Baffle
7	114	56	49	58	51	1.04	Repositioned Front Baffle
8	106	46	43	60	57	1.30	Tilted Front Baffle up
9	118	66	56	52	44	0.79	Removed Front Baffle
10	124	62	50	62	50	1.00	Replaced Front Baffle
11	126	70	55	56	45	0.80	Enlarged Hole in Front Baffle
12	276	220	80	56	20	0.25	Placed White Strip of Paper in Viewing Path of Collection Optics in front of Back Baffle. Front Baffle was removed

terms of reducing the light trap illumination of the collection optics viewing region. The reduction resulting from this adjustment was small, however. The addition of a black backplate mask over the bright face of the aluminum adapter flange produced an almost negligible improvement. The purpose of the mask was to reduce the amount of light scattered back from the light trap which reflects off the adapter flange and falls on the collection optics viewing region.

The addition of the conical front baffle to the test arrangement produced a relatively significant effect on the surface scattering background level. The function of this baffle was to partially block unfocused laser light from the laser input optical port from illuminating the sides of the extension arm and the collection optics viewing region in particular. Tilting this baffle up, which maximized the blocking effect of the baffle, produces the lowest level of surface scattering interference obtained in the test. Other adjustments only increased the interference level.

The final part of the surface scattering test was the placement of a white piece of paper over the portion of the extension arm viewed by the collection optics. This increased the surface scattering interference level to three times the previous level without the front baffle in place. This confirms that the surface scattered light comes primarily from the viewing region of the collection optics and is not caused by defects in the collection optics which might have caused the optics to view an area directly illuminated by the focused portion of the laser light.

The surface scattering test provides strong evidence that the main source of surface scattered interference is the direct illumination of the collection optics viewing region by stray, unfocused light coming from the laser input optical port. It is believed that this high level of stray light is caused by reflections from the surfaces of the two laser input focusing lenses, although tests have not been conducted which prove this hypothesis. If this belief is correct, then the stray light level can be substantially reduced by coating the laser input optics with a high performance antireflection coating. A factor of 4 reduction in the surface reflection will produce a factor of 16

reduction in the stray light level, which will greatly improve the signal-to-noise level of the Rayleigh scattering measurements.

3.3 Laser/Pinhole and Laser/Fiber Coupling Tests with Unstable Resonator Optics

Two types of tests were carried out to characterize the performance of the laser with the unstable resonator optics. Measurements of the fraction of laser power transmitted through various combinations of pinholes and laser focusing lenses were first performed. Following the pinhole characterization, laser/optical fiber coupling tests were performed in which the fractional power coupled into and transmitted through several different fibers was measured. A third test with the laser was also performed in which a dichroic filter was used to characterize the distribution of energy between the 510 nm and 578 nm lines of the laser. These tests will now be discussed in greater detail.

Pinhole Tests

Pinholes constructed from 0.010 inch brass sheet were used for the pinhole tests. It was found in preliminary tests with the stable resonator optics that commercially available pinholes constructed from 0.0005 inch stainless steel foil were easily damaged by the 20 W copper vapor laser. The brass pinholes were easily made by drilling holes in the brass sheet. Diameters of nominally 250, 400, 500, 600, 800, 1000, and 1300 μm were made.

The results of the pinhole tests were previously presented in Figure 1.3 and are repeated in Figure 3.4. The fractional transmission is presented as a function of d_p/f where d_p is the pinhole diameter and f is the focal length of the laser focusing lens. Use of the quantity d_p/f as the independent variable allows the results from different combinations of pinhole diameters and lens focal lengths to be ideally represented by a single curve. For a transmission of 100%, d_p/f would be equal to the divergence of the laser beam if the beam is characterized by a single divergence, since the focused spot diameter of a laser beam is given (to first order) by the product of the beam divergence, θ_d, and the lens focal length

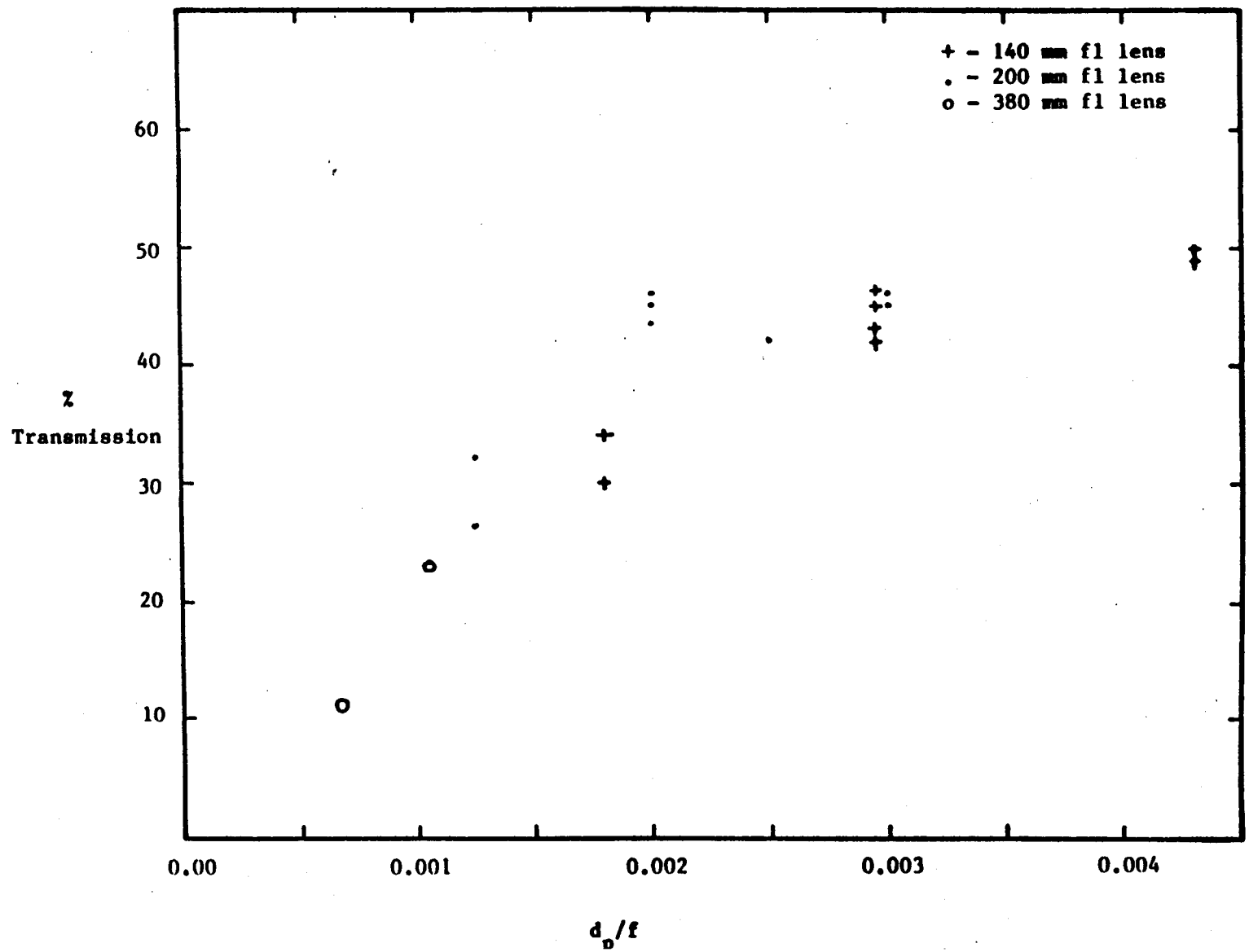

Figure 3.4. Pinhole Test Results for Copper Vapor Laser

$$d_{spot} = f\ \theta_d.$$

The copper vapor laser, however, emits radiation over a distribution of divergences. The d_p/f value at less than 100% transmission represents the largest divergence of the fraction of radiation which is transmitted.

The results of Figure 3.4 show that roughly 30 - 40% of the laser beam is emitted at a relatively low divergence of 1 - 2 mr, while over 50% of the beam is emitted at divergences exceeding 4 mr. This was particularly noticeable in the testing with pinhole/lens combinations having a value of d_p/f greater than 2×10^{-3} since little increase in transmission was obtained as larger pinholes were used. The unstable resonator optics, in comparison with the stable resonator optics, yielded roughly a factor of 2 improvement in the divergence characteristics of the radiation emitted at low divergence based on the pinhole tests. For example, the unstable resonator optics produced 20% power at $\theta_d < 1$ mr, and 40% power at $\theta_d < 1.75$ mr compared with 20% at $\theta_d < 2$ mr, and 40% at $\theta_d < 3.4$ mr for the stable resonator optics.

Several comments should be made regarding the nature of the pinhole tests. Because the detector was rated for a maximum power of 10 W, a screen was placed at the outlet of the laser to attenuate the beam so that the maximum power experienced by the detector was less than 10 W. The screen had a transmission of 34%. The optical setup, then, consisted of the attenuation screen, a focusing lens, a pinhole mounted on an X-Y-Z translation stage, and the calorimeter-type detector (Scientech). The fractional power transmitted by a pinhole is determined by the ratio of the detector power readings with and without the pinhole. Only the pinhole is removed in determining the reference power level. Measurements indicated that the presence of a screen affects the transmission of a pinhole, although contrary to what might be expected, the fractional transmission of a pinhole is greater when a screen is included in the optical system. The results in Figure 3.4, therefore, overstate the actual transmission of the pinholes. The pinholes were visually inspected under a microscope for signs of damage or reduced quality which may have occurred during the pinhole tests and no sign of deterioration was evident. Translation of the pinhole along the optical axis showed little sensitivity of the transmission to the axial position of the pinhole for

displacements of roughly 5 mm about the center of the focused region. This suggests that the transmission should not be affected by the 0.25 mm (0.010") thickness of the pinhole.

Laser/Optical Fiber Coupling Tests

Based on the results of the pinhole tests, the optical configuration of the laser/fiber coupling tests included a 600 μm pinhole placed at, or slightly in front of, the focal point of the laser beam to block the portion of the beam having high divergence. This configuration greatly reduced the amount of laser radiation which fell on the exterior surfaces of the fiber and fiber holder, thus reducing the potential for damage caused by the fraction of the beam which cannot be used. The optical configuration for the laser/fiber coupling test therefore consisted of a 200 mm f1 focusing lens, a 600 μm pinhole mounted on an X-Y-Z translation stage, an X-Y-Z adjustable fiber holder, and a detector. At the start of a test, the pinhole was positioned to maximize the power transmitted by the pinhole. The position of the pinhole along the optical axis was determined by moving the pinhole from the center of the waist toward the lens until a decrease in transmitted power was noted. The fiber was then initially positioned behind the pinhole in line with the center of the pinhole. From this point, the fiber position was adjusted to maximize the power transmitted through the fiber and onto the detector.

Three power measurements were made in the tests to obtain the "relative" coupling efficiency and the absolute coupling efficiency. The relative coupling efficiency is defined as the ratio of the power exiting the fiber to the power transmitted through the 600 μm pinhole. The absolute coupling efficiency is defined as the ratio of the power exiting the fiber to the total laser power. The three power measurements therefore are the total laser power (measured after passing through the laser focusing lens), the power transmitted through the pinhole, and the power exiting the fiber. The first measurement required the use of an attenuation screen since the total laser power was generally in excess of 10 W (the maximum power rating of the detector). Separate measurements in which the total laser power was less than 10 W were used to determine the exact transmission of the attenuation screen. An attenuation screen was not used for the second and third power measurements

since the power was less than 10 W and because the use of a screen or neutral density filter altered the focusing characteristics of the laser beam. (Several measurements of the power transmitted through the pinhole were inadvertently made with a screen before the adverse effects of the screen were realized). The effects of a screen or neutral density filter on the transmission through a pinhole and transmission through a fiber are, paradoxically, opposite. As mentioned in the pinhole tests, the relative transmission through a pinhole was greater when a screen or neutral density filter was used. The presence of a screen increased the relative transmission of a 600 μm pinhole by 36%, while the presence of a metallic-type neutral density filter increased the relative transmission by 33%. On the other hand, the relative coupling of the laser beam into a fiber was substantially reduced when a screen was used, but unaffected by the presence of a neutral density filter. The reduction in relative coupling of the laser beam into a fiber varied from 35% to 65%. The cause of these differing effects of a screen and neutral density filter is unknown. Diffraction is a possible cause, but the diameter of the screen holes is roughly 1000 times the laser wavelength (0.5 mm vs. 0.5 μm) so diffraction effects should be small. Quite possibly, these effects are due to some peculiar characteristics of the Cu vapor laser beam.

The results of the laser/optical fiber coupling tests are summarized in Table 3.2. Two fiber diameters and three fiber manufacturers were evaluated in the tests. Since the probe is designed to use 200 μm core diameter fibers, this size was emphasized in the testing. (It should be noted that the General Fiber Optics fiber used in these tests is not the same type of fiber as the laser input fiber, since the latter fiber was obtained after the tests were performed). The "maximum power" entry in Table 3.2 is the maximum power exiting the fiber during the test, but does not necessarily represent the maximum power capability of the fiber since the laser was not operated at maximum power for most of the tests. (The total laser power can be determined by dividing the maximum power entry by the absolute coupling entry). The maximum power capability of a fiber is strongly influenced by the quality of the cleaved surface of the fiber, so the same fiber can exhibit different power capabilities due to differences in surface quality. This point is illustrated by the results with the EOTec 200 μm fiber in which the power

TABLE 3.2

Summary of Laser/Fiber Coupling Tests

Fiber	Maximum Power	Relative Coupling	Absolute Coupling	Comments
General Fiber Optics, 200μm (4 m length)	3.8 W	92% - 72%	30% (est)	Decrease in Relative Coupling was probably due to laser damage
	5.3 W	98%	40%	Fiber showed evidence of Laser Damage after Test
Diaguide, 200μm (3 m length)	4.5 W	99%	30% (est)	Fiber was not inspected after test
	3.5 W	78%	37%	254 mm focusing lens was used.
	6.5 W - 6.0 W	60%	35%	254 mm lens was used. Fiber showed evidence of Laser Damage after test
	4.0 W	67%	25%	254 mm lens was used. Laser Rep Rate = 10 kHz. Surface Pitting was evident after test
EOTec, 200μm (1.5 m length)	1.8 W	50%	15% (est)	Fiber surface had some defects due to cleaving procedure
	3.3 W	90%	30% (est)	Same fiber as above test but with newly cleaved surface
Diaguide, 400μm (1.5 m length)	6.5 W	150%	45%	Fiber was not inspected after test
EOTec, 400μm (1.5 m length)	6.6 W	150% (est)	42%	Fiber was not inspected after test

through the fiber was nearly doubled by improving the surface quality of the laser input end of the fiber. In several tests, the absolute coupling efficiency was not determined directly because a measurement of the laser power without a pinhole was not performed. Estimated values are given instead and denoted by "est".

Several results and observations from the fiber coupling tests merit discussion. The first is that the maximum power capability of the 200 μm core fibers appears to be on the order of 5 to 6 W. The Diaguide 200 μm fiber briefly transmitted 6.5 W before dropping off to 6.0 W. The drop off was probably caused by laser damage to the fiber surface. After the test, the laser input surface of the fiber was found to be chipped on one side, with bubbles or pits in the region between the core and cladding on the side opposite from the chip. The peak laser flux on the fiber corresponding to 6.5 W, a 6 kHz pulse rate and 25 ns pulse width is 1.4 MW/mm^2, which is above the limit of 1 MW/mm^2 quoted by one fiber manufacturer. Since other fiber manufacturers quote limits of 10 MW/mm^2, the maximum power limit of the fiber may be higher under ideal conditions - uniform flux on the fiber surface, a perfectly cleaved surface, and a particulate free atmosphere. It should be pointed out, however, that even if a 200 μm fiber were capable of accepting greater power, it may not be possible to couple more than 35% of the total laser power into the fiber due to the divergence characteristics of the laser.

A second observation which can be drawn from the tests is that the use of a 400 μm fiber results in an increased coupling efficiency, but the increase is not proportional to the increase in fiber surface area. This indicates that the beam profile at the focused laser beam waist has a small diameter region of high intensity, with the intensity rapidly falling off outside of this region. The relatively small increase in absolute coupling efficiency of the 400 μm fiber over the 200 μm fiber also supports the suggestion in the previous paragraph that the power capacity of a 200 μm fiber may be limited to 35% of the total laser power by the divergence characteristics. This limit on the coupling efficiency will actually be a function of the focal length of the laser focusing lens. A shorter focal length will result in a higher coupling efficiency, but will also increase the intensity of the small central region of the beam and increase the probability for laser damage. A longer focal

length lens will reduce the numerical aperture with which the beam is coupled into the fiber, which is desirable for the probe optical design, but result in a lower coupling efficiency.

A third point observed in the laser/fiber coupling tests is that the numerical aperture (N.A.) of the laser light exiting the fiber is greater than the N.A. with which the laser beam was coupled into the fiber, but substantially less than the fiber N.A.. The numerical aperture of the light exiting the 200 μm fibers was approximately 0.13, while the input N.A. was 0.08 and the fiber N.A. was 0.20. The N.A. of the light exiting the fiber was determined by measuring the diameter of the bright spot on a target at a known distance from the fiber end. A very low intensity spot could also be detected on the target. This spot roughly corresponds to light which exits at the N.A. of the fiber. For the 400 μm core diameter fibers, the numerical aperture of the light exiting the fiber was measured to be 0.09 and 0.11 for the Diaguide and EOTec fibers respectively, while the input N.A. and fiber N.A. were the same as for the 200 μm fibers. The exact reason for the lower effective N.A. of the 400 μm fibers is uncertain. One possible cause is that the greater stiffness of the 400 μm fibers resulted in their assuming a greater radius of curvature along the path between the laser input and the detector. This increased radius over the 200 μm fibers produced less bending of the light inside the fiber. Care was taken in the tests to avoid tightly bending the fibers, but differences in the radius of curvature between the 200 μm and 400 μm fibers could have existed.

In the fiber tests conducted to date, no evidence has been found of laser damage to the output end of the fiber. This is significant since the output end of the fiber will be mounted in the probe and will be relatively difficult to repair if damaged. The laser input end, on the other hand, will be quite accessible and relatively easy to repair if damaged. The quality of the output end of the fiber was found to affect both the coupling efficiency of the fiber, and the quality of the output beam. One 200 μm fiber (General Fiber Optics) which was tested had a cleaved input surface and a "micropolished" output surface. The coupling efficiency of this fiber was 50% less than that of the same fiber after the "micropolished" surface was replaced by a cleaved surface. In addition, the edge of the bright spot with

the micropolished surface was not distinct, while the edge of the bright spot with the cleaved surface was very sharp.

Laser Tests With Dichroic Filter

A test was performed with a dichroic filter to characterize the relative power emitted on the 510 nm and 578 nm lines as a function of the laser tube pressure. The tests were run using a laser pulse rate of 6 kHz and a screen (34% transmission) to reduce the laser beam intensity to the range acceptable by the laser power detector. The results of the test are shown in Table 3.3. The entry $I_{510+578}$ is the sum of the power measured individually on the 510 nm and 578 nm lines. Measurements were also made of the total laser power without the dichroic filter and were, to within the resolution of the power meter, equal to the sum of the measurements on the individual lines. Thus, the dichroic filter separates the lines with no noticeable loss in power. The results in Table 2 bear out the general statements of the laser manufacturer: that the power split between the 510 nm and 578 nm is roughly 2/3 and 1/3 respectively; and that the fraction of power on the 578 nm line increases with pressure.

Measurements made just after the lasing action was initiated show a higher fraction of power on the 510 nm line. This is due to the laser tube being relatively cool, which favors the 510 nm line. After the laser reached steady state operating conditions (~15 minutes), the split was close to the manufacturer's specification. The main factor governing the split between the two lines is the tube temperature, with the 510 nm line being favored by cool temperatures and the 578 nm line being favored by higher temperatures. Since the tube temperature increases as the pressure in the tube is increased (due to a lower neon flow rate), the fraction of power emitted at the 578 nm line increases with pressure. It should be noted, however, that as the pressure is increased, the total power emitted on the 510 nm line also increases. This increase, however, is relatively not as great as the increase on the 578 nm line, thus resulting in an increase in the fraction of power at the 578 nm line. The measurements indicate that for maximum power, both overall and on the 510 nm line, the laser should be run at 40 torr (the upper limit of the recommended pressure range of the Cu vapor laser). One other point to note in

TABLE 3.3

Spectral Characteristics of the Copper Vapor Laser+

Pressure (torr)	I_{510} (W)	I_{578} (W)	$I_{510+578}$ (W)	I_{510}/I_{tot}	Comments
24	1.35	0.30	1.65	0.82	Measured just after Lasing Action Commenced
24	2.55	1.35	3.90	0.65	
24	2.8	1.5	4.3	0.65	
24	2.7	1.5	4.2	0.64	Neon flow rate was increased for this measurement only
20	2.6	1.3	3.9	0.67	
25	2.65	1.4	4.05	0.65	
29	2.7	1.6	4.3	0.63	
37	2.9	1.75	4.65	0.62	
42	3.2	2.1	5.3	0.60	
24	2.85	1.8	4.65	0.61	

+ A 34% transmission screen was used for these measurements.

the test results is that the fraction of power on the 510 nm line remains low after the pressure in the tube is lowered from 42 torr to 24 torr. This is due to the fact that the tube cools down very slowly, and therefore is still at a relatively high temperature at the time that the measurement was taken.

Power measurements on the 510 nm and 578 nm lines were also taken after focusing the beam through 250 μm, 400 μm, and 600 μm pinholes. The measurements showed that the power distribution between the two lines is unchanged by focusing the beam through a pinhole.

IV. RECOMMENDATIONS

The Rayleigh scattering diagnostic system as delivered to NASA represents the system as initially designed. The RSD system does not contain modifications which were identified during the testing process as being desirable or necessary to improve the performance of the system. This section presents recommendations for both necessary and optional modifications to the RSD system and for further tests which would allow a better characterization and improvement of the system's performance.

This section is organized into three parts - recommendations for improving the precision and accuracy of the RSD system, recommendations for improving or increasing the capabilities of the RSD system, and recommendations for additional system tests. Modifications to some components such as the laser input optics are suggested in both the first and second parts, so any changes made in these components should be done in light of the suggestions in both parts.

4.1 Recommendations for Improving Measurement Precision and Accuracy

Power Monitor Electronics

The power monitor gated integrators, as discussed in section 3.1, have a precision of 10% as opposed to a precision of 1% for the SRS gated integrators and other electronics. This relative lack of precision could be due to greater susceptibility to RF interference, poor grounding, a bad component, or simply a limitation in the design of the Evans Electronics boards. Since the power monitor signals for both the 510 nm and 578 nm lines have low precision, the problem is probably not a bad component. Grounding is also not believed to be the source of the problem. The cause of the poor precision of the Evans Electronics boards should either be found and corrected, or the boards should be replaced by more reliable, high precision gated integrators. SRS gated integrators may be "overkill" for use as power monitor gated integrators, but they have been proven acceptable for the system.

Reduction of Interference from Surface Scattered Light

The main source of interference due to surface scattered light in the calibration cell is the direct illumination of surfaces in the collection optics viewing region by unfocused light from the laser input optical port. (Refer to section 3.2 for a complete discussion). This will remain to be the primary source of surface scattering interference for all applications in which the focused laser beam is effectively suppressed. Therefore, for applications in which surfaces close to the probe are viewed by the collection optics, measures should be taken to substantially reduce the level of unfocused light originating from the laser input optical port. (For applications having only distant surfaces, the surface scattering interference may be acceptably small).

The obvious measure to be taken to reduce the surface scattering interference due to unfocused laser light is to antireflection coat the laser input lenses. Before this is done, however, it is recommended that the reflectivity of the lenses be measured so that an assessment of the reduction to be obtained by a more efficient coating can be made.

A second measure which could be taken in addition to the antireflection coating is to reduce the size of the collection optical fiber. A reduction in size (core diameter) will reduce the area viewed by the collection optics and thus reduce the scattered light interference. This will have only a small effect, however, and will have other ramifications. A reduction in the collection fiber size will reduce both the interaction distance in the measurement volume and the measurement volume size. Thus, the Rayleigh scattering signal will be reduced but the spatial resolution and ability to tolerate particles will be increased. The sensitivity to misalignment will also be increased. In light of these additional effects, a reduction in the collection fiber diameter should not be considered for reducing scattered light interference alone, but should be done in concert with desired changes in other system characteristics.

Modifications to Increase Rayleigh Scattering Signal Level

The main limitation on the precision of the Rayleigh scattering temperature or density measurement is, as discussed in section 3.1, the low level of the Rayleigh scattering signal. Typical signal levels on the 510 nm line were 50 - 100 photoelectrons per laser pulse. While the final design of the collection optics resulted in a loss of collection solid angle due to vignetting, the primary cause of the lower signal level is the low level of laser power being transmitted through the laser input fiber. While 6 W of laser power was transmitted through fibers 3 to 4 m in length (see section 3.2), only 1 W was transmitted through a 10 m fiber. It should be noted that this 1 W maximum transmitted power was obtained with both the Diaguide and General Fiber Optics 10 m fibers, indicating that the transmission loss was not peculiar to one fiber.

Additional laser/fiber coupling tests should be performed before modifications are made to the RSD system to address the transmission loss problem. One reason which has been suggested to account for the transmission loss is that most of the power being coupled into the fiber is actually coupled into the cladding, which is capable of carrying the power over short distances but not over long distances. This is an unlikely probability, since the light emerging from both the short and long lengths of fibers formed a bright central spot with a distinct edge. A test of this theory would be, however, to use a shorter focal length lens (e.g. 100 - 150 mm) to focus the light into the fiber. While producing a smaller spot size, the shorter focal length lens will also increase the probability of damaging the fiber. A more likely reason for the transmission loss is the presence of nonlinear processes in the fiber. These processes may be reduced be either reducing the input laser power, increasing the fiber diameter, decreasing the fiber length, or some combination of the three. One method of reducing the input laser power is to use a longer focal length lens for focusing the laser beam. While increasing the focused spot size and thus reducing the power coupled into the fiber, it will also reduce the divergence of the beam being coupled into the fiber - a potentially positive effect. A second method of reducing the laser power is to run the laser at a lower input power (2800 - 3200 W). If the transmission loss mechanism is highly nonlinear, a reduction in input power

may at some point lead to an increase in transmission. Since this effect would probably be accompanied by hysteresis, the test should be performed with increasing, rather than decreasing, power levels.

Tests characterizing the fiber length vs. transmission loss characteristics should start with the longest length of fiber anticipated being used, and should possibly be performed in conjunction with additional input power variation tests. Since the General Fiber Optics and Diaguide fibers exhibited the same degree of transmission loss with 10 m fibers, Diaguide fibers should be used in the tests since they are inexpensive and readily available. Transmission loss vs. fiber length tests should be performed for both 200 μm and 400 μm core diameter fibers. These tests will identify the best combination of fiber length, core diameter, and input power for the RSD system.

Of the above measures to reduce the power transmission loss, the change which will have the greatest impact on the RSD system is an increase in the laser input fiber diameter. A change to 400 μm, the next standard core diameter size, will at least double the measurement volume size. Unless a special, low NA 400 μm core fiber were obtained, the change will also result in an increase of the input fiber NA to ~0.20 from 0.13. If the fiber-to-lens distance is decreased so that the laser light emitted from the fiber does not overfill the laser input lenses, the focused spot diameter at the measurement volume will increase further. The laser input lens closest to the fiber will also have to be replaced so that the focal length matches the new fiber-to-lens distance. If the fiber-to-lens distance is not decreased to handle the higher fiber NA, then the laser input lens will be overfilled, causing an increase in the unfocused laser light being emitted from the laser input optical port. This will most likely increase the surface scattering interference and adversely affect the measurement precision. Black anodizing the laser input lens tube plug will help to reduce the increase in surface scattering.

4.2 Recommendations for Improving the Capabilities of the RSD System

Modifications to Increase the Standoff Distance

A limitation of the Rayleigh scattering probe, as currently designed, is that the standoff distance (distance from the end of the probe to the measurement volume) is only 25 mm (1"). This value was a result of the trade offs discussed briefly in section 1.7.2.1.1 and more completely in Appendix A. Generally, an increased standoff distance is obtained at the cost of a lower spatial resolution and tolerance for particles and a lower Rayleigh scattering signal. However, since the current laser input fiber NA results in the laser input lenses being underfilled and the lenses are set back an extra 3.5 mm from the probe face, the standoff distance can be increased by 50% without decreasing the spatial resolution or overfilling the laser input lenses. This modification would require laser input lenses with a back focal length 10 mm greater than the current lenses, or 43 mm, and the repositioning of the 3.5 mm spacer from the front of the laser input assembly to the rear of the assembly. In addition, the canted lens and wedge of the collection optics will need to be replaced to match the new measurement volume location. While the Rayleigh scattering signal will be lower with this increased standoff distance, the reduction will be partially offset by the reduced degree of vignetting of the collection optics and the longer interaction length in the measurement volume.

Further increases in the standoff distance will require, for the same focused laser spot size, either a laser input fiber NA lower than 0.13 or overfilling the laser input lenses. If the spot size were allowed to increase, the standoff distance could be increased without overfilling the lenses. This latter option may be preferable if the measurement environment is known to be relatively "particle free".

Modifications to Increase the Spatial Resolution and Reduce Sensitivity to Particles

Reductions in the measurement volume size to increase the spatial resolution and reduce the sensitivity to particles can be accomplished by reducing the images of the laser input and collection fiber ends at the

measurement volume, by reducing the optical aberrations, or by a combination of both. The best approach to reducing the aberrations is to use either best form or achromat lenses for the optics. Achromat lenses should be avoided if the probe is to be used in an environment having a high temperature blackbody background. Before modifications to reduce the size of the fiber images in the measurement volume are undertaken, an analysis should be performed to ensure that aberrations are not a limiting factor in determining the spatial resolution.

The images of the fiber ends at the measurement volume can be reduced by selecting the focal lengths of the optics to demagnify the fibers. In the case of the collection fiber, the fiber image can also be reduced by reducing the fiber diameter (an option not available to the laser input fiber because of the high energy density in this fiber). The problem facing a reduction in the input fiber image is that it either requires overfilling the lenses, which causes other problems, or using a fiber having an NA lower than 0.13. A reduction in the collection fiber image alone, while reducing the measurement volume size, will also reduce the Rayleigh scattering signal level. The portion of the focused laser beam which is not observed by the collection fiber is effectively wasted laser power. This may be an acceptable trade off for some applications, but it is not without drawbacks.

Preliminary SSME Probe Specifications

Several significant differences exist between the requirements for a probe which is to be used in a general combustion application and a probe which is to be used on a SSME test engine. The probe for the SSME application must be approximately 11 mm in diameter, but does not require a small measurement volume since the particulate loading will be very low. This latter factor along with the very high gas density present in the SSME allow a probe diameter of 11 mm to be designed more easily than the probe constructed in the present effort.

For the preliminary calculations, a focused laser spot size of 1 mm, a standoff distance of 40 mm, a laser input fiber core diameter of 200 microns, and a fiber numerical aperture of 0.20 have been selected. These values

require an input lens clear aperture of 3.2 mm. If a probe design similar to the present probe is used, an 11 mm probe could be obtained by using a diameter of 4.0 mm for both the input and collection optical ports and a separation of 1.0 mm between the ports. For a collection lens clear aperture of 3.0 mm, a collection solid angle of approximately 4.4×10^{-3} sr is obtained. The interaction length which results from the above specifications is approximately 8.0 mm.

For a mixture of 87.5% H_2 and 12.5% H_2O, the differential Rayleigh scattering cross section is $\langle\sigma\rangle = 2.02 \times 10^{-28}$ cm^2 at 510 nm. The number density at the fuel preburner conditions of 5500 psia and 970 K is 2.84×10^{21} cm^{-3}. The values of η, ε_1, ε_2, and ε_3 (refer to Appendix G) are assumed to be 0.17, 0.20, 0.67, and 0.82, respectively.

The signal intensity which is calculated from the above parameters is 2.6×10^5 counts/pulse at a 5 kHz laser pulse rate and 6.85×10^{15} photons/pulse at 510 nm. The precision of a measurement with this signal intensity is 0.2%. This signal intensity is very large and allows much room for trade offs in the probe design, such as reducing the interaction length by reducing the focused beam spot diameter, while still maintaining a high level of precision. In addition, because the Rayleigh scattering signal is very large owing to the high density, the relative interference from surface scattering will most likely be much reduced.

4.3 Recommended Tests for Additional System Characterization

Two main tests are recommended for further characterizing the performance of the RSD system. One test is the characterization of the system performance in the presence of particles. This test can be performed in the calibration cell using several approaches. A very simple approach used in the final testing of the RSD system was to direct a stream of ambient air through the cell at atmospheric pressure (with the top flange of the cell removed). This procedure tests the ability of the RSD system to reject particles - it actually pointed out a flaw in the particle rejection software which was later addressed but not retested - but it does not quantitatively characterize the

ability of the system to handle particles since the particle size distribution and number density are unknown. A more quantitative approach is to direct a stream of known number density and particle size distribution (or preferably, several tests with monotonic size distributions) through the measurement volume in the calibration cell. A top flange assembly for the calibration cell is provided which directs a central particle stream and a shroud stream through the center of the calibration cell. An outlet flange providing a fitting which can be connected to an exhaust source such as a vacuum cleaner is also provided. An approximate characterization can be performed with this apparatus if the number density in the input particle stream is known. Of particular interest from this test will be the ability of the RSD system to reject particles at high particle number densities as a function of particle size, and the resultant accuracy and precision of the measurements. A further valuable piece of information which can be obtained from the tests is whether the ratio of 510 nm to 578 nm signal can be used in addition to the absolute magnitude of the signals to reject particles. This may be particularly important in rejecting smaller particles or particles which pass through the edge of the measurement volume.

The second main test which can be performed to better characterize the RSD system is a test of the accuracy of the probe power monitor concept. The primary question is whether the light signal transmitted through the power monitor fiber is proportional to the laser input power on both the 510 nm and 578 nm lines. This test can be performed in a straightforward manner by setting up the calibration cell to allow for the detection of the Rayleigh scattering signal at 90°, as discussed in section 1.8. By observing the variation of both the 90° Rayleigh scattering signal and the probe power monitor signal with a variation in input laser power, the ability of the power monitor subsystem to accurately yield the relative laser power can be determined. While not necessarily required for the RSD system to yield accurate results, the ability of the power monitor subsystem to accurately determine the absolute laser power is also of great interest. An aspect of the power monitor subsystem which may be very important for the ability of the RSD system to yield accurate absolute values of density and temperature, is the sensitivity of the power monitor signal to adjustments in the laser input

fiber position. If the power monitor signal is sensitive to these adjustments, then the RSD system will accurately yield only relative values for density and temperature unless the fiber position remains untouched after the system calibration prior to a measurement. The above power monitor test will also allow the present or revised power monitor gated integrators to be checked out, the need for which was discussed earlier in section 4.1.

Several other smaller tests should be performed since they were not performed in the RSD system development or testing activities. The dependence of the spectral transmittance and reflectance of the dichroic filters used in the Rayleigh scattering and power monitor detector optical systems needs to be determined. The 35° angle of incidence currently used in the detector arrangements is based on a 10% shift to shorter wavelengths at a 45° angle of incidence which was quoted by Corion. A measurement of the spectral characteristics as a function of the angle of incidence will allow the optimum angle to be determined. A second test which should be performed to better characterize the performance of the SRS gated integrators is to determine the value of the residual remaining from the previous sample. A maximum value of 5% is specified by SRS. The actual value may be important in determining the accuracy of measurements with high particle loadings. Since the presence of a particle in the measurement volume will usually produce a large signal, the succeeding measurement may be contaminated if the residual is as high as 5%. Thus, knowledge of the actual value of the residual will be important in further refinements of the data reduction software to handle particles.

APPENDIX A

PROBE OPTICAL DESIGN TRADE OFFS

The selection of 25.4 mm as the outer diameter of the probe places significant constraints on the optical design of the probe. The probe design allows 18.65 mm for the sum of the clear apertures for the input and collection lenses. This available clear aperture distance must be divided between the input and the output lenses based on considerations which include maximizing the Rayleigh scattering signal, minimizing interference by surface scattered light, and minimizing interference due to presence of particulates. A discussion of the factors influencing the design of the input and collection optics will first be presented, followed by a discussion of the trade offs in the optical design.

The characteristics which are desirable for the input optics are a small diameter, the ability of the optics to focus to a small spot size all of the laser light exiting the fiber, and the ability to focus the laser light at least one inch, and preferably several inches, from the front of the probe. These characteristics are interrelated by the following formula:

$$D_{lens} = \frac{2\ N.A.\ L_{standoff}\ D_{optical\ fiber}}{D_{spot}}$$

where D_{lens} = clear aperture of the input lens

$L_{standoff}$ = standoff distance of the measurement volume from the lens

N.A. = numerical aperture of the optical fiber

$D_{optical\ fiber}$ = core diameter of the optical fiber

and D_{spot} = diameter of the focused laser beam in the measurement volume

It can be seen that the desirable characteristics of a small D_{lens}, a small D_{spot}, and a large $L_{standoff}$ all conflict with each other. The two remaining parameters which can be selected to achieve the desirable characteristics to the extent possible, are the fiber numerical aperture and diameter. However, constraints exist on the selection of both the fiber diameter and the numerical aperture.

The constraint on the fiber diameter is the energy density threshold for damage to the fiber surface. Recommendations from fiber manufacturers vary significantly on the value of this constraint. At the low end, Fiberguide Industries states a damage threshold limit of 1 MW/mm^2 based on the peak pulse power, while at the high end, General Fiber Optics states a limit of 11 MW/mm^2. Both of these limits are for silica core/silica clad fibers. For a copper vapor laser power of 20 W, a pulse rate of 5 kHz, and a pulse width of 25 ns, the peak pulse power is 160 kW. This corresponds to a minimum fiber core diameter of 450 microns for the low damage threshold value and 135 microns for the high value. This introduces over a factor of 3 uncertainty into the selection of the lens diameter, standoff distance, and focused spot size. Tests with 200 micron core diameter fibers showed occasional signs of laser damage, suggesting that the damage threshold was between these two values, but probably towards the high end.

The constaint on the numerical aperture of the fiber is primarily one of availability, although limits imposed by the divergence of the laser beam also come into play. The lowest numerical aperture of standard commercially available fibers is 0.18, with many manufacturers having slightly higher values of 0.20 to 0.22. (Fibers having a core diameter of 50 to 100 μm are available with numerical apertures of 0.11 to 0.14, but these will not meet the energy density constraint). Usually at a significantly higher cost, fibers can be specially made with a numerical aperture as low as 0.10, but the energy damage threshold of these fibers cannot be tested in advance. The laser beam divergence may pose an additional limit on the numerical aperture of the fiber since the fiber N.A. must be equal to or greater than the N.A. of the lens which focuses the light into the fiber.

The characteristics which are desirable for the collection optics are a large collection solid angle and an optical design which minimizes the collection of stray light. The collection solid angle is directly affected by the input optics design and must be determined in an analysis of the trade offs in the optical design of the probe. The consideration of minimizing the collection of stray light involves matching both the image diameter of the measurement volume to the core diameter of the fiber, and the effective F# of the lens to the numerical aperture of the fiber. The formula which can be derived from the condition of matching the image and fiber diameters is:

$$S_{output} = S_{input} \frac{D_{optical\ fiber}}{D_{spot}}$$

where S_{input} = distance from measurement volume to collection lens

S_{output} = distance from collection lens to optical fiber

and D_{spot} = diameter of the focused laser beam in the measurement volume

The required collection lens focal length can be obtained from the relation

$$fl = \frac{1}{\frac{1}{S_{input}} + \frac{1}{S_{output}}}$$

By matching the fiber and image diameters, only the light which originates from, or passes through, the measurement volume will directly reach the fiber. Stray light can enter the fiber if this matching condition is met, but only by being reflected off of the interior surface of the lens tube.

The condition of matching the effective F# of the collection lens to the fiber numerical aperture also reduces the amount of stray light which enters the collection fiber. The relation which can be derived from this matching condition is

$$D_{lens} = 2 \text{ N.A. } S_{output}$$

where D_{lens} = clear aperture of the collection lens

By matching the collection lens F# and the fiber N.A., only light which passes through the collection lens can be transmitted by the fiber. This eliminates the collection of stray light which is reflected off the interior surface of the lens tube. Thus, by matching the image and fiber diameters as well as the effective lens F# and fiber N.A. only stray light which passes through the measurement volume can be accepted by the collection fiber. However, it may not be possible or desirable to meet both matching conditions due to the constraints this would impose on the overall optical design of the probe. (Specification of the parameters D_{lens}, S_{input}, and D_{spot} also affects the input optical design. In addition, only discrete values of N.A. and $D_{optical}$ fiber are available). The consideration of minimizing the collection of stray light is then also involved in the optical design trade off analysis.

The optical design of the probe requires trade offs among the considerations of maximizing the Rayleigh scattering signal, minimizing the collection of scattered light, reducing interference due to scattering by particulates, and increasing the standoff distance. Table A.1 illustrates the trade offs in the input optical design in which the input lens clear aperture is given as a function of the standoff distance, focused laser beam spot size, input fiber numerical aperture, and input fiber core diameter. A discussion of the preliminary selection of the probe optics specifications based on the results presented in Table A.1 now follows. While this discussion does not reflect the final specifications selected after the probe mechanical design constraints and optical component availability are considered, it does elucidate the basis for the nominal probe specifications.

For the design of the general purpose probe, nominal values for two of the parameters in the input optical design have been set - the standoff distance and the spot size - with the remaining parameters following from these. A nominal standoff distance of 25 mm was selected because a much smaller distance may significantly decrease its usefulness for performing measurements in real systems. In fact, a larger standoff distance will be

TABLE A.1

Minimum Input Lens Clear Aperture

Standoff Distance, mm	Spot Size = 0.2 mm						Spot Size = 0.5 mm					
	NA = 0.10			NA = 0.20			NA = 0.10			NA = 0.20		
	Fiber Core Dia.			Fiber Core Dia.			Fiber Core Dia.			Fiber Core Dia.		
	200 µm	400 µm	600 µm	200 µm	400 µm	600 µm	200 µm	400 µm	600 µm	200 µm	400 µm	600 µm
10	2.0	4.0	6.0	4.0	8.0	12.0	0.8	1.6	2.4	1.6	3.2	4.8
15	3.0	6.0	9.0	6.0	12.0	18.0	1.2	2.4	3.6	2.4	4.8	7.2
20	4.0	8.0	12.0	8.0	16.0	24.0	1.6	3.2	4.8	3.2	6.4	9.6
25	5.0	10.0	15.0	10.0	20.0	30.0	2.0	4.0	6.0	4.0	8.0	12.0
30	6.0	12.0	18.0	12.0	24.0	36.0	2.4	4.8	7.2	4.8	9.6	14.4
40	8.0	16.0	24.0	16.0	32.0	48.0	3.2	6.4	9.6	6.4	12.8	19.2
50	10.0	20.0	30.0	20.0	40.0	60.0	4.0	8.0	12.0	8.0	16.0	24.0
75	15.0	30.0	45.0	30.0	60.0	90.0	6.0	12.0	18.0	12.0	24.0	36.0
100	20.0	40.0	60.0	40.0	80.0	120.0	8.0	16.0	24.0	16.0	32.0	48.0

used if it can be reasonably obtained. A focused laser spot size of 0.2 mm was selected because it would allow measurements to be made in the presence of a particle concentration of approximately $10^4/cm^3$. Since this is a low particle concentration, an even smaller spot size would be desirable so that the probe could accommodate higher particle concentrations. This value was selected, however, as a reasonable compromise. The remaining variables in the design of the input optics are the fiber core diameter, numerical aperture, and input lens clear aperture. Due to the significant cost of fibers having an N.A. of 0.10, a fiber N.A. of 0.2 was selected for the initial probe development. (Towards the end of the program, a fiber having an N.A. of 0.13 was obtained on a special basis at a reasonable cost). This will allow an input lens clear aperture of 10 mm under the assumption that a 200 μm core fiber is acceptable from the standpoint of laser damage. For an 18.65 mm limit on the sum of the input and collection lens clear apertures, this leaves 8.65 mm for the collection lens clear aperture - a low but acceptable value. After experience with the performance of the probe using the above optical design has been obtained, it may be desirable to redesign the input optics based on the use of the more costly 0.10 N.A. optical fibers to obtain an improvement in the probe's characteristics.

The above analysis of the design of the input optics did not take into consideration any trade offs with the design of the collection optics. This is because values for the fiber core diameter and input lens clear aperture directly proceeded from the specification of the standoff distance and spot size, and the decision to at least initially avoid the high cost of the 0.10 N.A. fibers. This then fixes two parameters in the collection optics design - a collection lens clear aperture of 8.65 mm and a value of S_{input} of roughly 30 mm. S_{input} is the distance between the measurement volume and the canted lens. This leaves only the diameter of the collection fiber, the fiber numerical aperture (both of which are generally available only in discrete values), and S_{output} as free variables. This will allow either the matching condition for the image and fiber diameters or the matching condition for the lens F# and fiber N.A. to be met, but will not generally allow both matching conditions to be met. For a 200 micron collection fiber, the first matching condition yields a value of S_{output} of 30 mm, but for the second matching condition to be met a fiber having an N.A. of 0.083 would be required. A 100

micron collection fiber may allow both matching conditions to be nearly met since the corresponding fiber N.A. is 0.17 (close to the values offered by some manufacturers).

If the requirements of the two matching conditions are widely divergent, the image and fiber diameter matching condition will be given preference since this condition also affects the measurement volume size. A fiber core diameter which is much greater than the laser spot image will yield a large measurement volume and an increased sensitivity to interference from particle scattering. A fiber core diameter which is smaller than the laser spot image will yield a lower signal intensity and measurement precision. In the final optical design, however, an attempt will be made to satisfy the two matching conditions as closely as possible.

APPENDIX B

PHOTODIODE GATED INTEGRATOR AND PROGRAMMABLE TIME DELAY MANUALS

EVANS ELECTRONICS

MODEL 414

PROGRAMMABLE TIME DELAY MODULES

Voltage - Model 4141

Digital - Model 4145

Digital Extender - Model 4146

- Delays from 10^{-9} to 10^{2} Sec.
- Voltage or Crystal-Based Digital Control
- Low Jitter
- Pos. or Neg. True Input/Output
- Variable Pulse Widths
- Boxcar Interface to Model 4130 Integrator
- On-Board IC Voltage Regulators

DESCRIPTION:

Both Models 4141 and 4145 have three outputs, each of which generates a time-delayed pulse following a trigger pulse, or transition, applied to a single input. One output produces a reference pulse having a fixed delay relative to the input. At another, a pulse is delayed beyond the reference by an amount determined by external programming. The third generates a pulse coincident in time with the programmed delay interval. The widths of the reference pulse and delayed pulse are independently adjustable with on-board pots. All pulse inputs and outputs are TTL type logic with either positive or negative true available.

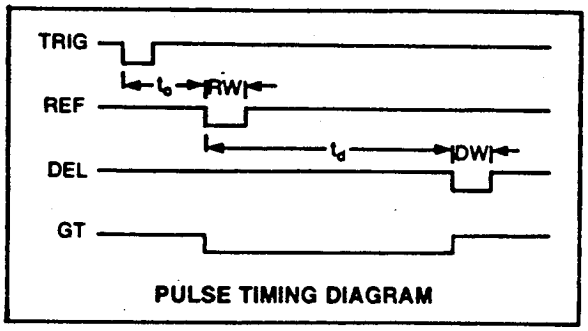

PULSE TIMING DIAGRAM

The Model 4141 has an RC type time base. Its delay is voltage-programmable from external sources; however, there is an on-board pot. available for local control, if desired. The 4141 is especially suited to generating continuously variable time delays with resolution below 1 ns.

The Model 4145 has a crystal-controlled oscillator which establishes an accurate time base—typically $< \pm 0.005\%$. Digital delay programming is accomplished with external digit switches, counters, holding registers, etc., via negative true logic input lines arranged as either 4 or 5 decade BCD. Jitter, due to random phasing of the input trigger relative to the oscillator cycle, is reduced by a special interpolating circuit.

The Model 4146 is a separate, supplementary module which can be used to extend the range of a 4145 to include four additional decades of BCD programmable time delay.

Whether under manual or computer control, the Models 4141, 4145, and 4146 provide a flexible, inexpensive means of generating delays ranging from nanoseconds to tens of seconds. Although designed for broad application these modules are compatible with the EE Model 4130 Gated Integrator for the performance of boxcar and other time-delay dependent integrations.

EVANS ELECTRONICS

P.O. Box 5055, Berkeley, California 94705 • Phone (415) 653-3083

APPLICATIONS:

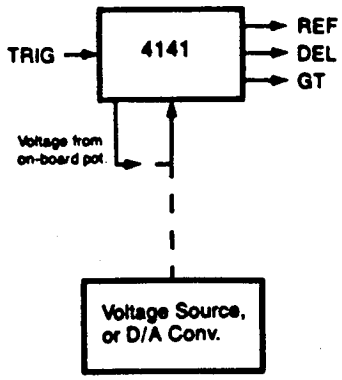

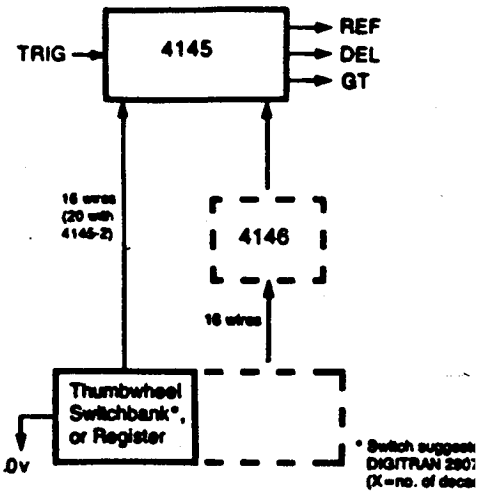

SPECIFICATIONS:

MODEL NO.:	4141	4141-1	4141-2	4141-3	4145	4145-1	4145-2	4146
TYPE OF CONTROL:	Voltage	Voltage	Voltage	Voltage	Digital	Digital	Digital	Digital
NOM. FIXED DELAY, t_o:	120ns.	500ns.	5μs.	50μs.	450ns.	3.5μs.	450ns.	—
VARIABLE DELAY, t_d:	0 - 1μs.	0 - 10μs.	0 - 100μs.	0 - 1ms.	0 - 999.9μs.	0 - 9999μs.	0 - 999.99μs.	0 - 9.999sec. 0 - 99.99sec.
MIN. DELAY INCREMENT:	<1ns.	<1ns.	<10ns.	<100ns.	100ns.	1μs.	10ns.	1ms. (1) 10ms. (2)
MAX. JITTER + DRIFT, t_o:	<±1ns.	<±5ns.	<±50ns.	<±500ns.	<±1ns.	<±3ns.	<±1ns.	—
MAX. JITTER + DRIFT, t_d:	<±1ns.	<±5ns.	<±50ns.	<±500ns.	<±2ns.	<±5ns.	<±2ns.	<±10ns. (1) <±30ns. (2)
TRIGGER INPUT:	TTL type. Positive or negative true. (3) →							—
PROGRAM INPUT:	0 to + 10v. full scale. Source impedance <10K. →				TTL type. Negative true. Binary-coded decimal (8-4-2-1) 4 decades.	4 decades.	5 decades.	4 decades.
OUTPUTS:	TTL type. Positive or negative true. (3) →							—
ADJ. PULSE WIDTH:	20 - 100ns.	0.1 - 1μs.	0.1 - 10μs.	1 - 100μs.	20 - 100ns.	0.1 - 1μs.	20 - 100ns.	—
MAX. SUPPLY CURRENT, @+15v.:	250ma.	250ma.	250ma.	250ma.	100ma.	100ma.	100ma.	—
@−15v.:	50ma.	50ma.	50ma.	50ma.	50ma.	50ma.	50ma.	—
@+5v.:	—	—	—	—	660ma.	660ma.	660ma.	450ma.
OPERATING TEMP. RANGE:	10°C - 40°C. →							
DIMENSIONS:	.062" pc board. 4-1/2"W x 6-1/2"L. 7/8" clearance required on component side. Board edge mates to standard 2 x 22 pin connector on .156" centers (e.g., TRW Cinch 50-44A-30).							

(1) added to 4145 or 4145-2

(2) added to 4145-1

(3) polarity set by on-board jumpers. Normally shipped as negative true

EVANS ELECTRONICS

P O Box 5055 Berkeley California 94705 • Phone (415) 653-3083

OPERATING NOTES

1. VC (pin 20) is the voltage control input. The on-board potentiometer R1 can be used as a control by connecting VS (pin X) to VC (pin 20).
2. Logic polarity (positive or negative true) is determined by the position of an on-board jumper for each of TRIG, REF, DEL, AND GT. See Locator diagram.
3. Output pulse widths, RW and DW, are adjustable with pots. R19 and R15 respectively.
4. R33 is an initial alignment pot. It is normally set for 120 ns. of delay of the DEL pulse (pin 3) with respect to the TRIG pulse (pin 8) with VC (pin 20) grounded.
5. R7 is also an initial alignment pot. Normally it is set for coincidence of the leading edges of the pulses from REF (pin 4) and DEL (pin 3) when VC (pin 20) is grounded.
6. R11 is a calibrating pot. Normally it is set for rated full scale relative time delay between the leading edges of the pulses from REF (pin 4) and DEL (pin 3) with +10v. at VC (pin 20). If R11 is readjusted Steps 4. and 5. should be repeated until further adjustments are not required.
7. When cable or transmission line is connected to any of the outputs, it is desirable to terminate in the characteristic impedance at the far end as follows:

for $Z_o \geqq 100$ ohms,

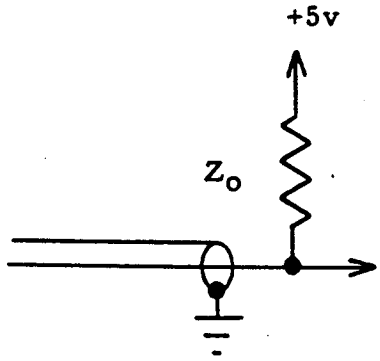

for $Z_o < 100$ ohms,

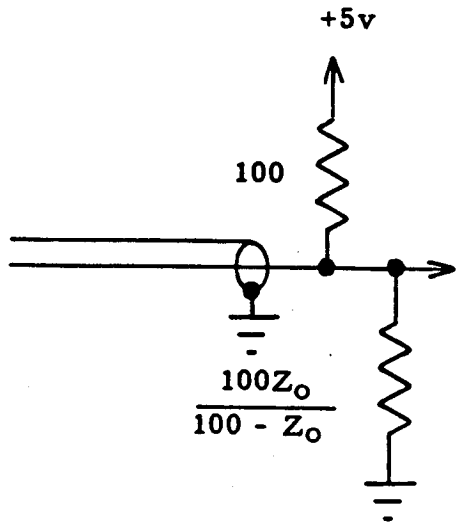

EVANS ELECTRONICS
Berkeley, CA

PIN CONNECTIONS

Bottom View of Connector

Solder side ←

→ Component sid

0 v	22	Z	0 v
NC	21	Y	0 v
VC	20	X	VS
NC	19	W	0 v
NC	18	V	0 v
NC	17	U	0 v
NC	16	T	0 v
NC	15	S	0 v
NC	14	R	0 v
NC	13	P	0 v
NC	12	N	0 v
NC	11	M	0 v
NC	10	L	0 v
NC	9	K	0 v
TRIG	8	J	0 v
NC	7	H	0 v
-15 v	6	F	-15 v
+15 v	5	E	+15 v
REF	4	D	0 v
DEL	3	C	0 v
GT	2	B	0 v
0 v	1	A	0 v

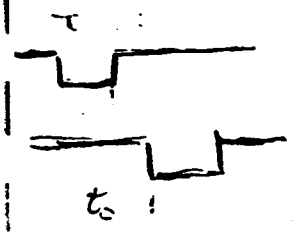

Pulse Timing

EVANS ELECTR
BERKELEY, CA

LOCATOR

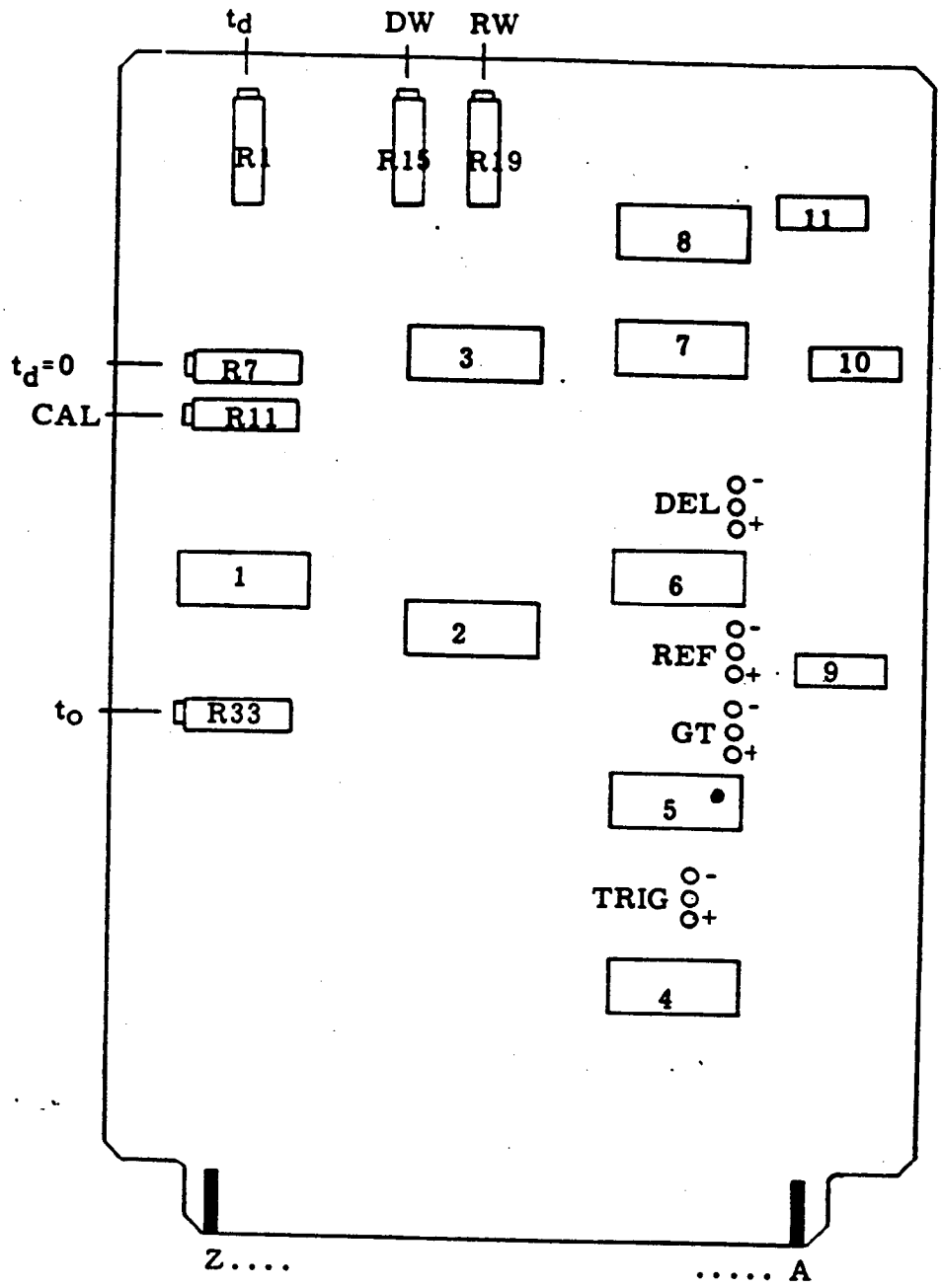

EVANS ELECTRONICS
Berkeley, CA

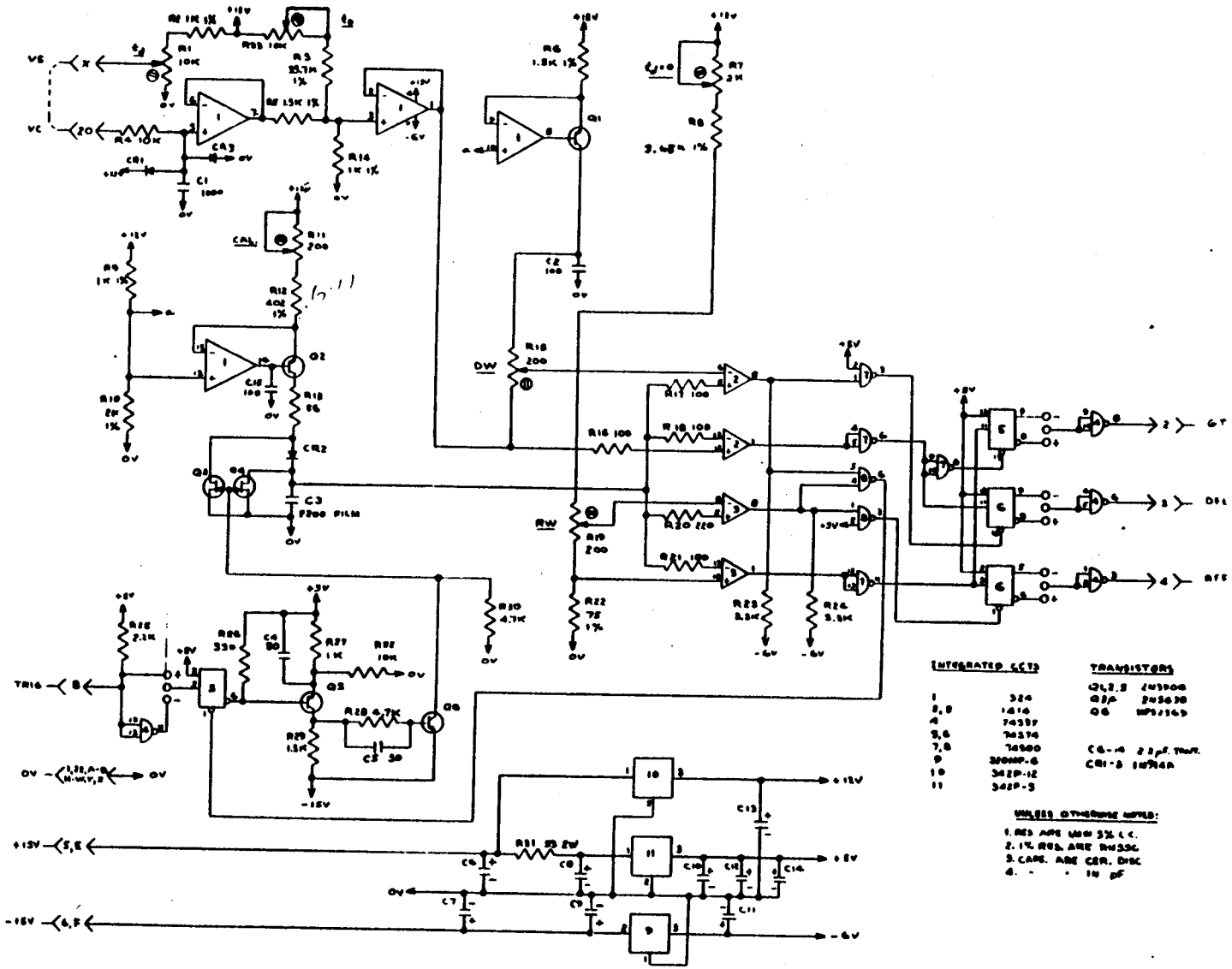

SCHEMATIC PROGRAMMABLE TIME DELAY MODEL 4141

GATED INTEGRATOR MODULE

- 30 ns. Minimum Gating Time
- 1 pa. Maximum Leakage Current
- Fast Input Voltage Follower
- Adaptable to Boxcar Integration
- Automatic Baseline Correction (2 Modules)
- Automatic Limit Reset
- On-Board IC Voltage Regulators

The Model 4130A is a fast, low-leakage integrator having an input isolating gate which can be opened, under external control, for periods ranging from dc down to 30 ns. The output voltage closely approximates 1/RC x the time integral of the input voltage, with the integration proceeding only during open-gate intervals; the integral is held constant while the gate is closed. Two logic outputs indicate continuous comparisons (greater than or less than) of the integral with 2 voltage levels preset in with on-board potentiometers. A reset, returning the output voltage to zero, can be actuated with either a direct logic input, or a trigger applied to an internal pulser.

Signal input to the 4130A is accessible through a fast unity-gain buffer amplifier, and also through 2 direct connections. Each input is essentially independent of the others, and may be used to provide a separate input for zero offset, baseline correction, or feedback.

In addition to totalizing applications, the Model 4130A is especially well suited to boxcar integration in which sequential, or otherwise selected, segments of a repetitive signal are to be averaged over many cycles. Programmable time delays for boxcar applications are available in the EE Models 4141, 4145 modules.

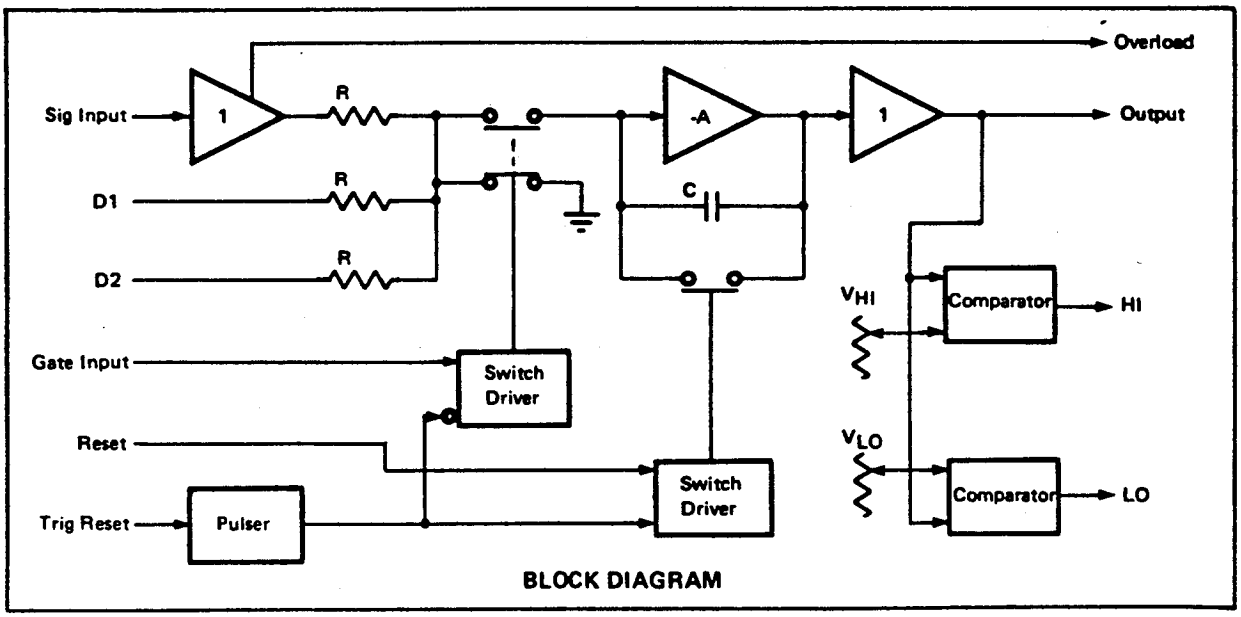

BLOCK DIAGRAM

EVANS ELECTRONICS
P O Box 5055, Berkeley, California 94705 • Phone (415) 653-3083

APPLICATIONS:

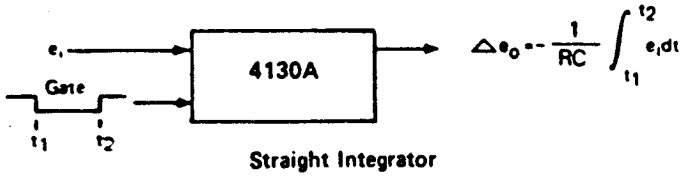

Straight Integrator

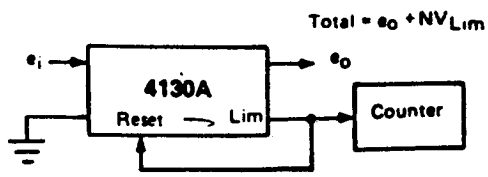

Long Term Integrator

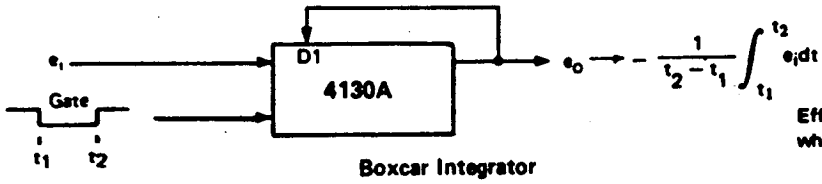

Boxcar Integrator

Effective time constant = $\frac{RC}{n(t_2 - t_1)}$, where n = repetition rate.

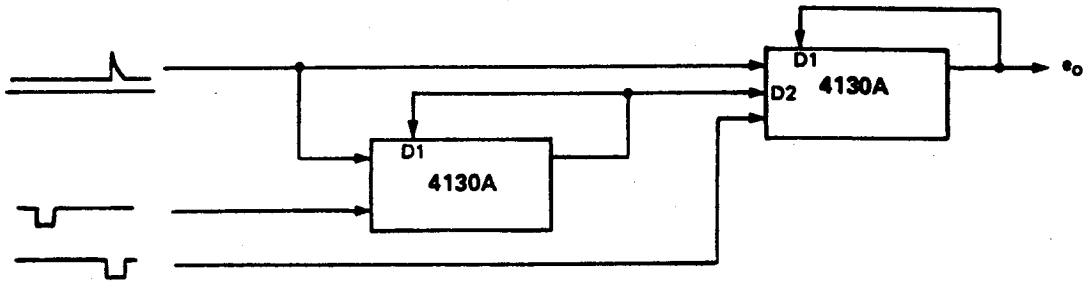

Boxcar with Automatic Baseline Correction

SPECIFICATIONS @25°C:

INTEGRATING TIME CONSTANT

10^{-4} sec. ±10%. R=10K, C=10,000 pF. Board space allows user substitution of RC values covering 10^{-6} to 10^{3} sec. Special order RC's available.

ANALOG OUTPUT

Max. swing, ±5v @10ma.

LEAKAGE

1 pa. max. with gate closed.

LINEARITY DEPARTURE

±.1% of full scale max.

DRIFT

70 μv/°C max, referred to output.

VOLTAGE FOLLOWER INPUT

Input impedance 1 megohm in paralled with <20 pf. AC or DC. 0.1 μF series capacitor on AC input. Rise time <4 ns. Temp. coeff. typically <10 μv/°C. Adjustment pot. to zero offset.

DIRECT INPUTS

Two inputs directly coupled to integrator junction through 10K resistors (other values can be substituted).

LOGIC INPUTS

Compatible with TTL, DTL, CMOS, and contact closure. Negative logic. Min. off voltage +2v (or open circuit). Min. on sink current, 5 ma. (or short circuit to ground).

1. Gate. Min. open time, 30 ns.
2. Reset. Places <100 ohms across integrating capacitor. Delay time to turnoff, <100ns.
3. Pulsed Reset. Negative input transition triggers 12 μs. resetting pulse. Other RC values can be substituted for longer pulses as desired.

LOGIC OUTPUTS

Negative logic. Open-collector transistor. Min. sink current typically >16 ma.

1. Overload. Indicates when input voltage follower swing exceeds ±3v
2. Hi, Lo. Indicates when integral output voltage exceeds preset values. Both Hi and Lo reference voltages adjustable over ±5v.

POWER REQUIREMENTS

+15v ± 1v, <150 ma. -15v ± 1v, <75 ma.

DIMENSIONS

.062" pc board. 4½"W x 6½"L. 7/8" clearance required on component side. Board edge mates to standard 2 x 22 pin connector on .156" centers (e.g., Cinch 50-44A-30).

OPERATING TEMP. RANGE

10° C.–40° C.

EVANS ELECTRONICS
P O Box 5055, Berkeley, California 94705 • Phone (415) 653-3083

OPERATING NOTES

1. When used in the boxcar configuration as shown on the 4130A data sheet, the open-gate gain is determined by the ratio of 2 of the resistors R1, R2, R3 utilized as the feedback and input resistors respectively. With the 10K resistors supplied, the gain is approx. -1. Other values can be substituted; the integrating time constant is the product of C and the feedback R.

2. In the automatic baseline correction configuration, the gain of the 2nd compensating module should be equal to the ratio of the net forward gains referred to the 2 inputs of the 1st module. A potentiometer in the external feedback path of the 2nd module is recommended for exact nulling.

3. There is a small charge transferred with each gate transition. As the gate duration is decreased (below approx. 10 μs) this effect begins to contribute a measurable equivalent input error current which is constant for a given RC selection and gate width. This current can be effectively balanced out, if desired, by connecting V_x (pin 8) to any of the unused dc inputs, and adjusting R66 for zero OUTPUT (pin 10) with zero input. An external series resistor may be added for finer adjustment.

4. R10, R37, and R43 are local zeroing pots., and should require only minor and infrequent adjustment. The following procedure is recommended:
   a. Connect the OUTPUT (pin 10) directly to the DC SIG INPUT (pin 20).
   b. Ground the RESET (pin D).
   c. Locate R41 (1K, 1W), and attach a dc voltmeter (or scope) having a resolution of at least 0.1mv. to the end of R41 nearest the center of the card.
   d. Adjust R37 for 0v.
   e. Remove voltmeter and attach it to OUTPUT (pin 10).
   f. Adjust R43 for 0v.
   g. Remove the ground at RESET (pin D)
   h. Ground the GATE (pin C).
   i. Adjust R10 for 0V. at the OUTPUT (pin 10).

5. R54 and R61 are the HI and LO limit adjustments respectively. A convenient arrangement for establishing the limit points is to ground the GATE (pin C), connect the OUTPUT (pin 10) directly to one of the dc inputs (D1, D2, or DC SIG INPUT), and connect V_x to another of the dc inputs. R66 can then be varied while monitoring the OUTPUT, and the desired limit established. Subsequently, R54, or R61, can be varied while HI (pin 2) and LO (pin B) logic status is observed. Note that HI and LO are open-collector outputs, and require resistor returns to a positive voltage in order to determine status.

EVANS ELECTRONICS
Berkeley, CA

OPERATING NOTES (Cont'd)

6. The HI (pin2) or LO (pin B) can be used for automatic reset connecting either output directly to both RESET (pin D) and TRIG RESET (pin 4). No external output pull-up resistors ar required in this arrangement. For complete resetting action C23 should be approx. .01C1.. This configuration is useful f long term integration, and for generation of ramps and time delays.

7. When integrating from a very high impedance, or constant current, source, e.g., a collector electrode in vacuum, it i preferable to use the D1 (pin 12) or D2 (pin 13) input. If, addition, the voltage follower is not being used, it will be important to remove R3, since any path to ground during open gate intervals will result in error current generated by inp offset (note that even a 10 μv. offset with R3=10K produces 1 na.).

8. The integrating capacitor should be a film type, preferably polystyrene, teflon, or polycarbonate. Other film types, su as polyester, or mylar may be quite satisfactory where leaka resistance, temperature coefficient, or dielectric absorptio are not critical. When a new capacitor is substituted, the board area inside the guard ring enclosing one capacitor ter nal should be cleaned on both sides of the board with freon, other flux remover. Caution: polystyrene capacitors can be irreversibly damaged upon contact with many solvents, includ freon.

9. If the AC or DC SIG INPUT is not used, the DC SIG INPUT (pin should be grounded to prevent pickup.

10. The module is sensitive to light in the guard ring area, and exhibit leakage rates > 1pa. under normal ambient light. It be necessary to shade the board if minimum leakage is requir

11. CAUTION: Do not use a soldering gun when substituting compon AC line voltages can destroy the semiconductor devi Use only soldering irons which are grounded through 3-wire plug.

PIN CONNECTIONS

Bottom View of Connector

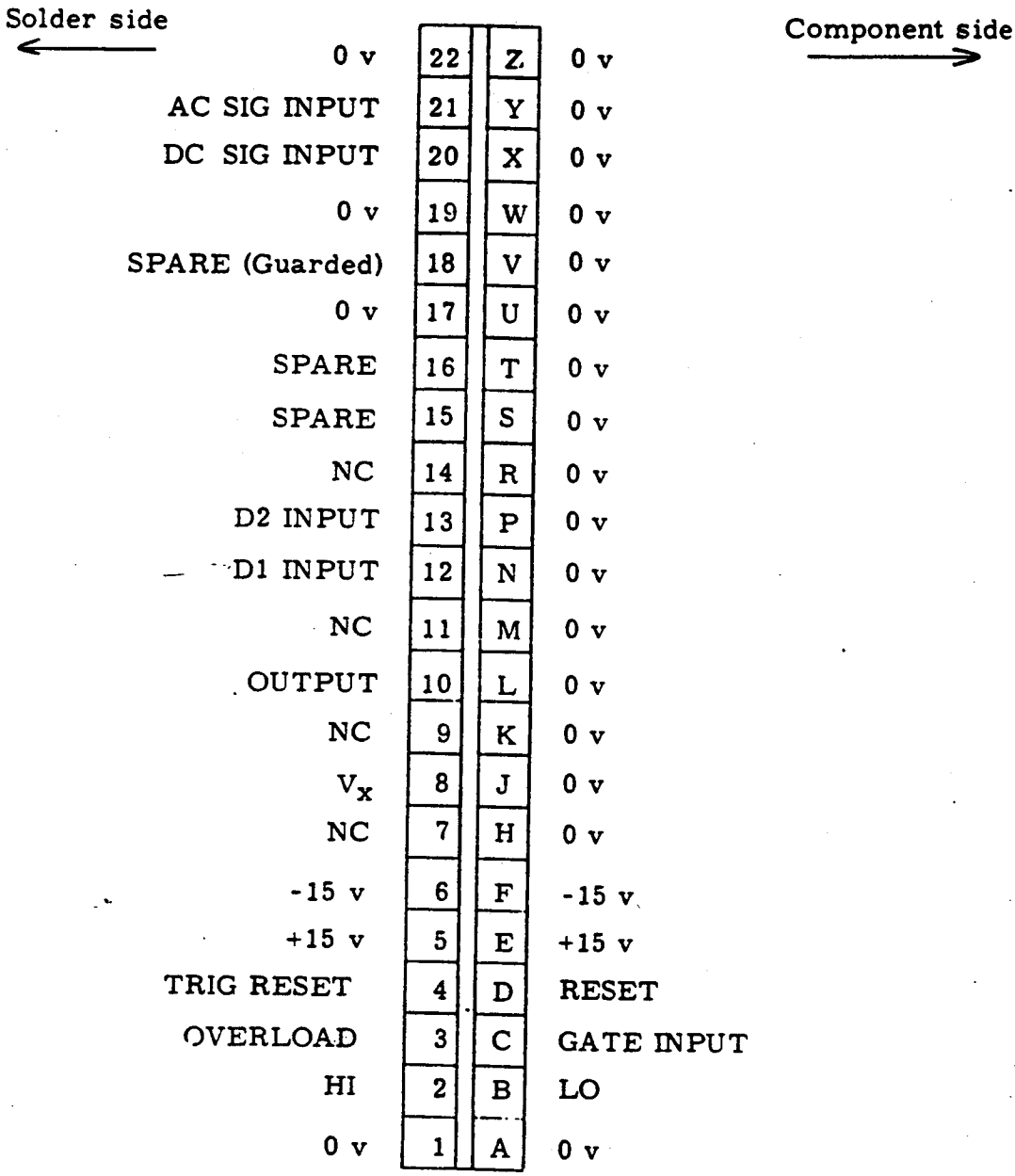

LOCATOR

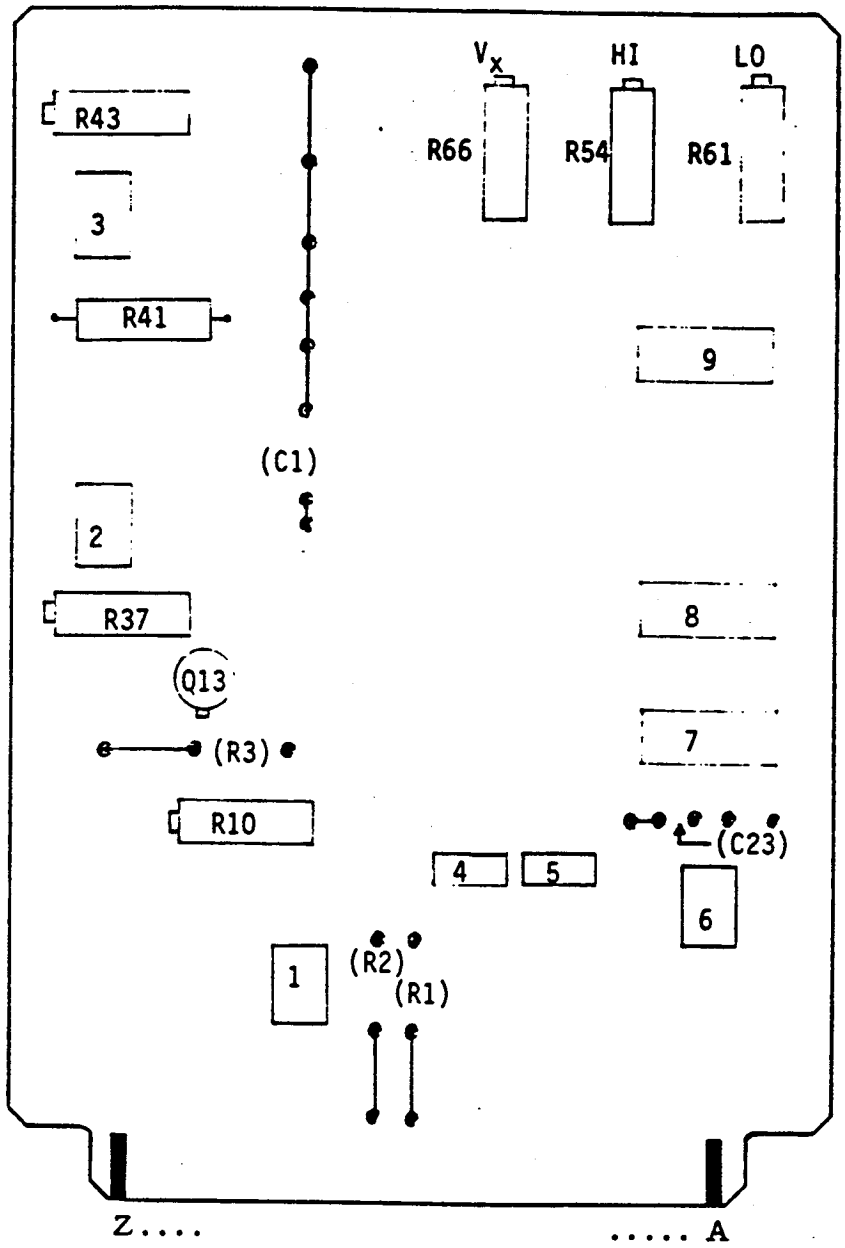
V_x
HI
LO
R43
R66
R54
R61
3
R41
9
(C1)
2
R37
8
Q13
(R3)
7
R10
(C23)
4
5
6
1
(R2)
(R1)
Z....
..... A

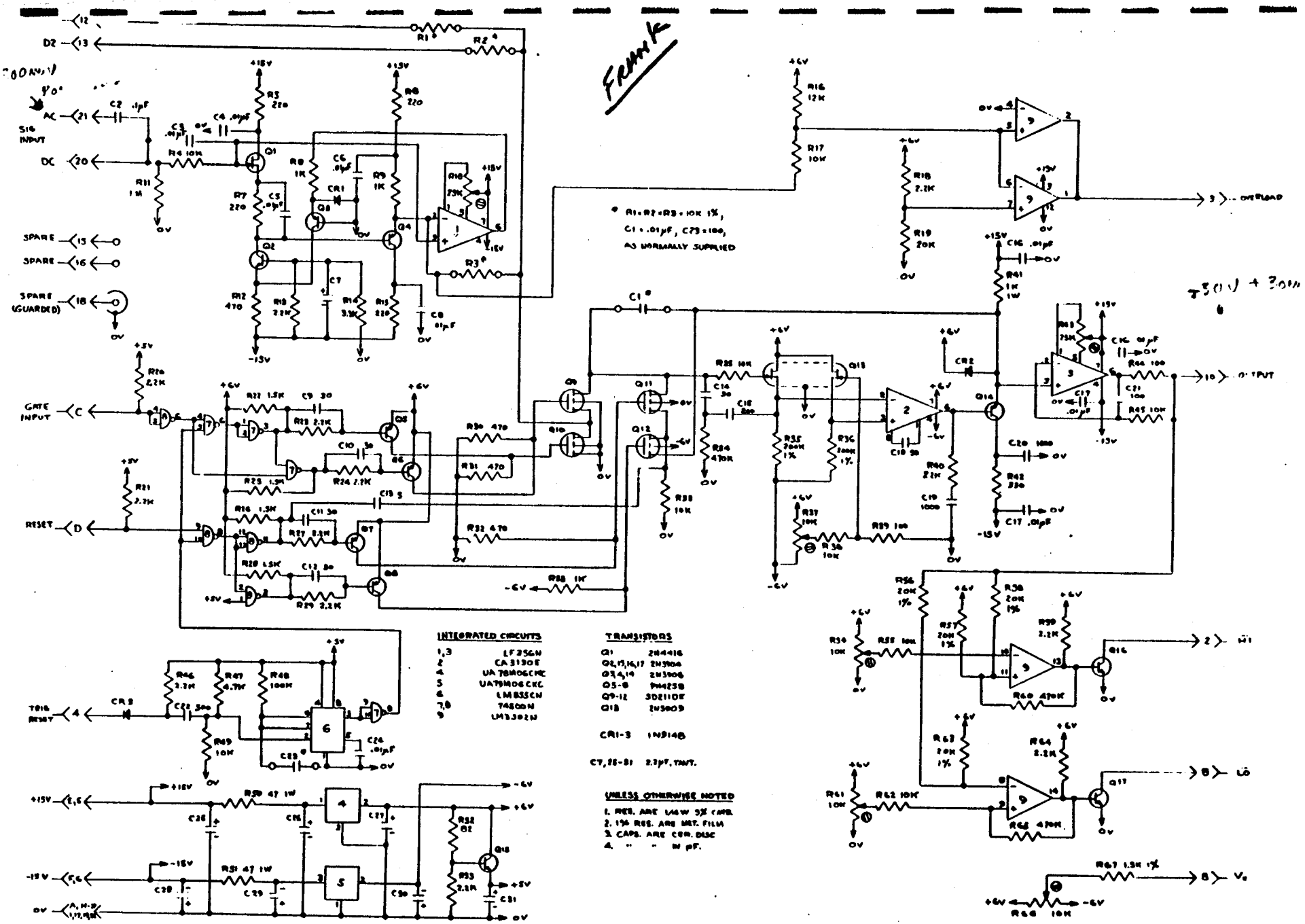

SCHEMATIC GATED INTEGRATOR MODEL 4130A

APPENDIX C

PURGE GAS PRESSURE REGULATION

A requirement for using the Rayleigh scattering measurement system at elevated pressures is the ability to regulate the purge gas pressure and flow rate as the pressure level of the measurement environment changes with time, e.g., during startup and power level changes in a gas turbine engine. While a computer controlled system using electronic mass flow controllers is possible, a simpler and more elegant solution is to use a differential pressure regulator referenced to the measurement environment pressure. The differential pressure regulator supplies gas at a constant pressure differential with respect to the reference pressure. An example of the operation of this pressure regulation technique in a gas turbine engine test will now be given.

In an advanced gas turbine engine, the combustion chamber pressure varies from 1 atm (before ignition) to approximately 30 atm (at full power). Before the engine is started, the pressure differential is set to the desired value for the operating conditions of the test (or the first of a series of steady state conditions). If a 10% $\Delta p/p$ of the purge gas across the lens optics is desired at an operating pressure of 30 atm, then a differential of 3 atm or 44.1 psi is set on the differential pressure regulator. At low pressure, a 3 atm differential is much higher than needed, although the stress imposed by this differential on the optical components is well within the strength of the components. As the engine is brought to operating conditions, the 3 atm differential produces the desired mass flow rate and relative pressure drop ($\Delta p/p$). Figure C.1 shows the variation of the mass flow rate, purge gas exit Mach number, and purge gas supply pressure with the combustor pressure for a 3 atm differential and a purge gas composition of 90% He and 10% N_2. Figure C.2 shows the dependence of the same quantities on the combustor pressure for a purge gas composition of 100% N_2. These figures show that the mass flow rate of the purge gas increases with combustor pressure and the exit Mach number decreases with combustor pressure. These results were obtained by a purge gas flow model which considered the contraction pressure drop at the entrance to the flow passages in the lens tube, the isentropic expansion pressure drop as

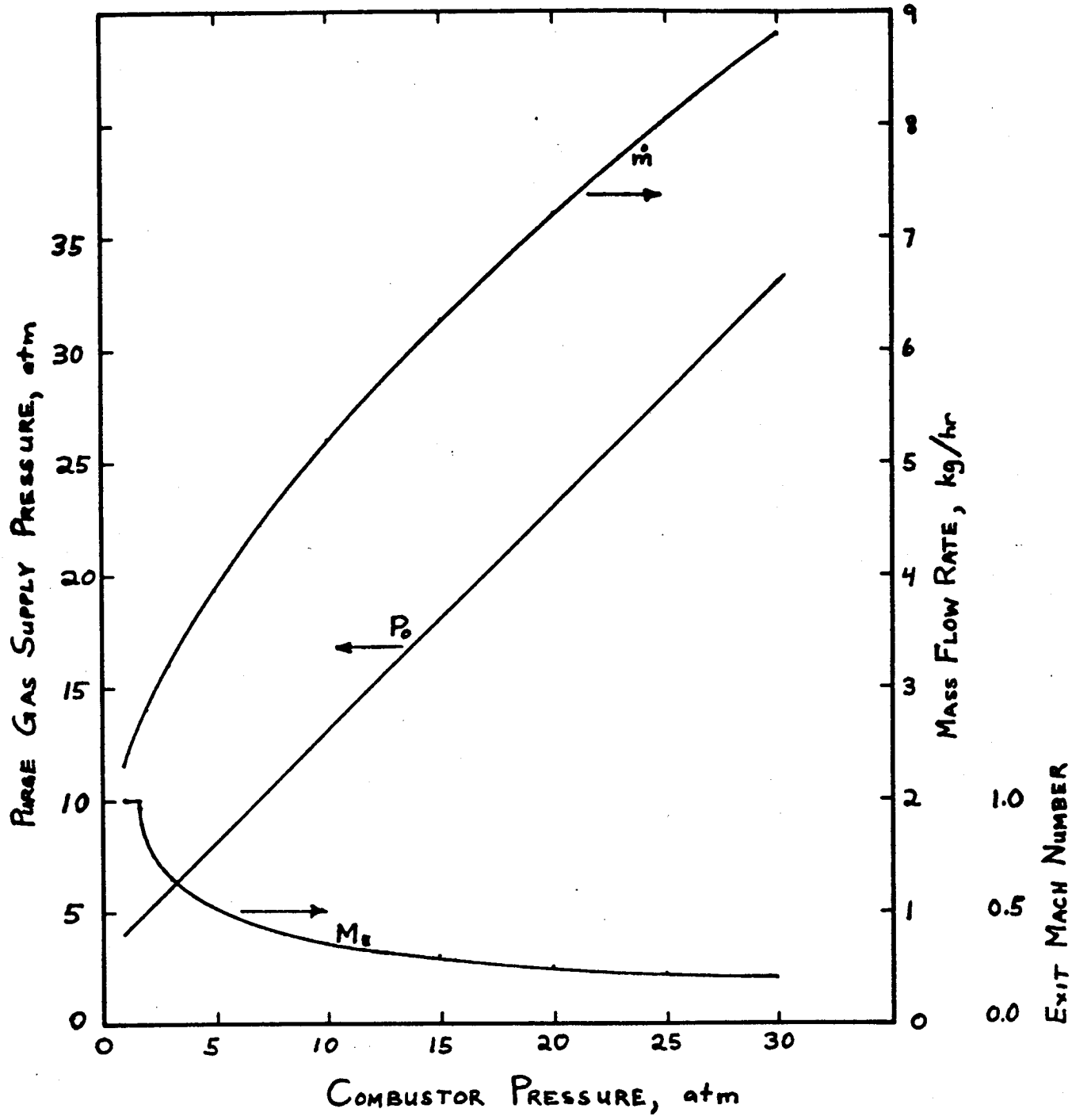

Figure C.1 Purge Gas Flow Characteristics for 3 atm Pressure Differential and 90% He/10% N_2 Gas Composition (Transmitter Optical Port)

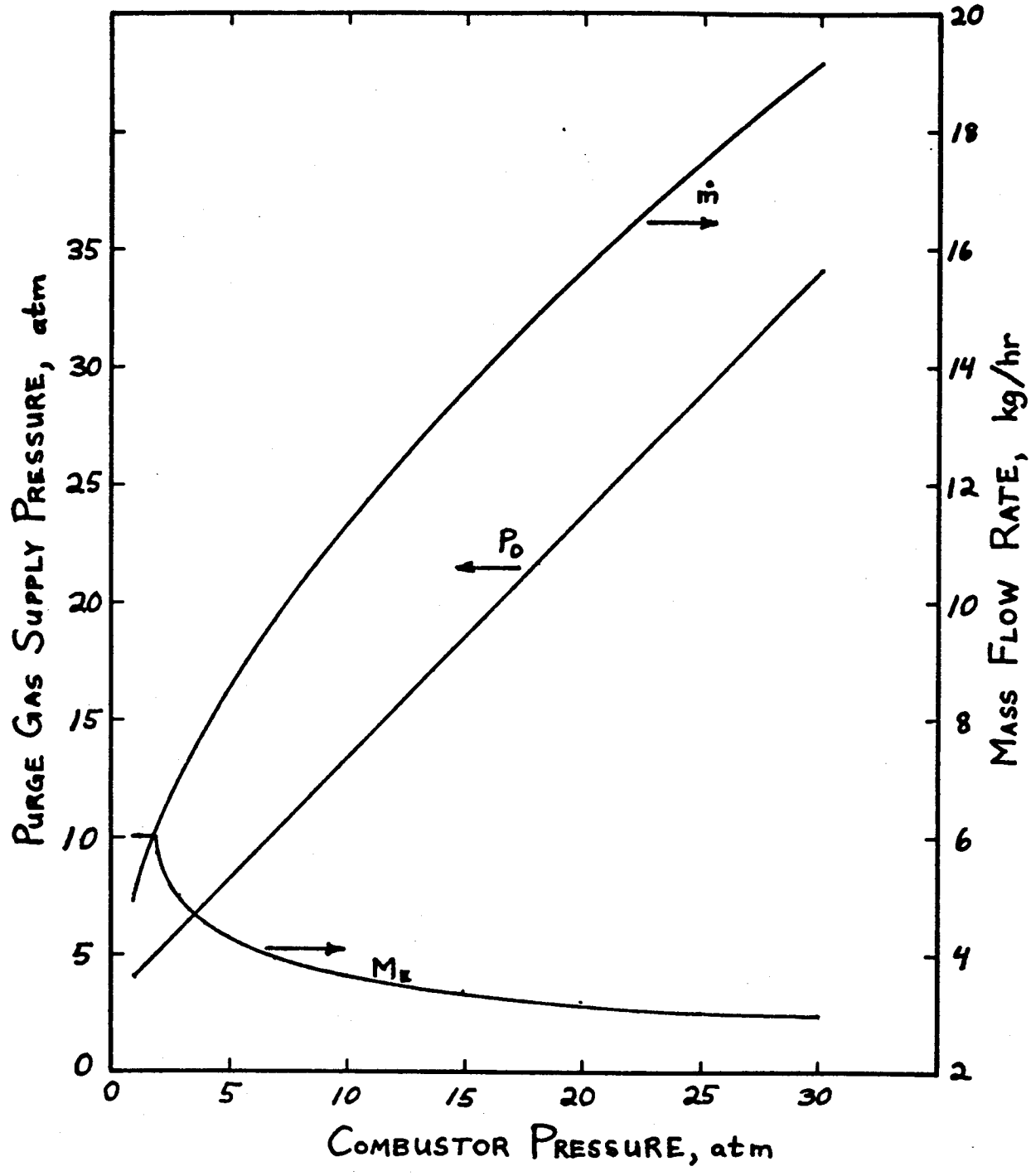

Figure C.2 Purge Gas Flow Characteristics for 3 atm Pressure Differential and 100% N_2 Gas Composition (Transmitter Optical Port)

the flow accelerates to the entrance velocity at the flow passage inlet, and the combined friction and flow acceleration pressure drop experienced as the purge gas flows through the lens tube passages. The calculations were performed for the transmitter lens tube passages which have a total flow area of 1.8 mm^2, a hydraulic diameter of 0.316 mm, and a length of 14 mm. Due to the flow acceleration caused by frictional losses, the flow at the exit of the purge gas passages is choked (M_e = 1) for both the He/N_2 and N_2 purge gas compositions at a pressure differential of 3 atm and a combustor pressure of 1 atm. For He/N_2, the purge gas flow remains choked until the combustor pressure rises to 1.4 atm, while for pure N_2, the flow remains choked until the combustor pressure reaches 1.7 atm.

The dependence of the purge gas mass flow rate on the pressure drop (i.e., differential pressure setting) is shown in Figure C.3 for combustor pressures of 10 atm and 30 atm and for purge gas compositions of 100% N_2 and 90% He/10% N_2. The results in this figure illustrate that the purge flow rate can be easily controlled by selection of the differential pressure setting. Flow rates of 5 to 15 kg/hr of N_2 or 2 to 7 kg/hr of 90% He/10% N_2 can be obtained with relative pressure drops of 5 to 10% during operation at elevated pressures. The response time of differential pressure regulators is approximately 0.1s. This should be adequate for normal turbine engine pressure transients. If a test requires operating at several pressure levels, the differential pressure setting can either be manually adjusted for each or a remote control activator can be used to adjust the setting.

The main requirement for implementation of the differential pressure purge gas system is the availability of a pressure tap for the measurement environment pressure. Ideally, a pressure tap in a location near the Rayleigh scattering probe should be used. If no suitable reference pressure source is available or feasible, the Rayleigh scattering probe could be modified to provide the source. The simplest modification would be to remove the pressure transducer and use the pressure port as the reference pressure source. An alternate modification would be to drill an additional hole in the probe to provide the source. The compact design of the probe makes this latter option somewhat risky, since great care would need to be taken to avoid breaking through existing passages. The first option, on the other hand, can be easily implemented.

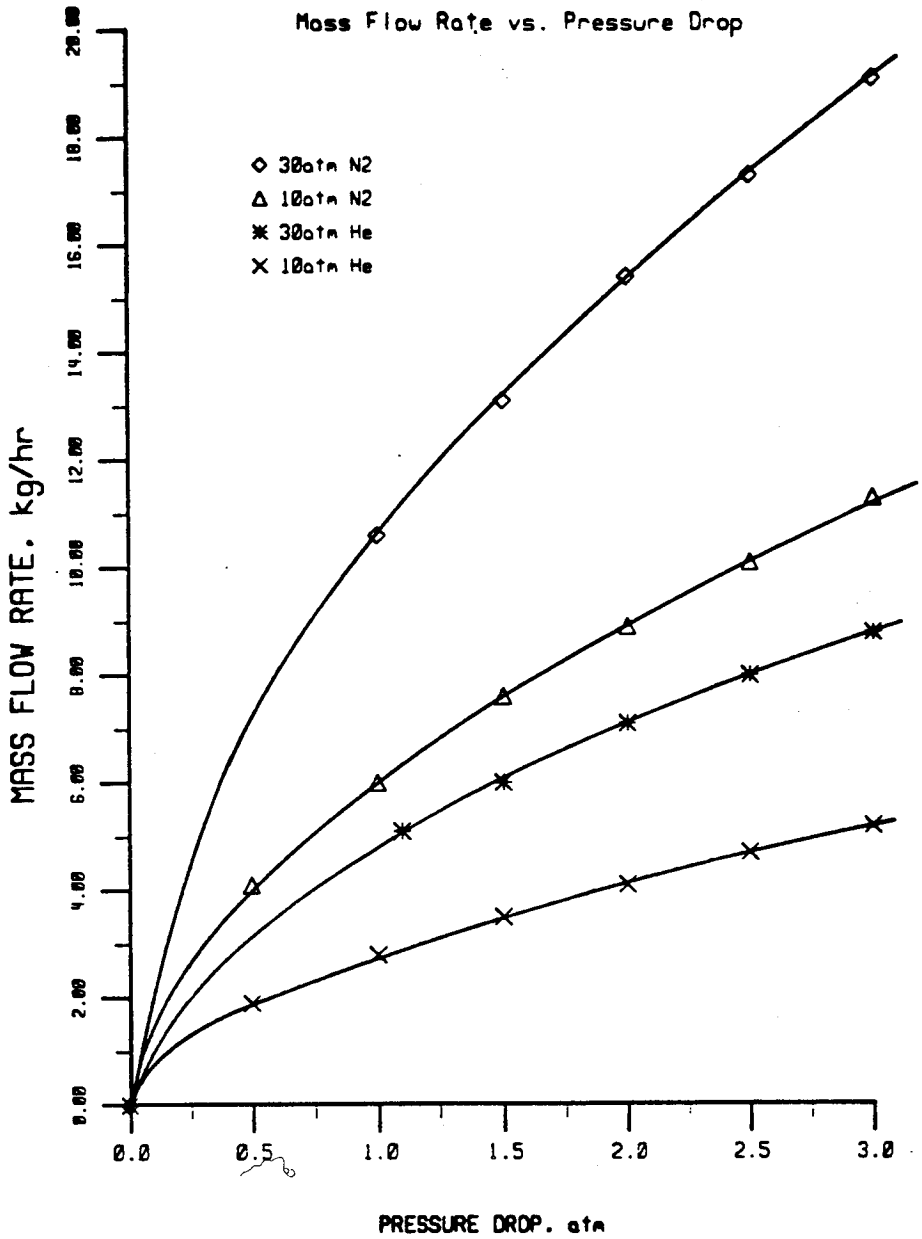

Figure C.3 Purge Gas Flow Rate as a Function of Pressure Drop for Transmitter Optical Port

APPENDIX D

LENS STRESS AND TEMPERATURE CALCULATIONS

Calculations were performed to determine the maximum stress on the optical components due to the pressure differential and the maximum temperature of the optics due to radiative heating. The stress calculations showed that the maximum expected stress was well within the strength limits of fused silica. The temperature calculations showed that if natural convection and radiation were the only cooling mechanisms, the optical components will rise to relatively high temperatures in some applications. The details of these calculations now follow.

The stress component which is most significant in the three dimensional bending of a thin circular plate which is supported along its periphery is the radial stress. For a plate of uniform thickness, this stress is maximum at the center of the plate. The expression for the radial stress at the center of a uniformly loaded circular plate is given by Timoshenko and Goodier (Theory of Elasticity, 3rd Edition, McGraw-Hill, 1970, p.385) to be

$$\sigma_r = q \left[\frac{2 + v}{8} \frac{z^3}{c^3} - \frac{3}{8} \frac{2 + v}{5} \frac{z}{c} + \frac{3(3 + v)}{32} \frac{a^2 z}{c^3} \right]$$

where q = load per unit area

v = Poisson's ratio

z = coordinate in direction perpendicular to the plate with the origin at the center of the plate

c = half thickness of the plate

a = radius of the plate (at the point of support)

For a pressure differential (q) of 50 psi, v = 0.21, a = 6 mm, c = 0.6 mm, the radial stress at z = c and r = 0 is 1510 psi. The CRC Handbook of Applied Engineering Science gives the tensile strength of fused quartz to be 7000 psi, which is over four times greater than the maximum radial stress. Even this calculation is conservative because it is based on the edge thickness of a lens or wedge. The thickness of both these components will be greater in the center, thus reducing the maximum stress. For the optical components and pressure differentials being considered for the probe therefore, failure due to stress should not be a problem.

The estimated lens temperature can be calculated from an energy balance for the lens in which the energy input from radiative energy transfer is set equal to the energy output from radiative energy transfer and natural convection. An approximate equation for the energy balance can be written as

$$\sigma\alpha\, T_w^4 = 2\,\sigma\,\varepsilon\, T_{lens}^4 + (T_{lens} - T_{probe})\, h_{nc}$$

where T_w = temperature of measurement environment surfaces

T_{lens} = steady state lens temperature

T_{probe} = probe temperature

σ = Stefan-Boltzmann constant

α = effective absorptivity of lens in receiving radiative energy from the measurement environment

ε = effective emissivity of lens in emitting radiative energy to the probe

h_{nc} = heat transfer coefficient for natural convection

The approximations used in this equation are that the radiative energy input to the lens from the probe can be neglected relative to the input from

the measurement environment, and that the emissivity and absorptivity of the probe and measurement environment are unity.

In this equation, the effective absorptivity is a function of the optical characteristics of the lens material and the temperature of the surfaces in the measurement environment. Likewise, the effective emissivity is a function of the lens material and the temperature of the lens.

The heat transfer coefficient for natural convection can be evaluated from a correlation given by Kreith (Principles of Heat Transfer, 3rd ed., Intext, New York, 1973, p. 396),

$$\frac{h_{nc}\, L}{k} = 0.555\ (Gr_L\ Pr)^{0.25} \qquad (10<GrPr<10^9)$$

where $Gr_L = \rho^2 g\ \beta\ (T_{lens} - T_\infty)\ L^3 / \mu^2$

and Gr_L = Grashof number based on height L

ρ = density (of purge gas)

g = gravitational acceleration

β = temperature coefficient of volume expansion (= 1/T)

T_∞ = temperature of probe purge gas

L = surface height (= lens diameter)

μ = viscosity of purge gas

k = thermal conductivity of purge gas

The calculation of the steady state temperature of the optics requires an iterative process using the above equations and the temperature dependence of the gas properties and optical material properties. Results of a series of

calculations for three optical materials, two measurement environment wall temperatures, and two pressures are shown in Table D.1. The results show that for high wall temperatures and low pressures, the optical component temperatures can be quite high; however, wall temperatures of 1400 K will usually only be encountered in pressurized systems. The effect of a high (30 atm) pressure on the optical component temperatures is significant. This result of lower temperatures at high pressures is due to the increase of the free convection heat transfer coefficient with pressure. The variation in temperature due to the optical material characteristics is also substantial. Sapphire is clearly the material of choice from temperature considerations, due to its high transmittance out to 6 microns in wavelength. The IR fused silica is an improvement over the standard UV fused silica because it does not have the strong absorption band at 2.7 microns. Both fused silicas are effectively opaque for wavelengths longer than 4 microns.

Table D.1
Optical Component Temperatures

Optical Material	P = 1 atm		P = 30 atm	
	Tw = 1400 K	Tw = 1000 K	Tw = 1400 K	Tw = 1000 K
UV fused silica	1005 K	700 K	695 K	470 K
IR fused silica	915 K	661 K	600 K	445 K
Sapphire	770 K	570 K	475 K	385 K

APPENDIX E

Pressure Transducer Freqency Response Calculations

Two pressure measurement configurations were considered for the Rayleigh scattering probe. These configurations were a short passage terminated by a pressure transducer and a long, narrow passage terminating into a cavity in which a transducer is mounted. A third configuration, the infinite line probe configuration, was also considered but was judged to be less desirable for the present application than the first configuration.

The "organ pipe" formula for the primary resonant frequency,

$$f_r = c/4L$$

where c = adiabatic sound speed

and L = pressure tube length,

is valid only for the case of very low viscous damping. The low damping requirement can be expressed as a constraint on the maximum tube length. This constraint has been given as (R. D. Samuelson, "Pneumatic Instrumentation Lines and their Use in Measuring Rocket Nozzle Pressure", Aerojet-General Corp., RN-DR-124, July 1967),

$$L < \frac{\rho\, cA}{1800\mu}$$

where ρ = gas density

A = tube cross sectional area

μ = gas viscosity

An additional restriction on the use of the "organ pipe" equation is that the cavity volume of the pressure transducer must be small with respect to the tube volume. Samuelson gives this constraint as

$$V = (L)(A)/60$$

where V is the transducer cavity volume

A second order approximation can be used to model the response function of the "organ pipe" probe configuration. Samuelson gives the gain response function to be,

$$G = \frac{1}{[(1 - u^2)^2 + (2\delta u)^2]^{1/2}}$$

where $u = f/fr$ = dimensionless frequency

δ = damping coefficient

The damping coefficient for the low viscous damping conditions being considered is essentially zero, thus simplifying the relationship to be

$$G = \frac{1}{1 - u^2}$$

The above formulas can now be applied to determine the frequency response and constraints on the "organ pipe" pressure measurement configuration. Assuming that the pressure measurement tube is purged with the same gas which will be used for the optical components (90% He and 10% N_2), the sound speed, viscosity and density at 300 K and one atmosphere are $c = 800$ m/s, $\mu = 2 \times 10^{-5}$ kg/m s and $\rho = 0.26$ kg/m^3. For a tube inner diameter of 2.5 mm (0.10"), the low viscous damping restriction on the use of the "organ pipe" formula for the primary resonant frequency is $L < 2.9$ cm. For the transducers being considered the transducer cavity volume constraint will not be a problem. The primary resonant frequency for a transducer mounted 2 cm from the front face of the probe is then 10,000 Hz, and is twice this value for a transducer

mounting depth of 1 cm. The above equation for the gain response function can be used with these primary resonant frequencies to determine the frequency at which the gain deviates 5% from unity. For f_r = 10,000 Hz, a 5% gain deviation occurs at f = 2,200 Hz. The 5% deviation frequency at f_r = 20,000 Hz is 4,400 Hz. A 20% deviation is obtained at approximately twice the frequency for a 5% deviation.

The above results indicate that very good pressure reponse can be obtained with the "organ pipe" configuration up to frequencies in the kilohertz range. This type of frequency response will permit accurate temperature measurements to be performed at these frequencies, provided that the pressure gradient between the measurement volume and the front of the probe is negligible.

The second pressure measurement configuration considered for the probe consisted of a long, narrow tube terminating in a cavity. It was determined, however, from the formulas in Samuelson's report that the high viscous damping regime could not feasibly be obtained with the current probe design. For example, if the tube length were limited to 8 cm, the tube diameter would need to be 65 microns or less. Furthermore, even if this regime could be obtained the gain response function for frequencies in the kilohertz range would be much less than unity. For these reasons, the "organ pipe" configuration was selected.

APPENDIX F

OPTICAL PERFORMANCE ASSESSMENT

The optical performance of the laser input and collection optics was evaluated by employing a ray tracing program written for that purpose. Good spatial resolution without too high a sacrifice in light gathering capability was the principal design objective. Spatial resolution was assessed by determining the spread of a bundle of rays generated by a source at the fiber location as the laser axis was crossed. Since loss of resolution caused by the use of a wedge is most acute in the plane defined by the optical axes of the transmitter and collection systems, the calculations were carried out in this plane only.

The initial calculations modeled the original optical design of the collection system, which consisted of a biconvex lens placed close behind the wedge and operating at a magnification of one. They indicated that poor resolution was obtained with such a design (see Table F.1) due to spherical aberration caused by such a low f-number lens and, more importantly, to aberration caused by the wedge. One solution to both of these problems is to use a long focal length lens placed some distance behind the wedge. The increased f-number of such a system results in decreased spherical aberration and more closely parallel light rays passing through the wedge, hence less wedge aberration. In Figure F.1, the results of some of these calculations are shown for the case of point source illumination. The improvement in resolution (distance along the transmitter axis imaged) as higher f-number optics are used is apparent, and for small standoff distances the f-number is more important than the $1/\sin\theta$ effect resulting from the crossing angle of the transmitter and collection paths. In the limit of parallel incident light the wedge introduces no aberration. The accompanying loss of light gathering capability (which scales as $1/d^2$, where d is the lens to focal volume distance) makes this approach unattractive, however.

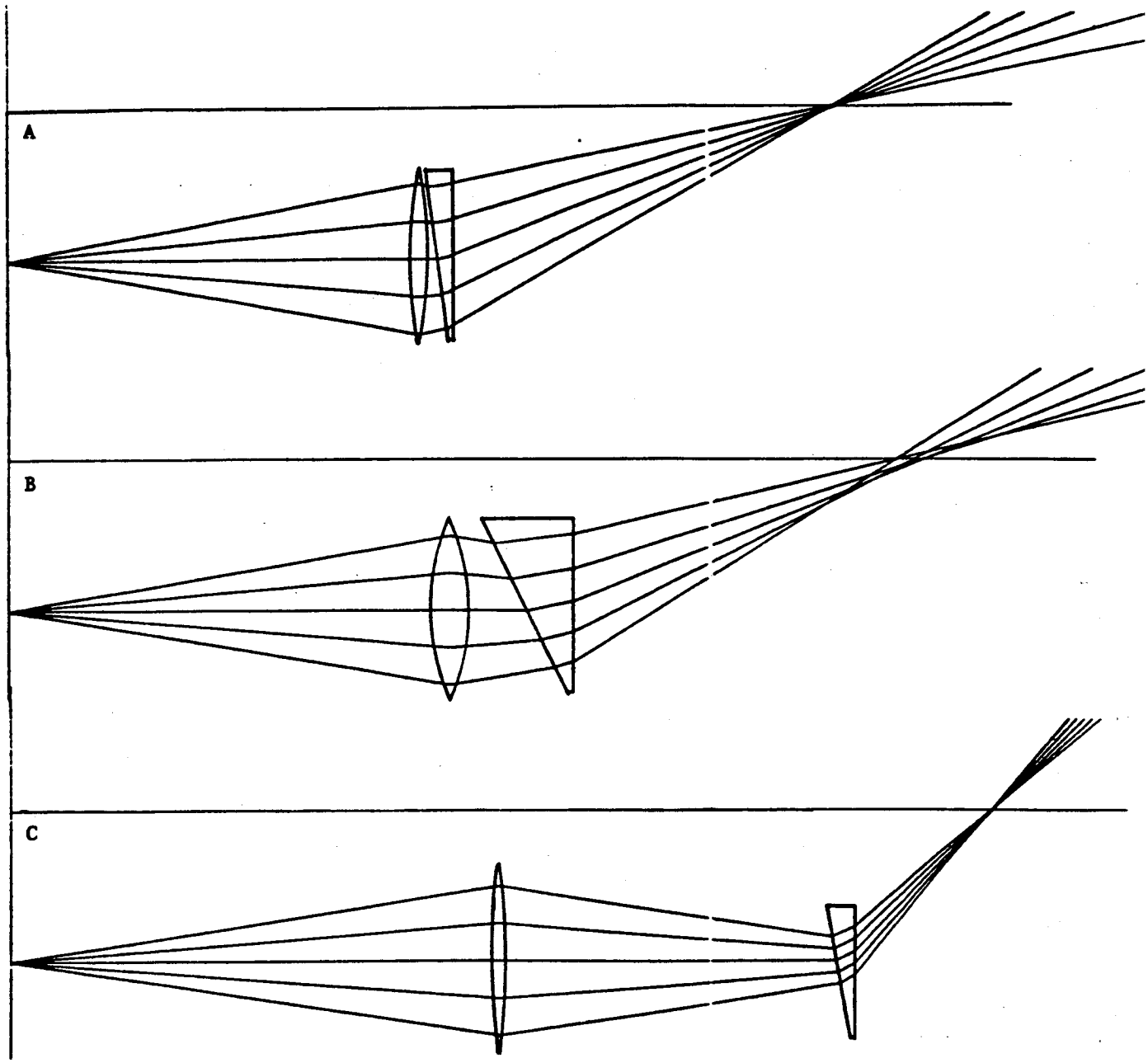

Figure F.1 Ray training calculations for 3 collection optics configurations, all with a single biconvex lens and a point source.

A) 3 inch standoff, f = 42mm, S^1 = 84mm, resolution = 1mm.
B) 1 inch standoff, f = 18mm, S^1 = 36mm, resolution = 2.2.5mm.
C) 1 inch standoff, f = 50mm, S^1 = 100mm, resolution = 0.31mm.

Scales are not equal.

TABLE F.1

Summary of Model Results for Collection and Transmitter Optics

Lens System	Focal Length	Eff. f/#	Fiber Size	Resolution*
Single Biconvex (d=8.89) with wedge	20	4.5	0	2.78
Single Biconvex (d=8.89 with wedge	35	7.9	0	0.84
Ideal lens with wedge	20	4.5	0	1.63
Segmented wedge, Ideal lens	20	4.5	0	1.1
Plano-Convex Lens Pair with wedge	32.8, 32.8	3.7	0	0.245
Plano-Convex Lens Pair with wedge	32.8, 32.8	3.7	0.1	0.63
Plano-Convex Lens Pair with wedge	66.3, 32.8	3.7	0.1	0.32
Transmitter, Plano-Convex Lens Pair (d_1=12.7)	32.8, 32.8	2.6	0.1	0.428
Transmitter, Plano-Convex Lens Pair (d_1=12.7)	66.3, 32.8	5.2, 2.6	0.1	0.214

*For collection system, resolution is the distance along the laser beam imaged ("interaction length"). For the transmitter, resolution simply means the spot size.

In the basic design discussed above the main source of aberration is the wedge, as can be seen in Table 2, in which the resolution obtained for single lens systems at different focal lengths is compared for the real case and an ideal case in which the lens is "perfect" and introduces no aberration. Thus, an alternate approach is to correct for the wedge aberration in some fashion. Calculations investigating the effect of using a segmented wedge as a means of making the correction were made. They showed insufficient improvement in performance to warrant the increased cost and fabrication difficulties associated with such a wedge (see Table F.1).

Another design approach that was tested eliminates the wedge aberration by ensuring that parallel light passes through the wedge. This is accomplished by placing the wedge between two plano-convex lenses operating at infinite conjungate ratio. This design also reduces spherical aberration because the two plano-convex lens combination performs better than a single biconvex lens. Another advantage of this design is that it places the first lens as close as possible to the focal volume. The main disadvantage is the vignetting caused by the angled placement of the first lens. This arrangement of the collection optics can be seen in Figure F.2. The reduction in gathered light caused by the vignetting is approximately 50%. The improvement in spatial resolution is substantial, however (see Table F.1), and thus this design was chosen for the collection system.

A pair of equal focal length plano-convex lenses was also chosen for the laser input optics owing to their better performance compared to a single biconvex lens. This can also be seen in Figure F.2. The lower spot size obtained is 0.43 mm, which is about twice as large as the desired size. To achieve a 200 μm spot either best form lenses (custom), achromats (not suitable for use at high temperature), or an unequal focal length pair of plano-convex lenses (magnification <1) are needed. In Figure F.3 the performance of 3 transmitter configurations are compared. The single lens transmitter is clearly inadequate. Figures F.3b and F.3d show the point source and 200 fiber source cases for the design chosen for the probe evaluation. Figure F.3c shows the still smaller spot size obtained with a magnification of 0.5 lens pair.

The overall resolution of the probe is thus: $res_1 \times res_2 \times res_3 = 430\ \mu \times 240\ \mu \times 630\ \mu = 6.5 \times 10^7 \mu m^3$ (vs. $8 \times 10^6\ \mu m^3$ design target), eight times larger than desired. However, the current design should be adequate for characterizing the actual probe performance. If needed, the design can be changed to incorporate an unequal focal length pair of lenses and should easily meet the 200 μm x 200 μm x 200 μm desired resolution.

TABLE F.2

Comparison of Performances of Single-Lens/Wedge Collection Configuration for "real" and "perfect" lens cases.

f	Δx real	Δx perf.
20mm	2.78mm	1.63mm
35mm	0.84mm	0.55mm
50mm	0.39mm	0.31mm

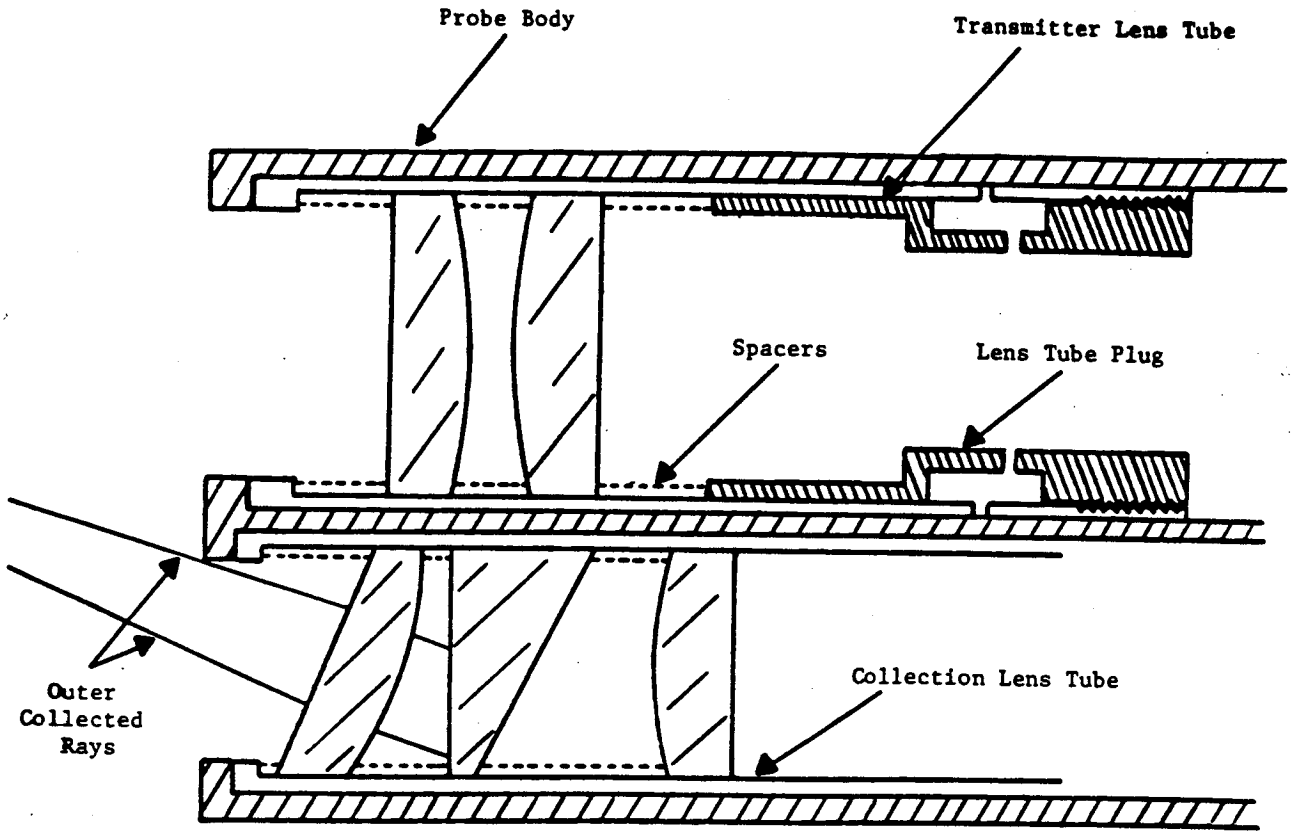

Figure F.2 Rayleigh Scattering Probe Optical Design

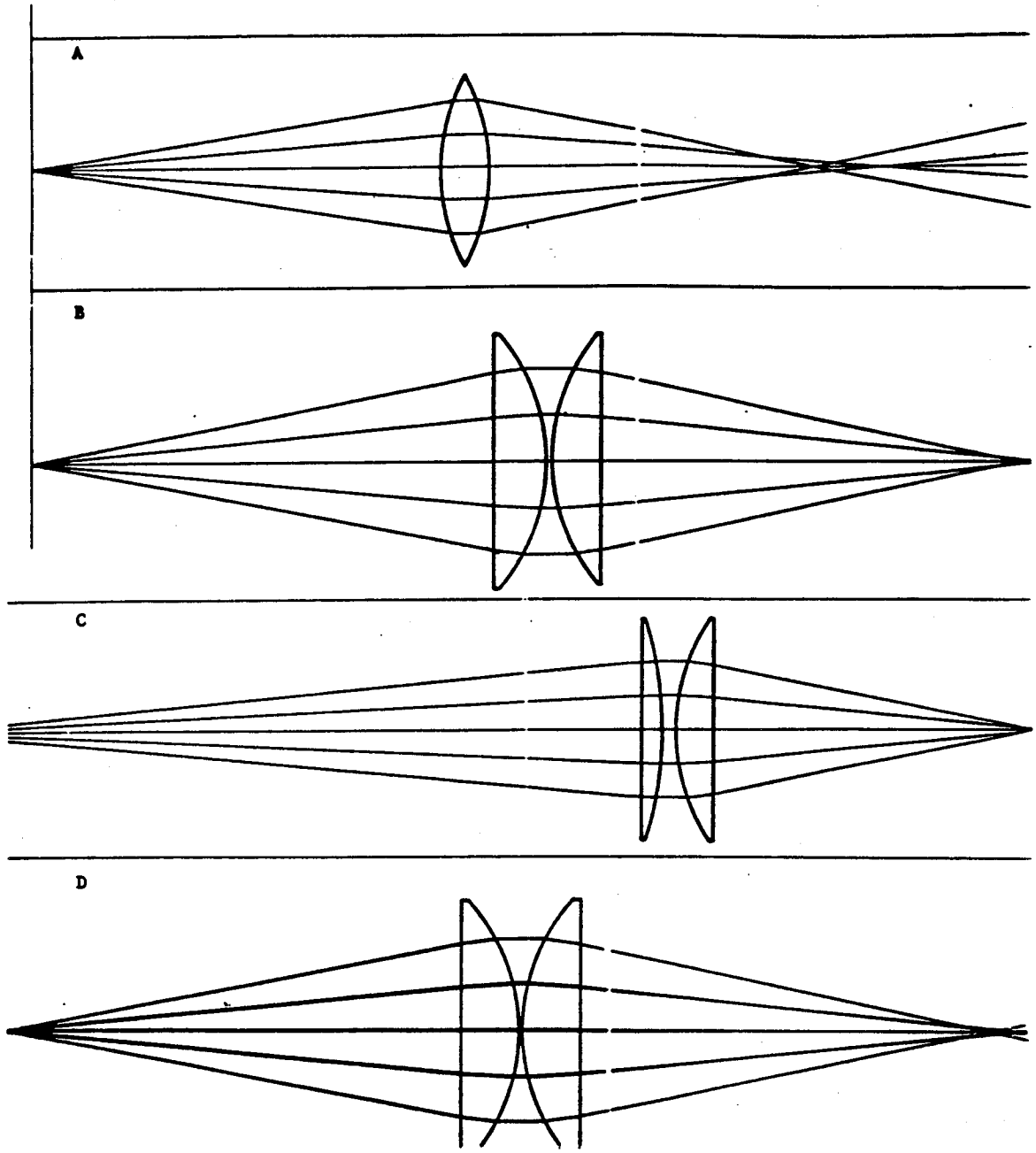

Figure F.3 Ray Tracing Calculations for 3 Transmitter Configurations a) Single bi-convex lens (f = 20 mm, S_1 = 40 mm) with point source. Spot size is 0.73 mm. b) Two plano-convex lenses (f_1 = f_2 = 32.8 mm, S_1 = 32.8 mm) with point source. Spot size is 0.27 mm. c) Two plano-convex lenses (f_1 = 66 mm, f_2 = 32.8 mm, S_1 = 66 mm) with point source. Spot size is 0.15 mm. d) Two plano-convex lenses (f_1 = f_2 = 32.8, S_1 = 32.8) with a 200 μm fiber source. Spot size is 0.43 mm. Scales are not equal.

APPENDIX G

ANALYTICAL FORMULATION OF RAYLEIGH SCATTERING MEASUREMENTS

The elastic scattering of light by gaseous molecules is a well known phenomena and its "discovery" is attributed to Lord Rayleigh (John William Strutt).[1-3] The principles of elastic light scattering in gases are well understood and documented.[3-5] This section describes how Rayleigh scattered light can be used to ascertain the temperature or number density of a gas sample.

The intensity I of light scattered by a unit volume of gas into an infinitesimal solid angle at scattering angle θ is

$$I = I_o N L \sigma(\theta) \tag{1}$$

where I_o is the incident intensity, $\sigma(\theta)$ the scattering cross section, L is the effective length of the irradiated sample which is observed, and N is the number density of the gas. Through the ideal gas law

$$N = \frac{P}{kT} , \tag{2}$$

where P is the gas pressure and k is Boltzmann's constant, Equation (1) gives that I/I_o is inversely proportional to temperature. This simple relationship makes Rayleigh scattering a reasonable, nonintrusive method for measuring temperature.

For unpolarized light, the scattering cross section is defined[4] by

$$\sigma(\theta) = \frac{2}{3}\left(\frac{2\pi^4}{\lambda}\right) \alpha^2 \left(\frac{6 + 3p_n}{6 - 7p_n}\right) P(\theta) \tag{3}$$

where α is the molecular polarizability of the gas, λ is the wavelength of incident light, and p_n (depolarization factor) is a small correction term which accounts for the molecular anisotropy of the gas. This equation

illustrates the familiar λ^{-4} wavelength dependence. The angular part of Equation (3) is

$$P(\theta) = \frac{3}{4(1 + 2\gamma)} [(1 + 3\gamma) + (1 - \gamma) \cos^2 \theta]; \gamma = p_n/(2 - p_n) \quad . \quad (4)$$

For light polarized perpendicular to the observation plane, the first term in the square brackets is used, and the second term is used for parallel polarization. Again, γ is related to p_n and is a small correction term.

The molecular polarizability α is related to the molar refractivity R_L and index of refraction n by

$$\alpha = \frac{3R_L}{4\pi N_o} = \frac{3}{4\pi N} \frac{n^2 - 1}{n^2 + 2} \quad (N_o = \text{Avogadro's number}). \quad (5)$$

The molar refractivity is slightly wavelength dependent and can be very accurately measured (~1 part in 10^4). It can be represented by a function of the form

$$n_{STP} - 1 = \frac{a}{b - \lambda^{-2}} \quad (6)$$

where a and b are coefficients fit to the available experimental data. Values of a, b, p_n, and γ are given in Table G.1 for some common gases. Since n^2-1 is also proportional to N,[4] α is independent of number density. A compilation of R_L data for most of the common combustion gas species, including explicit wavelength dependence, is available in Reference 6. From this, the Rayleigh scattering cross section for any gas species of interest can be accurately obtained for a given λ.

For a mixture of gases, the total cross section is simply an average of individual cross sections, weighted by their fractional (molar) abundance, χ_i. Thus, for a gas mixture Equation (1) can be written as

$$I/I_o = N L \langle\sigma\rangle = N L \sum_i \chi_i \sigma_{\lambda,i}(\theta) \qquad (7)$$

TABLE G.1

Refractivity and Anisotropy Data for Combustion Species

Species	Refractivity Coefficients[a] $a \times 10^{12}$	$b \times 10^{6}$	Anisotropy Terms[b] ρ_n	γ
Ar	520.33	1.8768	0.0	0.0
CH_4	599.53	1.2964	0.0	0.0
CO	404.39	1.2356	0.013	0.007
CO_2	681.39	1.5571	0.097	0.051
H	87.47	0.7839	0.0	0.0
H_2	187.53	1.3783	0.0	0.0
H_2O	291.48	1.1869	0.020	0.010
NH_3	328.85	0.8021	0.010	0.005
NO	393.40	1.3648	0.027	0.014
N_2	562.45	1.9097	0.036	0.018
O	71.63	0.6049	0.0	0.0
OH	105.76	0.3209	0.0	0.0
O_2	380.37	1.4334	0.065	0.034

[a]Using Equation (6) with λ in A

[b]See Equations (3) and (4)

For a given experimental geometry and wavelength, the scattered light signal observed can be written as

$$\boxed{\text{Signal} = I_o C N \langle\sigma\rangle} \quad , \qquad (8)$$

or

$$\boxed{\text{Signal} = I_o \frac{CP}{RT} \langle\sigma\rangle} \quad , \tag{9}$$

illustrating the simple dependence on number density or temperature.

The constant C contains all fixed parameters of the system and essentially becomes the overall calibration constant. It can be empirically determined using the calibration procedure described in section 2.6 of this report, but for signal analysis calculations it can be written as

$$C = \eta \varepsilon_1 \varepsilon_2 \varepsilon_3 L \, d\Omega \quad , \tag{10}$$

where

η = quantum efficiency of photomultiplier

ε_1 = overall efficiency for transmitting incident light through fiber optics and focusing into gas sample

ε_2 = overall efficiency for collecting scattered light and transmitting it through fiber optic to detector

ε_3 = transmission of interference filter

$d\Omega$ = solid angle (sr) subtended by collection optics

In a nonideal system, the signal measured at each wavelength is made up of a Rayleigh scattered component (S) and a surface scattered background (B),

$$\text{Sig} = S + B \tag{11}$$

The Rayleigh scattered component is given by:

$$S = CIN\sigma \tag{12}$$

where I is the laser intensity, N the number density of scatter, σ the effective Rayleigh scattering cross section, and C a system dependent constant. The background is given by

$$B = CC'I \tag{13}$$

where C' is a constant. Thus

$$\frac{Sig}{I} = CN\sigma + C'C \tag{14}$$

The expected response is therefore linear, and a least squares fit to the calibration data with y = Sig/I and x = Nσ yields the slope, C, and intercept CC'. The least squares fit is done according to

$$\text{slope} = C = \frac{n\Sigma xy - \Sigma x\Sigma y}{n\Sigma x^2 - (\Sigma x)^2} \tag{15}$$

$$\text{intercept} = CC' = \frac{\Sigma y\Sigma x^2 - \Sigma x\Sigma xy}{n\Sigma x^2 - (\Sigma x)^2}$$

where n is the number of conditions.

From equations (11) - (14), the expression for the surface scattered background component can be found to be

$$B_{\lambda 1} = \frac{Sig_{\lambda 1} - Sig_{\lambda 2} \dfrac{I_1\sigma_1C_1}{I_2\sigma_2C_2}}{1 - \dfrac{C_2'\sigma_1}{C_1'\sigma_2}} \tag{16}$$

REFERENCES

1. J. W. Strutt, Philos. Mag (4) 41, 107 (1871); Sci. Papers I, 87 (1899).

2. J. W. Strutt, Philos. Mag (5) 12, 81 (1881); Sci. Papers I, 518 (1899).

3. A. T. Young, "Rayleigh Scattering", in Physics Today, American Institute of Physics, New York (1982), p. 42.

4. Earl J. McCartney, Optics of the Atmosphere, Chap. 4, J. Wiley and Sons, New York (1976).

5. R. Siegel and J. R. Howell, Thermal Radiation Heat Transfer, Chap. 20-21, McGraw Hill, New York (1972).

6. W. C. Gardiner, Jr., Y. Hidaka, and T. Tanzawa, "Refractivity of Combustion Gases", Comb. Flame 40, 213 (1981).